In compliance with the
Canadian Privacy Legislation
some supporting forms
may have been removed from
this dissertation.

While these forms may be included
in the document page count,
their removal does not represent
any loss of content from the dissertation.

Motion mechanisms and cortical areas in human vision: psychophysics and fMRI

Serge O. Dumoulin

Department of Neurology and Neurosurgery,

McGill University, Montréal, Canada.

February, 2003.

A thesis submitted to the Faculty of Graduate Studies and Research

in partial fulfillment of the requirements of the degree of Doctor of Philosophy.

Your file Votre référence
ISBN: 0-612-88455-4
Our file Notre référence
ISBN: 0-612-88455-4

Abstract

OUR visual world contains both luminance- (first-order) and contrast-defined (second-order) information. Distinct mechanisms underlying the perception of first-order and second-order motion have been proposed from electrophysiological, psychophysical and neurological studies. In this thesis psychophysical and human brain imaging (fMRI) experiments are described that support the notion of distinct mechanisms, but extend the previous studies by providing evidence for a functional dissociation and a relative cortical specialization for first- and second-order motion.

Using psychophysical methods, a directional anisotropy was found for second-order but not first-order motion in peripheral vision. This anisotropy is interpreted as a functional dissociation implicating the second-order mechanism in optic flow processing.

Identification of early visual cortical areas is a prerequisite to any functional assessment of these visual areas. To this aim a novel human brain mapping method has been developed which automatically segments early human retinotopic visual areas. Unlike previous methods this procedure does not depend on a cortical surface reconstruction and thereby greatly simplifies the analysis.

In a combined psychophysical and fMRI study, distinct cortical regions, in occipital and parietal lobes, were preferentially activated by either first- or second-order motion. These results provide evidence for the idea that first-order motion is computed in V1 and second-order motion in later occipital visual areas. In addition the results suggest a functional dissociation of the two kinds of motion beyond the occipital lobe consistent with a role for the second-order mechanism in optic flow analysis.

Résumé

Le monde visuel contient à la fois des informations de luminance (de premier ordre) et des informations de contraste (de deuxième ordre). Des études électrophysiologiques, psychophysiques et neurologiques ont proposé des mécanismes distincts pour la perception du mouvement du premier et du second ordre. Dans cette thèse sont décrites des expériences psychophysiques et d'imagerie cérébrale humaine (IRMf) qui supportent cette distinction, mais aussi étendent les études précédentes en démontrant une distinction fonctionnelle et une relative spécialisation corticale pour le mouvement du premier et du second ordre.

En utilisant des méthodes psychophysiques, une anisotropie directionnelle a été mise en évidence en vision périphérique pour le mouvement du second ordre seulement. Cette anisotropie est interprétée comme une dissociation fonctionnelle qui implique un mécanisme du second ordre dans le traitement du flot optique.

L'identification des premières aires visuelles corticales est une condition préalable à l'évaluation fonctionnelle de ces aires visuelles. Pour y parvenir nous avons développé une nouvelle méthode de cartographie cérébrale qui segmente automatiquement les premières aires visuelles rétinotopiques. Contrairement aux autres méthodes, celle-ci ne dépend pas de la reconstruction de la surface corticale, simplifiant ainsi grandement l'analyse.

Dans une étude combinant psychophysique et imagerie cérébrale, des régions corticales distinctes ont été préférentiellement activées dans les lobes occipital et pariétal soit par du mouvement du premier ordre, soit par du mouvement du second ordre. Ce résultat supporte l'hypothèse que le mouvement du premier ordre est calculé par l'aire V1, et que le mouvement du second ordre est calculé par des aires visuelles d'ordre supérieur. Ce résultat suggère en outre une dissociation fonctionnelle des deux types de mouvement au-delà du lobe occipital en accord avec un rôle du mécanisme du second ordre dans l'analyse du flot optique.

Samenvatting

ONZE visuele wereld bevat informatie over helderheid (eerste-orde) en contrast (tweede-orde). Aparte mechanismen voor de waarneming van eerste- en tweede-orde beweging zijn beschreven door electrofysiologische, psychofysische en neurologische studies. In dit proefschrift zijn psychofysische en menselijke hersenscanning (fMRI) experimenten beschreven die het idee van de aparte mechanismen ondersteunen, maar die tevens een bewijs leveren van een functionele onderscheiding en een relatieve corticale specialisatie voor het verwerken van eerste- en tweede-orde beweging.

In het perifere gezichtsveld is er, met behulp van psychofysische methoden, een richtingsanisotropie gevonden voor de tweede-orde bewegingen, maar niet voor de eerste-orde bewegingen. Deze anisotropie is geïnterpreteerd als een functionele onderscheiding waarbij het tweede-orde-systeem betrokken is in het verwerken van optische stromingsvelden.

Identificatie van visuele corticale gebieden is een vereiste voordat er een functioneel onderzoek van deze gebieden gedaan kan worden. Tot dit doel is er een nieuwe brain mapping methode ontwikkeld die automatisch de visuele retinotopische gebieden onderscheidt. In tegenstelling tot andere methoden, hoeft voor deze werkwijze het corticale oppervlak niet gereconstrueerd te worden, waardoor de analyse een stuk eenvoudiger wordt.

In een gecombineerd psychofysisch en fMRI studie worden aparte corticale gebieden geactiveerd, in de occipitaal- en parietaalkwab, door eerste- of tweede-orde bewegingen. De resultaten bevestigen het idee dat eerste-orde bewegingen worden verwerkt in V1 en tweede-orde bewegingen in latere occipitale visuele gebieden. Verder duiden de resultaten op een functioneel onderscheid van de twee soorten bewegingen voorbij de occipitaalkwab, in overeenstemming met een rol voor het tweede-orde systeem in de analyse van optische stromingsvelden.

Acknowledgments

I am thankful to many people who have provided assistance and support throughout this project. First, I would like to express my gratitude to my supervisors Curtis Baker, Alan Evans and Robert Hess for their continuing support, guidance and enthusiasm, making this thesis possible.

I would also like to express my appreciation to the members of the McGill Vision Research Unit and the McConnell Brain Imaging Centre for their help in various stages of this dissertation, in particular Rebecca Achtman, Gareth Barnes, William Beaudot, Véronique Bohbot, Louis Collins, Mike Ferreira, Rick Hoge, Tim Ledgeway, Kathy Mullen, Vali Petre and Bruce Pike. I would also like to thank all the subjects for their cooperation and patience, and the MR technicians for their assistance. Furthermore, I would like to express my gratitude to Lucia Vaina of Boston University for providing data for figure 4.4. For their help in McGill's administrative challenges, I would like to thank Monique Ledermann and Elizabeth Wong.

I gratefully acknowledge my family, family-in-law and friends, in both continents, for their support, interest and providing a "life outside science". Mijn grootste waardering gaat uit naar mijn ouders voor alle mogenlijkheden die ze mij geboden hebben en hun niet aflatende steun. Ook gaat mijn dank uit naar mijn zusje Daphne en Opa voor hun steun en vertrouwen. Finally, I would like to thank Gisele and Daniel for their love, support, and my happiness.

This research was supported by Natural Sciences and Engineering Research Council of Canada (NSERC) grant OGP0001978 to Curtis Baker, Canadian Institutes of Health Research (CIHR) grants MT 10818 and MST 34695, and NSERC grant 0GP0046528 to Robert Hess, and International Consortium for Brain Mapping (ICBM) grant MH52176-06 to Alan Evans.

Preface

THIS thesis describes a cortical specialization for two motion mechanisms, known as first- and second-order, and additionally suggests a functional dissociation between these two kinds of motion. Furthermore, a novel human brain mapping methodology was developed to automatically identify early human visual areas. The dissertation is based on the following manuscripts:

> Dumoulin, S.O., Baker Jr, C.L., Hess, R.F. (2001) Centrifugal bias for second-order but not first-order motion. *Journal of the Optical Society of America A.* 18(9): 2179–2189.
>
> Dumoulin, S.O., Hoge, R.D., Baker Jr., C.L., Hess, R.F., Achtman, R.L., Evans, A.C. (2003) Automatic segmentation of human visual retinotopic cortex. *NeuroImage.* 18(3): 576–587.
>
> Dumoulin, S.O., Baker Jr., C.L., Hess, R.F., Evans, A.C. (2003) Cortical specialization for processing first- and second-order motion. *Cerebral Cortex.* Submitted.

These papers appear in chapters 2 to 4, respectively. At the time of writing two of these manuscripts are published and the third is "submitted". The first two manuscripts are reproduced with permission of their respective publishers.

Contributions of authors

THE contributions of the authors to the manuscripts on which this thesis is based are as follows. Mr. Dumoulin developed the major parts of the methodology (chapter 3), designed, implemented and conducted the experiments, and wrote the bulk of the manuscripts. The supervisors, Drs. Baker, Evans and Hess provided guidance and supervision in the different fields of visual psychophysics (chapters 2 and 4), human brain mapping methodology (chapter 3), and applied functional imaging (chapter 4). The additional co-authors Dr. Hoge and Ms. Achtman provided valuable assistance in methodological development and data acquisition (chapter 3).

Table of contents

List of figures

List of tables

List of abbreviations

1D, 2D, 3D ..... one, two, three dimensional

2AFC ..... two-alternative forced choice

AIR ..... automated image registration

aMRI ..... anatomical magnetic resonance imaging

ASPL ..... anterior superior parietal lobule

BOLD ..... blood oxygenation level dependent

CC ..... corpus callosum

CS ..... calcarine sulcus

CeS ..... central sulcus

CiS ..... cingulate sulcus

CSF ..... cerebral spinal fluid

$\mathbf{D_{min}}$ ..... minimal displacement needed to detect motion

EEG ..... electroencephalography

EPI ..... echo-planar imaging

fMRI ..... functional magnetic resonance imaging

FOE ..... focus of expansion

FRF ..... filter-rectify-filter

fwhm ..... full-width-half-maximum

GE ..... gradient echo

INSECT ... intensity normalized stereotaxic environment for the classification of tissues

IPS ..... intra-parietal sulcus

HM ..... horizontal meridian

hMT+ ..... human MT including parts of adjacent areas

HRF ..... hemodynamic response function

LCD ..... liquid crystal display

LIP ..... lateral intraparietal area

LO ..... lateral occipital

MAE ..... motion after effect

medline ..... medical literature analysis and retrieval system online

MEG ..... magnetoencephalography

MeSH ..... medical subject headings

MO ..... medial occipital

MRI ..... magnetic resonance imaging

mse ..... mean square error

MSPL ..... middle superior parietal lobule

MT ..... middle temporal area (V5)

mVFS ..... visual field sign map weighted by a magnitude map

PC ..... precuneus

PET ..... positron emission tomography

POS ..... parieto-occipital sulcus

ROI ..... region of interest

SF ..... sylvian fissure

SNR ..... signal-to-noise ratio

SPAM ..... statistical probability anatomical map

STS ..... superior temporal sulcus

TE ..... time to echo

TMS ..... transcranial magnetic stimulation

TR ..... repetition time

tVFS ..... visual field sign map weighted by a *t*-statistical map

V1 ..... visual area 1 (presumed homologue of area 17, striate cortex)

V2 ..... visual area 2 (presumed homologue of area 18)

V3 ..... visual area 3, dorsal counterpart of VP

V3a ..... visual area 3 accessory

V3b ..... visual area 3b

V4v ..... ventral part of visual area 4

V5 ..... visual area 5 (MT)

V7 ..... visual area 7

V8 ..... visual area 8

VFS ..... visual field sign

VM ..... vertical meridian

VOI ..... volume of interest

voxel ..... volume element

VP ..... ventral posterior area, ventral counterpart of V3

VSG ..... visual stimulus generator

Chapter 1

Introduction

THIS chapter provides an overview of the scientific background related to this dissertation. A general background of motion perception, in particular the concepts of first-order and second-order motion, is described. Furthermore, an introduction to functional magnetic resonance imaging is given, with the emphasis on visual area identification and motion perception. Lastly, a brief overview of the thesis is provided.

1.1 Visual motion

The ability to move is an essential property of almost all animals. With this ability comes the requirement to detect motion of ourselves and others. Most animals, including humans, use their visual system to obtain information about their own movements and their environment. Consequently, visual motion processing is a fundamental property of any visual system, regardless of the degree of development or use. The essential nature of visual motion processing is evidenced by the observation that no visual system has been shown to lack mechanisms for motion processing (Nakayama, 1985; Goldstein, 1999), and is further illustrated by certain animals, e.g. toads, where stimulus movement is essential for eliciting behavioral responses (Ewert, 1974; Camhi, 1984; McFarland, 1993), and, lastly, by the profound behavioral deficits exhibited by humans with lesions that selective impair motion perception (Zihl et al., 1983; Hess et al., 1989; Baker et al., 1991).

Image motion provides us with information about our environment, most obviously detection of moving objects. In addition, image motion supports several other visual functions. Relative velocities may be used to distinguish shapes and forms (form-from-motion), and to provide depth-clues (depth-from-motion) (Wallach and O'Connell, 1953; Rogers and Graham, 1979; Wilson et al., 1983; Nakayama, 1985). Furthermore, visual motion can not only provide information about the environment, but also about the observer's own motion and posture in relation to their environment, thus serving as a proprioreceptive sense (Gibson, 1954; Koenderink, 1986). The motion patterns on our retina elicited by our own movements are known as optic flow. Thus image motion can be used to provide information about ourselves, e.g. to guide our movements and navigation, and inform us about the environment, e.g. to segment our visual world and detect movements of others.

Several distinctions in the mechanisms underlying motion perception have been proposed (see for instance: Braddick, 1974; Chubb and Sperling, 1988; Cavanagh, 1992; Lu and Sperling, 1995; Van der Smagt et al., 1999; Burr and Ross, 2002), which may not seem surprising given the many functional roles for image motion. This dissertation focuses on the mechanisms proposed to mediate the perception of luminance- (first-order) and contrast-based (second-order) motion.

1.2 First- and second-order motion

Motion can be defined by first- or second-order stimulus attributes (see for example figure 1.1). First-order image statistics are luminance and color, and second-order attributes are variations of luminance (or color) over space (e.g. contrast or texture), time (temporal frequency), or ocularity (binocular disparity) (Chubb and Sperling, 1988; Cavanagh and Mather, 1989). However, in this monograph, second-order stimulus properties refer to contrast-defined image attributes. In the examples of figure 1.1 A-C, all image structures are defined by variations in luminance (dark-light bars), making them first-order stimuli. In panel D, however, the low spatial frequency is defined by contrast variations, i.e. second-order image statistics. Note that panel D necessarily also contains first-order information

(high spatial frequency, i.e. carrier). When the images in figure 1.1 are taken as space-time diagrams, with time increasing down the page, the high and low spatial frequency are moving to the left and right, respectively.

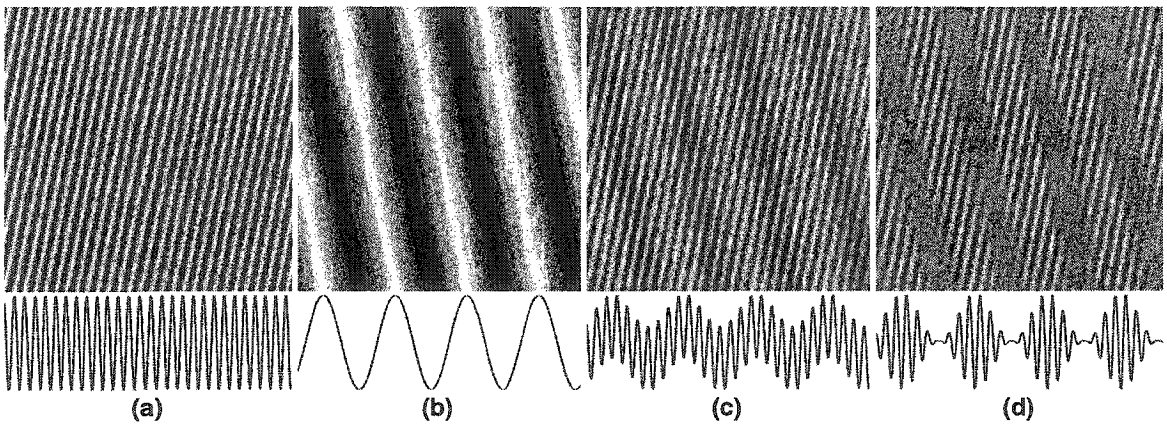

Figure 1.1: Examples of stimulus construction, containing images (top part of each panel) and a corresponding luminance profile (bottom part of each panel). Panels (A & B) illustrate a first-order high and low spatial frequency gratings, i.e. the gratings are defined by luminance variations. When added they give rise to the image in panel (C), when multiplied they give rise to the image in panel (D), where the contrast of the high spatial frequency (carrier, A) is modulated by the low spatial frequency (envelope, B), i.e. a second-order modulation. These images may represent spatial images or space-time diagrams. If interpreted as a space-time diagram with the time dimension increasing down the page, the high and low spatial frequencies are drifting left and rightwards, respectively. All images are displayed at a 100% contrast.

Psychophysical evidence suggests that first- and second-order motion stimuli are processed, at least initially, by distinct visual pathways and different mechanisms. For instance, alternating first- and second-order frames can not be integrated to detect the direction of motion (Mather and West, 1993; Ledgeway and Smith, 1994a). The idea of separate mechanisms is further illustrated by the observations that no cross-adaptation (Nishida et al., 1997) and no local cancelation (Scott-Samuel and Smith, 2000) occurs between first- and second-order motion signals, unlike first-order equivalents. First- and second-order mo-

tion also differ in their ability to induce motion-after-effects (MAE). Unlike first-order motion, second-order motion stimuli produce no MAE on a static background, but may induce MAE on a flickering background (Mather, 1991; Ledgeway and Smith, 1994b; Nishida et al., 1994; Gurnsey et al., 1998). Functional dissociations between the two motion systems have been found as well. For instance, first-order motion detectors are the primary input to the kinetic depth system (Landy et al., 1991; Hess and Ziegler, 2000). Eye-movements to second-order targets are impaired compared with first-order equivalents (Harris and Smith, 1992; Hawken and Gegenfurtner, 2001). Lastly, aging has been shown to have a different effect on first- and second-order processing (Habak and Faubert, 2000).

Using electrophysiological techniques, neurons have been found to respond to second-order stimuli in cat area 17 and 18 (Zhou and Baker, 1993, 1994, 1996; Mareschal and Baker, 1998a,b, 1999), with spatial and temporal frequency tuning which was different for first- and second-order stimuli within the same neurons. Neurons in primate striate and extra-striate cortex have also been shown to respond to second-order motion (Albright, 1992; Olavarria et al., 1992; Geesaman and Andersen, 1996; Chaudhuri and Albright, 1997; O'Keefe and Movshon, 1998), where area MT has been suggested to respond to motion independent of how it is defined (form/cue independent Albright, 1992), i.e. integrating first- and second-order motion.

Brain lesion studies indicate that each kind of motion perception can be affected separately while leaving the other intact, providing a neuropsychological "double dissociation". Relative impairments of either first-order (Greenlee and Smith, 1997; Vaina et al., 1998, 1999, 2000) or second-order (Plant et al., 1993; Plant and Nakayama, 1993; Vaina and Cowey, 1996; Greenlee and Smith, 1997; Braun et al., 1998; Vaina et al., 1999) motion perception have been described. Comparing the location of lesions affecting perception of either kind of motion, Greenlee and Smith (1997) found extensive overlap when transferring the lesioned areas to a standardized template (Seeger, 1978), whereas Vaina et al. (1999) suggested separate sites.

Thus, evidence for separate mechanisms for processing first- and second-order stimuli, both stationary and moving, have been provided by electrophysiological, human psy-

chophysical and neurological studies (for reviews see: Smith, 1994; Baker, 1999; Clifford and Vaina, 1999; Baker and Mareschal, 2001; Chubb et al., 2001; Lu and Sperling, 2001).

1.3 Models of motion perception

Models are of crucial importance to generate hypotheses and motivate experiments. The previous section proposes that first- and second-order stimuli are processed by two kinds of motion detectors, i.e. mechanisms detecting luminance-defined motion and separate ones processing second-order spatiotemporal correlations (e.g. contrast). In this section models of motion detection will be described with emphasis on second-order models. Please note that the first- and second-order distinction may occur both at the level of the stimulus (see previous section) as well as the properties of the mechanisms processing them; these two distinctions do not necessarily correspond fully.

First-order models of motion perception fall into three categories. The first category are so called Reichardt-detectors, where two retinal locations are compared after a time-delay for one of them, i.e. delay and compare (Reichardt, 1961; Van Santen and Sperling, 1985). The second type are gradient models, which divides the spatial derivative by the temporal derivative (Fennema and Thompson, 1979; Sobey and Srinivasan, 1991). The third computes spatio-temporal energy (Adelson and Bergen, 1985). Functionally, the first and third model are equivalent (with the appropriate assumptions, Adelson and Bergen, 1985; Van Santen and Sperling, 1985) and both closely predict the behavior of single neurons in early visual cortex. Therefore, these models are the most widely used and accepted. Their behavior is illustrated in figure 1.2 A and B for the stimuli in figure 1.1 C and D (see also figures 2.2 A, and 4.1). The spatial-temporal frequencies of the model filters are matched to high (A) and low (B) spatial-temporal frequency of the stimulus. As can be seen in the output images, both filters are able to correctly detect the first-order modulations. The second-order modulation (figure 1.2 B, right panel) is not detected since the mean luminance in the different sub-fields of the model is equal, hence no response of the model is elicited.

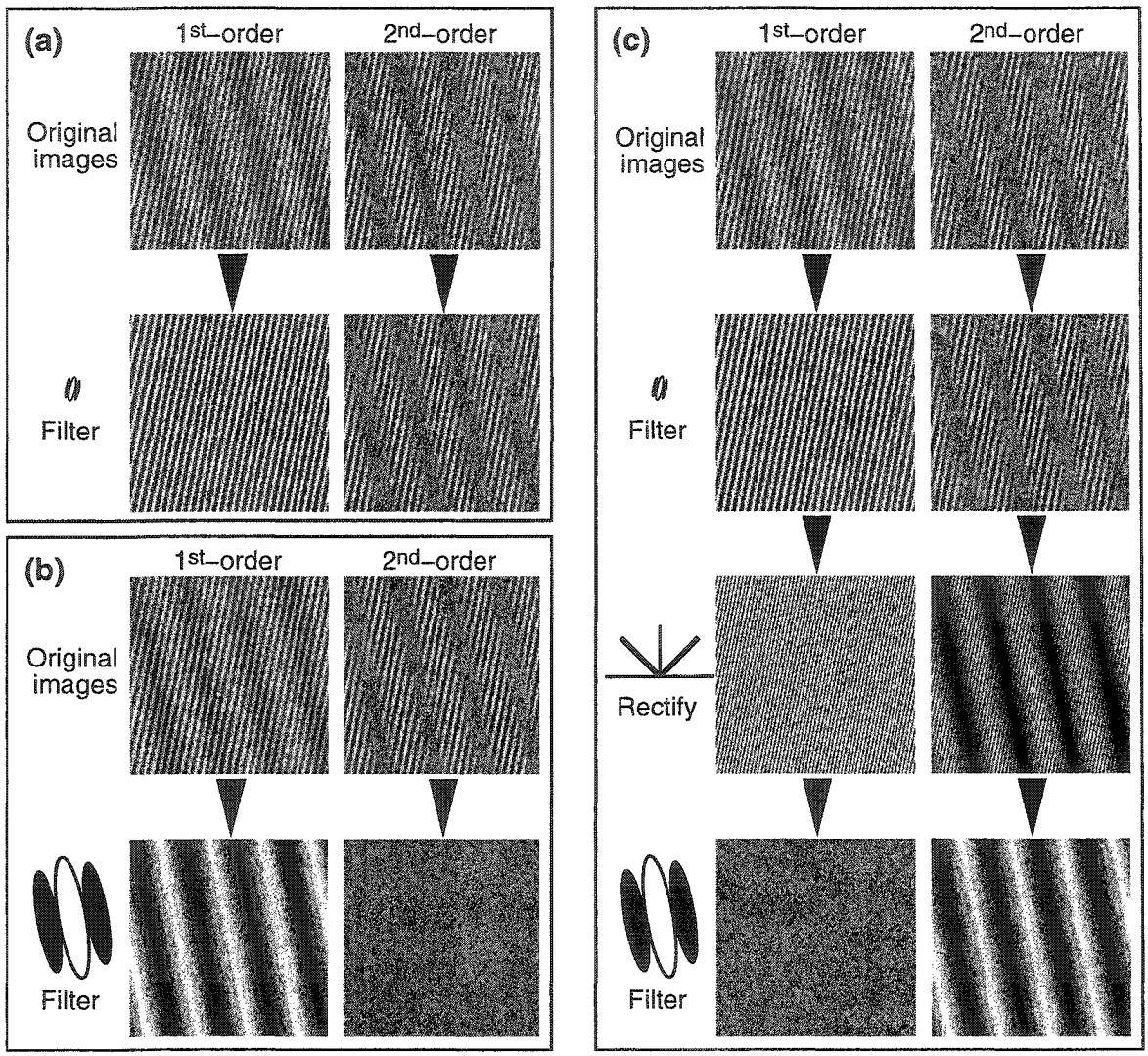

Figure 1.2: Models of first- and second-order mechanisms. The original (input) images are taken from figure 1.1 C & D. Panels A & B show the results of a linear filter model (Adelson and Bergen, 1985) at the appropriate high (A) and low (B) frequencies and orientations. These linear models are not able to detect the second-order modulation (top right image in panels A–C). Panel C demonstrates the filter-rectify-filter (FRF) model which detects the second-order modulation. These images may represent space-space or space-time diagrams, but the latter will be assumed since it relates to motion vision.

A separate model for second-order motion processing may not be necessary if second-order motion stimuli can be detected by first-order mechanisms (or if one model can account for responses to the different stimuli, e.g. Johnston et al., 1992; Benton et al., 2001). Early non-linearities can create luminance artifacts which a first-order model can detect. These non-linearities can arise in the stimulus presentation and/or early visual processing (He and MacLeod, 1998). However, psychophysical evidence suggest that these distortions are only detected at high contrast and high temporal frequencies (Scott-Samuel and Georgeson, 1999; Holliday and Anderson, 1994). Furthermore, these distortions do not occur in, and thus can not explain, certain types of second-order motion, such as motion-defined motion (Zanker, 1993; Zanker and Burns, 2001). Lastly, a large amount of psychophysical, electrophysiological and neurological evidence (see previous section) suggest distinct mechanisms (see also chapters 2 and 4). Thus early non-linearities may be a plausible explanation in some, but not all, cases.

The filter-rectify-filter (FRF) model is a prototypical second-order model due to input from established first-order channels, and due to its broad applicability, i.e. in motion and spatial vision and for different types of second-order stimuli. The behavior of the FRF model to our example stimuli (figure 1.1 C & D) is illustrated in figure 1.2 C. The output of the first-order filter is rectified, and then processed by a second filter at the spatial and temporal frequency of the envelope. This model is able to correctly detect the second-order modulation (figure 1.2 C, bottom panel). Wilson et al. (1992) proposes extraction of first- and second-order information of the FRF model at early (e.g. V1) and later cortical stages (e.g. V2), respectively. An even later site, e.g. MT, is suggested where both kinds of information may converge (but this may occur as early as area 17 and 18, e.g.: Zhou and Baker, 1993; Chaudhuri and Albright, 1997; Mareschal and Baker, 1998a).

Besides the relatively low-level models, higher-order attention- and/or position-based feature-tracking mechanisms have been proposed to mediate the perception of second-order motion (Seiffert and Cavanagh, 1998; Derrington and Ukkonen, 1999). This category of model tracks the position of image features over time. The exact nature of this mechanism is unclear, but generally, though not necessarily, some cognitive strategy is assumed.

Alternatively, such higher-order mechanisms have also been proposed as a parallel third(-order) mechanism mediating motion perception (Lu and Sperling, 1995; Bex and Baker, 1999; Ledgeway and Hess, 2000; Smith et al., 2001).

1.4 Function of second-order mechanisms

The utility of second-order mechanisms has been widely questioned because, firstly, it is assumed that generally second-order attributes co-occur with first-order information, i.e. the second-order information would not make a useful contribution. Secondly, psychophysical performances for second-order stimuli are generally weaker, i.e. higher thresholds for a number of stimulus dimensions, e.g. stimulus durations (Derrington et al., 1993; Ledgeway and Hess, 2002), amplitude (e.g. Schofield and Georgeson, 1999) and stimulus SNR (e.g. coherence: see chapters 2 and 4). Thirdly, in some visual functions, second-order mechanisms either do not seem to contribute, or at least to a lesser degree than first-order ones, e.g. motion functions such as depth-from-motion (Landy et al., 1991; Hess and Ziegler, 2000), eliciting eye-movements (Harris and Smith, 1992; Hawken and Gegenfurtner, 2001) and spatial functions such as contour-linking (Hess et al., 2000) and disparity defined shape (Ziegler and Hess, 1999).

Given the assumption that in most daily circumstances first- and second-order structure overlaps, second-order motion has been suggested to provide supplementary, refining, information (Smith, 1994). Indeed, first- and second-order cues do combine to improve perceptual accuracy at low (first-order) image contrasts (Smith and Scott-Samuel, 2001). Furthermore, first- and second-order cues are combined to compute the global motion direction in plaids (Derrington et al., 1992; Wilson et al., 1992).

In natural images first- and second-order (spatial) structure, but not magnitudes, are usually correlated (Johnson and Baker, 2003). Thus, the assumption that first- and second-order cues co-occur, is usually but not always correct (see also: Schofield, 2000). For example, illumination differences, like shadows, provide strong first-order (but not second-order) borders. These omnipresent borders may not always be useful in image segmentation (but

see: Kersten et al., 1997). Thus, second-order mechanisms would be useful in cases where the first-order information is weak or largely irrelevant, such as texture segregation and motion defined form, i.e. motion of objects rather than their constituent features, e.g. a moving soccer ball and zebra.

1.5 Functional magnetic resonance imaging

Functional magnetic resonance imaging (fMRI) has become one of the most widely used technologies for *in vivo* human brain imaging (see figure 1.3). The fMRI method is based on hemodynamic signals (e.g. Ogawa et al., 1990; Belliveau et al., 1991; Williams et al., 1992; Kwong, 1995; Ogawa et al., 1998) which are coupled to neuronal operations (Logothetis et al., 2001; Bandettini and Ungerleider, 2001; Heeger and Ress, 2002). The most common fMRI technique reveals changes in blood oxygenation (blood oxygenation level dependent, BOLD; Ogawa et al., 1990; Turner et al., 1991; Ogawa et al., 1992; Kwong et al., 1992; Bandettini et al., 1992). The popularity of the fMRI technology can be attributed to 1) the high spatial and temporal resolutions (compared to other hemodynamic techniques, e.g. PET), 2) relatively straightforward data-analysis and interpretation (compared to more direct measures of neuronal activity such as EEG and MEG), 3) its safe and totally non-invasive nature, allowing unlimited replications and experiments on the same subject (compared to other hemodynamic techniques, e.g. PET), and 4) the relatively easy accessibility of the MR equipment (most modern hospitals have MRI machines capable of taking fMR images).

On the other hand, there are a number of limitations of the fMRI technology that should be mentioned. Firstly, fMRI provides an indirect measure of neuronal activity, i.e. hemodynamic signals, and the spatial and temporal resolutions of fMRI is ultimately limited by the properties of the brain's circulatory system. Furthermore, the precise relationship between neuronal activity and hemodynamic responses are incompletely understood, which has implications for the analysis and interpretation of fMRI data, e.g. the fMR signal may be predominantly driven by synaptic activity rather than neuronal firing (Logothetis et al., 2001; Bandettini and Ungerleider, 2001; Heeger and Ress, 2002). Furthermore, due to the

low signal-to-noise and susceptibility to motion artifacts of fMRI data, extensive averaging, preprocessing and statistical analyses are required to detect the fMR signal. Lastly, the awkward environment of the MR machines severely limits experimental designs, i.e. the subjects are immobilized in a noisy narrow bore with a strong magnetic field. In spite of these limitations, fMRI has rapidly grown to be one of the most popular human brain imaging methodologies (see figure 1.3).

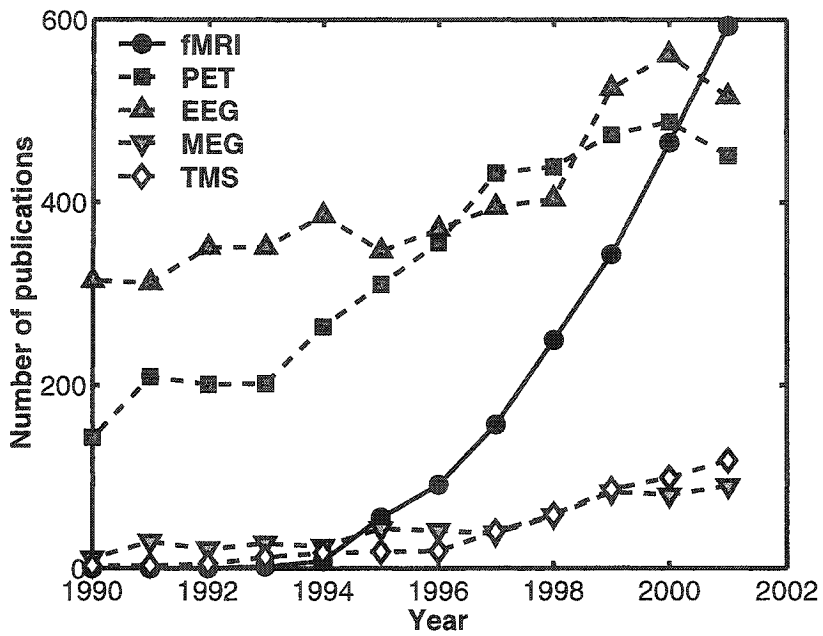

Figure 1.3: Number of published manuscripts in the last decade for five major techniques, which measure (fMRI, PET, EEG, MEG) or manipulate (TMS) neural activity *in vivo*. A literature search (medline) was used for the method acronym (see figure legend) within title, abstract, and keywords (MeSH) constraining the results to include the keywords: "human and (brain or cortex)". The result of this search is dominated by papers using or developing human brain mapping techniques, and shows the general trend of increasing publications within the last 12 years. Furthermore, the rapid growth of fMRI since the introduction of the method (Ogawa et al., 1990) relative to other human brain mapping technologies is revealed.

In the field of motion perception alone, fMRI has made numerous contributions (for reviews see: Tootell et al., 1996; Courtney and Ungerleider, 1997; Wandell, 1999; Culham

et al., 2001b). Using fMRI, results from other methodologies, such as psychophysics, electrophysiology and brain lesion studies were verified and expanded, and perhaps more importantly, fMRI provided a link between these methodologies (see for example chapter 4 and Brewer et al., 2002). Furthermore, fMRI bridges the gap between human and non-human primates by describing similarities (Tootell et al., 1995b; Logothetis et al., 1999; Rees et al., 2000; Vanduffel et al., 2001; Tolias et al., 2001) and discrepancies (e.g. reversed motion selectivity of areas V3 and V3A; Tootell et al., 1997; Vanduffel et al., 2001). Besides revealing locations and properties of known motion areas (Tootell et al., 1995a; Dumoulin et al., 2000; Dukelow et al., 2001; Huk et al., 2002), fMRI has also identified a number of motion responsive areas beyond the well described ones (Tootell et al., 1997; Van Oostende et al., 1997; Sunaert et al., 1999). Lastly, fMRI revealed substantial attentional (top-down) modulations in almost all early visual areas (O'Craven et al., 1997; Beauchamp et al., 1997; Somers et al., 1999; Kanwisher and Wojciulik, 2000), and allows visual activations to be correlated with awareness (Chun and Marois, 2002; Rees and Lavie, 2001; Rees et al., 2002).

One of the most prominent advances in fMRI methodology was the ability to precisely delineate (within $\sim$1mm: Engel et al., 1997) cortical areas using phase-encoded retinotopic mapping (see chapter 3, and for reviews see: DeYoe et al., 1994; Engel, 1996; Sereno, 1998; Tootell et al., 1998d; Warnking et al., 2002). The phase-encoded method sequentially stimulates each point in the visual field along the axes of a polar-coordinate system (Engel et al., 1994), thereby reconstructing the representation of the visual field on the cortex (Sereno et al., 1995). The analysis routine is unique because it relies on the phase of the MR signal rather than the amplitude, making the border identification independent of the widely used (amplitude) significance threshold. Furthermore, it reconstructs the entire visual representation and does not assume a particular a priori layout of the visual field (in contrast with mapping of the horizontal and vertical meridia: Fox et al., 1987; Shipp et al., 1995; Hasnain et al., 1998), allowing new areas to be described (i.e. V3B, V7, V8; see chapter 3 and Hadjikhani et al., 1998; Smith et al., 1998; Tootell et al., 1998a,c; Mendola et al., 1999; Press et al., 2001; Tootell and Hadjikhani, 2001).

Precise delineation of visual areas has several implications. Firstly, it allows quantitative insights into the organization of the visual cortex, e.g. by estimating cortical magnification factors (Sereno et al., 1995) or receptive field size (Smith et al., 2001). The quantitative measures furthermore permit interspecies comparisons (Sereno, 1998; Van Essen et al., 2001; Brewer et al., 2002) and a detailed analysis of the pathological visual system (Baseler et al., 1999; Morland et al., 2001; Baseler et al., 2002). Secondly, it enhances the interpretability of studies of the visual system's functional properties by allowing activations to be localized in, or constrained by, functional areas rather than anatomical locations (Di Russo et al., 2001). Furthermore, it allows a volume-of-interest (VOI) analysis, i.e. averaging of the same volumes (regions) in the individual brains with the underlying assumption of a homogeneous processing within the volume. A VOI-analysis increases signal-to-noise ratios (SNR) beyond standard stereotaxic averaging (i.e. averaging of similar coordinates after normalization for differences in position, size and orientation Collins et al., 1994; Talairach and Tournoux, 1988), due to intra- and inter-subject averaging (averaging of voxels within the same cortical area and the same cortical area across subjects, respectively, see also section 5.3).

1.6 Thesis overview

This thesis attempts to increase our understanding of first- and second-order motion processing by studying the mechanisms in peripheral vision and investigating a possible cortical specialization. In the latter part, visual areas, which have been hypothezised to be involved (Wilson et al., 1992), have to be identified first. To this aim a novel methodology has been developed to identify early visual areas without explicit reconstruction of the cortical surface.

1.6.1 Peripheral second-order motion and optic flow

At present there is a debate over whether the peripheral field can process second-order motion. Some studies suggest that second-order motion perception is present in the periphery (Smith et al., 1994; Solomon and Sperling, 1995; Smith and Ledgeway, 1997; Wang et al., 1997; Gurnsey et al., 1998; Smith et al., 1998; Allen and Derrington, 2000), whereas other have suggested that it is absent, or at least impaired compared to first-order motion in normal observers (Pantle, 1992; McCarthy et al., 1994; Zanker, 1997). A similar, perhaps related, controversy exists on the involvement of second-order motion mechanisms in optic flow analysis (Ashida et al., 1997; Gurnsey et al., 1998; Allen and Derrington, 2000).

Central and peripheral vision differ in a number of ways relating to their functional specialization. For instance, peripheral vision is more sensitive to lower spatial frequencies (e.g. Robson and Graham, 1981; Westheimer, 1982; Pointer and Hess, 1989), higher temporal frequencies (e.g. Tyler, 1987; Allen and Hess, 1992), and plays a major role in optic flow analysis (e.g. Warren and Kurtz, 1992; Bardy et al., 1999; Habak et al., 2002). Thus, an examination of the peripheral sensitivity to second-order motion may shed light on the above described controversies and bear upon the possible role of second-order motion.

Chapter 2 addresses the issues described above using a novel global motion stimulus developed by Baker and Hess (1998). The results support the notion that second-order motion can be perceived in peripheral vision, and reveal a directional bias for second-order but not first-order motion. This bias is mediated by an almost complete absence of the ability to detect second-order motion towards the fovea. A possible explanation for this phenomenon is that it reflects a role for second-order motion mechanisms in optic flow analysis, where, due to our predominantly forward movements, motion towards the center plays a minor role.

1.6.2 Visual area identification

Wilson et al. (1992) hypothezised differential involvement of early visual cortical areas in processing of first- and second-order motion. Between subjects, the locations of these areas can vary substantially, even within a stereotaxic space, i.e. a standard coordinate system

where brains are normalized for differences in position, size and orientation (Collins et al., 1994; Talairach and Tournoux, 1988), as described by various studies (Stensaas et al., 1974; Steinmetz et al., 1990; Steinmetz and Seitz, 1991; Watson et al., 1993; Rademacher et al., 1993; Gilissen et al., 1995; Aine et al., 1996; Gilissen and Zilles, 1996; Roland et al., 1997; Hasnain et al., 1998; Amunts et al., 2000; Dumoulin et al., 2000; Hasnain et al., 2001). Thus localizing these areas would be a prerequisite to determining the cortical specializations of these areas in processing either kind of stimuli. Furthermore, cortical area delineation offers the possibility of a volume-of-interest (VOI) analysis (see section 1.5). A VOI analysis can improve the signal-to-noise (SNR) ratio, beyond stereotaxic analysis, due to intra- and inter-subject averaging (for VOI and stereotaxic analysis see also sections 1.5 & 5.3).

All current methodologies identifying early retinotopic visual areas rely on an explicit cortical surface reconstruction, some of which require manual interference at several stages (Sereno et al., 1995; DeYoe et al., 1996; Engel et al., 1997). Use of this surface reconstruction can cause problems because of errors in the reconstruction, and due to the different spatial resolutions of functional and anatomical data. Even if the surface is accurately reconstructed, there is a problem of how to resample the 3D data onto the 2D sheet, e.g. if a given voxel intersects twice with the surface, or not at all.

Chapter 3 presents a volumetric method to extract early visual areas without any manual interference or the need to reconstruct the cortical surface, thereby greatly simplifying the analysis. If the primary goal of the area identification is a VOI-analysis, VOIs are directly supplied without an intermediate surface reconstruction/resampling step. Validations are provided by simulations and a comparison to surface-based methods.

1.6.3 Cortical processing of first- and second-order motion

Models of motion detection, derived from psychophysical, electrophysiological and neurological studies, propose parallel mechanisms at separate cortical sites (Chubb and Sperling, 1988; Wilson et al., 1992; Clifford and Vaina, 1999). However, cortical specializations for these mechanisms remain controversial in both the neurological (Greenlee and Smith, 1997;

Vaina et al., 1999) and brain imaging literature (Smith et al., 1998; Somers et al., 1999).

Previous human brain imaging attempts have implicated a variety of areas in processing both first- and second-order stimuli (Smith et al., 1998; Somers et al., 1999), with some responding more to second-order motion (Smith et al., 1998). These previous studies employed different first- and second-order stimuli, as is common in psychophysical experiments where only certain stimulus attributes can be used for a given task (e.g. figure 1.1 C & D). However, in brain imaging experiments, differential responses can be elicited by *any* stimulus differences or distinct processing at *any* level, e.g. stimulus, task or attentional. In particular, second-order stimuli necessarily contain first-order carriers, whereas the first-order stimuli did not contain any second-order structure. Thus, the previous experiments may have been biased towards detecting responses to second-order attributes, which could explain why no cortical regions were selectively activated by first-order motion. In addition, attentional modulation can substantially affect neuroimaging responses (Beauchamp et al., 1997; O'Craven et al., 1997; Somers et al., 1999), and could potentially be a confounding factor in the interpretation of these previous results (Huk et al., 2001). Therefore a careful control of attention is a prerequisite 1) to avoid activations elicited by differential attentional requirements of the experimental conditions, and 2) to minimize attentional tracking proposed to occur in second-order motion (Seiffert and Cavanagh, 1998; Derrington and Ukkonen, 1999).

In chapter 4 an fMRI experiment is described using a setup controlling for the previously mentioned confounds using a single kind of stimulus, which is based on previous psychophysical experiments (Baker and Hess, 1998; Ledgeway and Hess, 2000; Dumoulin et al., 2001, chapter 2). Data are processed using standard stereotaxic-based methods and a VOI-based analysis on identified visual areas (Dumoulin et al., 2000, 2003, chapter 3). A cortical specialization is described both in the occipital and parietal lobe, in agreement with psychophysical studies, brain-lesion sites and computational models. Furthermore, the activation pattern is consistent with a role for the second-order mechanism in optic flow analysis as suggested in chapter 2.

Chapter 2

Centrifugal bias for second-order but not first-order motion

In this chapter (published in *J. Opt. Soc. Am. A*: Dumoulin et al., 2001), the presence of first- and second-order motion mechanisms in peripheral vision are assessed. This issue is controversial since some previous studies (Pantle, 1992; McCarthy et al., 1994; Zanker, 1997) have argued that the periphery is impaired in second-order motion perception, while others (Smith et al., 1994; Solomon and Sperling, 1995; Smith and Ledgeway, 1997; Wang et al., 1997; Gurnsey et al., 1998; Smith et al., 1998; Allen and Derrington, 2000) have argued the opposite. A second question invokes whether directional anisotropies exist for either first- or second-order mechanism.

Abstract

Limited-lifetime Gabor stimuli were used to assess both first and second-order motion in peripheral vision. Both first and second-order motion mechanisms were present at a 20 degree eccentricity. Second-order motion, unlike first-order, exhibits a bias for centrifugal motion, suggesting a role for the second-order mechanism in optic flow processing.

2.1 Introduction

First-order motion consists of moving luminance-defined attributes. Second-order motion, on the other hand, consists of moving patterns whose motion attributes are not luminance-defined, e.g. moving contrast or texture borders (Chubb and Sperling, 1988; Cavanagh and Mather, 1989). The detection of first and second-order motion is thought to be mediated by different mechanisms, i.e. a quasi-linear (first-order) and a non-linear (second-order) mechanism (Smith, 1994; Baker, 1999). A variety of different patterns are considered to be second-order stimuli and further distinctions in stimuli and mechanisms have been suggested (Lu and Sperling, 1995; Bex and Baker, 1999; Ledgeway and Hess, 2000).

Psychophysical evidence suggests that first and second-order motion are processed, at least initially, by distinct visual pathways and different mechanisms. Early non-linearities in visual processing introduce significant artifacts only at high contrasts and at higher temporal frequencies, as shown by Scott-Samuel and Georgeson (1999) and Holliday and Anderson (1994). Dissociation between first and second-order motion has been shown by several studies. For instance, Landy et al. (1991) found that even though second-order motion could provide depth clues, first-order motion detectors are the primary input to the kinetic depth system. Harris and Smith (1992) found that only first-order and not second-order motion elicits optokinetic nystagmus. Further evidence for separate mechanisms is provided by the studies of Mather and West (1993) and Ledgeway and Smith (1994a), which showed that direction-discrimination fails when first and second-order frames have to be integrated to detect motion. Nishida et al. (1997) found no cross-adaptation between first and second-order motion, and Scott-Samuel and Smith (2000) found a lack of cancellation between directionally opposed first and second-order motion signals. First and second-order motion also differ in their ability to induce motion after effects (MAEs). Second-order motion stimuli produce no MAEs on a static background, but may induce MAEs on a flickering background (Mather, 1991; Ledgeway and Smith, 1994b; Nishida et al., 1994; Gurnsey et al., 1998). Furthermore, aging has been shown to have a different effect on first and second-order processing (Habak and Faubert, 2000). Brain lesion studies indicate that each kind of motion can be affected

separately while leaving the other intact (Vaina and Cowey, 1996; Vaina et al., 1998, 1999; Greenlee and Smith, 1997) providing a neuropsychological "double dissociation". Using electrophysiological techniques neurons have been found to respond to second-order stimuli in cat area 17 and 18 (Zhou and Baker, 1993, 1994, 1996; Mareschal and Baker, 1998a,b, 1999), with spatial and temporal frequency tuning which was different for first and second-order stimuli. Neurons in primate extra-striate cortex have also been shown to respond to second-order motion (Albright, 1992; Olavarria et al., 1992; Geesaman and Andersen, 1996; O'Keefe and Movshon, 1998).

Using a single stimulus constructed of Gabor micropattern arrays, first and second-order motion mechanisms can be dissociated by varying several stimulus parameters. The behavior of the first-order motion mechanism can be described by a spatio-temporal energy model (Adelson and Bergen, 1985), which for Gabor stimuli produces motion signals related to the carrier, rather than the envelope, of the micropatterns (Boulton and Baker, 1991; Clifford et al., 1998; Baker and Hess, 1998). The envelope of the Gabor micropatterns drives the second-order motion mechanism. Consequently changing the orientation, phase or frequency of the carrier on alternate frames leaves second-order motion intact but eliminates first-order direction-discrimination (Ledgeway and Hess, 2000; Baker and Hess, 1998; Boulton and Baker, 1994). Furthermore, temporal intervals (Boulton and Baker, 1994, 1993a; Bex and Baker, 1999), micropattern density (Clifford et al., 1998; Boulton and Baker, 1994, 1993b), percentage of distractor elements (Baker and Hess, 1998; Bex and Baker, 1997) and displacement (Ledgeway and Hess, 2000; Baker and Hess, 1998) can be used to dissociate the two kinds of motion.

Previous studies have differed over the presence of second-order motion processing in the periphery. Pantle (1992) reported immobility for a range of second-order stimuli in peripheral but not central vision. Similar results were reported by McCarthy et al. (1994) and Zanker (1997) for two specific kinds of second-order motion, i.e. flicker gratings and form-from-motion (θ motion) respectively. Even though the direction of motion could not be perceived, these stimuli could be detected in the periphery (Pantle, 1992; McCarthy et al., 1994; Zanker, 1997). Studies using contrast-defined second-order motion, however, suggest

that second-order motion can be perceived in peripheral vision under the appropriate spatio-temporal conditions (Gurnsey et al., 1998; Smith et al., 1994; Solomon and Sperling, 1995; Smith and Ledgeway, 1997; Wang et al., 1997).

Due to forward movement of ourselves relative to the world, we are more exposed to expanding patterns (Gibson, 1954). These optic flow patterns have been implicated in the guiding and regulation of the organism's own motion in relation to the environment (Nakayama, 1985). Therefore a higher sensitivity to expanding optic flow patterns would not be unexpected. Thus in peripheral vision the sensitivity of motion perception in different directions does not necessarily have to be equal. Indeed several studies have indicated anisotropies and inhomogeneities of the detection of the direction of motion using a variety of techniques (Georgeson and Harris, 1978; Ball and Sekuler, 1980; Mateeff and Hohnsbein, 1988; Fahle and Wehrhahn, 1991; Mateeff et al., 1991b,a; Van de Grind et al., 1992; Edwards and Badcock, 1993; Raymond, 1994; Ohtani and Ejima, 1997; Gros et al., 1998). These studies have revealed several anisotropies in the peripheral field, one of which is a difference in the perception of centrifugal (away from the center, expanding) and centripetal (towards the center, contracting) motion.

Using reaction-times to motion onset of an 8 deg. diameter random dot field, Ball and Sekuler (1980) found faster reaction times for the onset of centrifugal motion. Mateeff and Hohnsbein (1988); Mateeff et al. (1991b,a) reported shorter reaction times for a moving single dot if it moved towards the fovea (centripetal). They, however, confirmed the results of Ball and Sekuler (1980) when using larger, textured stimuli. Thus the bias found may depend on the stimulus, suggesting different underlying mechanisms.

Van de Grind et al. (1992), who measured signal-to-noise ratio (SNR) thresholds of random pixel arrays, found inhomogeneities and anisotropies throughout the visual field, but did not report either a strong centripetal or centrifugal preference. Measuring motion-detection coherence thresholds using radially expanding or contracting global-dot-motion stimuli (size 0 to 12 deg), Edwards and Badcock (1993) found lower thresholds for centripetal motion. An increase in eccentricity (16 to 24 deg), however, resulted in either a reduction or a loss of the observed centripetal bias. Raymond (1994), measuring the detection

of global motion in random dot kinematograms, also found lower thresholds for centripetal motion measuring the detection of global motion in random dot kinematograms (up to 12.5 deg). She, however, did not find a reduced centripetal bias with increasing eccentricity.

Anisotropies have also been indicated using motion-after-effects, which may have a similar basis. Larger motion aftereffects were found for apparent centrifugal motion, after adaptation to centripetal motion, than for apparent centripetal motion (Bakan and Mizusawa, 1993; Scott et al., 1966).

Georgeson and Harris (1978) reported an apparent centrifugal drift with counter-phase gratings. This result suggests that even in incoherently moving patterns with no net motion, e.g. random dot patterns, an apparent bias might be present.

Albright (1989) showed that more neurons in macaque middle temporal area (MT or V5) prefer motion in directions away from the center of gaze (centrifugal) than towards it (centripetal). This bias increased as a function of eccentricity.

The studies previously described do not distinguish between different motion mechanisms, i.e. first and second-order, which might underlie the perceptual judgements or the responses of neurons. Different mechanisms might have different functions and processes involved in optic flow processing might mediate a centrifugal bias whereas others might not. Investigating a centrifugal or centripetal bias of different motions might shed some light on the heterogeneity of previous results and on the functions of the mechanisms involved.

Researchers using stimuli constructed of arrays of Gabor patterns have identified distinct first and a second-order mechanisms underlying the processing of motion stimuli in central vision (Ledgeway and Hess, 2000; Clifford et al., 1998; Baker and Hess, 1998; Boulton and Baker, 1994, 1993a,b; Bex and Baker, 1997). The purpose of this study was i) to identify and characterize both first and second-order mechanisms in peripheral vision using an identical paradigm to Baker and Hess (1998), ii) to identify anisotropies related to centrifugal/centripetal biases in the detection of first and/or second-order motion.

2.2 Experiment 1

The purpose of the first experiment was to assess the relative contributions of first and second-order motion for a stochastic Gabor kinomatogram stimulus presented in the peripheral visual field.

2.2.1 Methods

For a more detailed description of the stimuli see Baker and Hess (1998). The visual stimuli were generated using a VSG 2/2 graphics card (Cambridge Research Systems), and displayed on a NEC XP17 monitor refreshed at 160 Hz. The raster consisted of 512x379 pixels with a pixel-size of 0.6mm. At a viewing distance of 57cm the pixels subtended 0.06 deg and the field size was 30.72 x 22.74 deg. The monitor intensity non-linearity was measured using a photometer (United Detector Technology, S370), and corrected by a method of Pelli and Zhang (1991) using appropriate functions from the VideoToolBox software package (Pelli, 1997). An ISR Video Attenuator (Institute for Sensory Research, Syracuse University, New York, U.S.A.) was used to resistively add the red, green and blue video signals to produce a monochrome signal having a higher intensity resolution (Pelli and Zhang, 1991). The monitor was operated using its green video input only.

The stimuli consisted of linearly added Gabor patterns each consisting of a 1D sinewave carrier enclosed by a 2D Gaussian envelope (see equation 2.1).

$$L(x,y) = L_0 \left[1 + C^{-\left(\frac{x^2}{2\sigma_x^2} + \frac{y^2}{2\sigma_y^2}\right)} \sin\left(\frac{2\pi x}{\lambda}\right) \right] \tag{2.1}$$

The whole stimuli were spatially scaled by a factor of 2 when presented in peripheral vision to compensate for the difference in central and peripheral acuity. Unless stated otherwise, the orientation of the Gabors was perpendicular to their direction of motion, the spatial wavelength (λ) was 1.43 deg (0.715 deg for central vision), the envelope size (σ) was $\frac{3}{4}\lambda$, the contrast (C) was 30% and the mean luminance (L_0) was 28.6 cd/m^2.

The Gabors were placed with respect to a grid with each Gabor having a (x and y) offset by a random amount with respect to their respective grid positions. This method pro-

vided a good density uniformity and prevented overlap between the Gabor patterns which could cause intensity saturation.

A Gabor position was maintained for 100ms (16 frames) before being re-plotted. Each stimulus presentation was 1000ms. Two kinds of Gabor micropatterns were used, which only differed in their motion trajectories. One set of micropatterns moved coherently by a fixed amount, the others were randomly jittered around their respective grid positions. The average probability of a micropattern moving coherently was determined by the coherence level. The Gabors had a limited-lifetime (400ms or 4 exposures), after which they were re-plotted at their respective grid positions, and it was freshly determined whether each would move coherently or not for the next set of displacements.

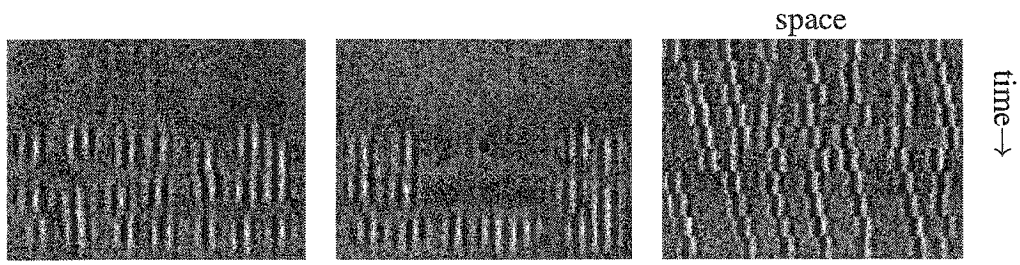

Figure 2.1: Spatial layouts (A & B) and a space-time diagram (C) of the visual stimuli. (A) Stimulus configuration for the periphery, the viewing distance was 57cm. (B) Stimulus used for central vision; the viewing distance was 114cm, i.e. the size of the stimulus was 50% of the stimulus presented in peripheral vision (A). (C) Space-time diagram along a horizontal transect of the stimulus. In this example the coherence was 50%, and the lifetime 4, and the spatial displacement $\frac{1}{4}\lambda$ rightwards.

The stimulus (see figure 2.1 A) was presented in the lower visual field with the center of the micropattern grid at a 20 deg eccentricity (eccentricity range: 14 to 26 deg). The stimulus used for central stimulation is depicted in 2.1 B; micropatterns falling in a central circular zone of radius 3.8 deg were not plotted, to avoid attentional tracking which has been shown to operate in the fovea (Cavanagh, 1992). The direction of motion of the Gabor patterns was either to the left or to the right. Percent errors in a forced-choice direction-

discrimination task were measured as a function of spatial displacement.

2.2.2 Results

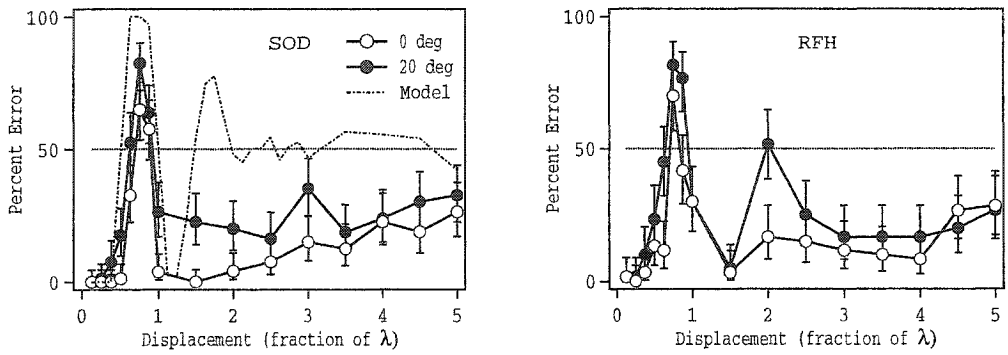

Figure 2.2: The psychometric functions for central vision (open circles) and at a 20 deg eccentricity (closed circles) for two subjects. For subject SOD the results of a linear filter model (Adelson and Bergen, 1985) are shown (dash-dotted line). The percentage errors in direction discrimination are plotted as a function of the spatial displacement of the Gabor micropatterns. The error bars indicate 95% confidence limits, n=80 (SOD) and n=60 (RFH). For smaller displacements the data follows the prediction of the model, however at larger displacements the model fails to predict motion detection. Baker and Hess (1998) suggested that motion perception in this stimulus is carried out by a first-order mechanism responding to the carrier frequency at small displacements and a second-order mechanism responding to the contrast envelopes at large displacements.

The resulting psychometric functions (see figure 2.2) showed an errorless performance at small displacements (around $\frac{1}{4}\lambda$), rising steeply to a reversal, i.e. high error percentages at $\frac{3}{4}\lambda$, then falling back to a relatively stable percent error level for a large range of displacements. The cyclic performance at smaller displacements ($< \lambda$) is predicted by a spatio-temporal energy model (Adelson and Bergen, 1985), which produces responses to the carrier, rather than the envelope, of the micropatterns. At larger displacements ($> \lambda$) the model fails to predict motion detection (see figure 2.2). Baker and Hess (1998) suggested that the

performance of the subjects at these larger displacements is mediated by a second-order mechanism responding to the contrast envelopes of the micropatterns. Further evidence that these distinct first and second-order mechanisms are underlying the perceptual judgements of this stimulus was presented by previous studies (Baker and Hess, 1998; Ledgeway and Hess, 2000).

The psychometric function for peripheral vision (figure 2.2, closed symbols) is similar to that of central vision (open symbols), except for larger error rates at larger displacements. The larger error percentages suggest, at this eccentricity, a significant although weaker contribution of the second-order mechanism.

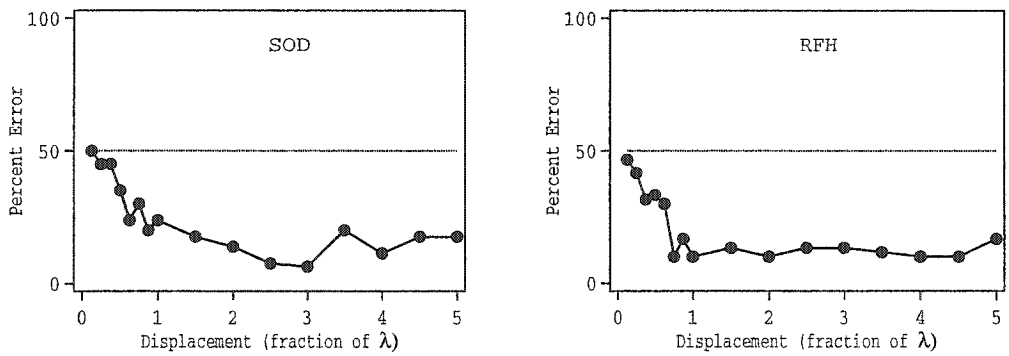

Figure 2.3: The psychometric functions at a 20 deg eccentricity for two subjects. The percentage errors in direction discrimination are plotted as a function of the spatial displacements of the Gabor patterns, n=80 (SOD) and n=60 (RFH). The carrier orientation of the Gabors was flipped by 90 deg on alternate exposures, thus eliminating the contribution of the first-order mechanism.

To further test the idea that a second-order mechanism is underlying the perceptual judgements at larger displacements, the carrier orientation was changed by 90 deg on alternate exposures. Changing orientations eliminates the perception of the direction of first-order motion, thus isolating the second-order motion (Boulton and Baker, 1994; Baker and Hess, 1998; Ledgeway and Hess, 2000). The results are plotted in figure 2.3. The cyclic performance at smaller displacements is abolished, though the performance at larger dis-

placements remains similar to figure 2.2, supporting the idea that changing the carrier orientation isolates the second-order mechanism. These data further illustrate the presence of a second-order mechanism in peripheral vision. Other manipulations of the stimulus variables verified the findings of Baker and Hess (1998), and are not reported.

2.2.3 Conclusion

Both first and second-order can be processed in peripheral vision using limited-lifetime random Gabor patterns. This supports the results of previous studies indicating that contrast-defined second-order motion can be perceived in peripheral vision (Smith et al., 1994; Solomon and Sperling, 1995; Smith and Ledgeway, 1997; Wang et al., 1997; Gurnsey et al., 1998), using a different kind of stimulus.

2.3 Experiment 2

Initial pilot experiments indicated large perceptual differences between centrifugal and centripetal direction of motion for second-order motion. While centrifugal motion was perceived as "normal" motion, centripetal motion, on the other hand, seemed perceptually similar to incoherent motion with no net directional component. The purpose of the second experiment was to assess centrifugal/centripetal directional anisotropies for both first and second-order motion in peripheral vision.

2.3.1 Methods

The methods were very similar to those for the first experiment. The stimuli (see figure 2.4) were presented at a nominal 20 deg eccentricity in either the left, right, upper or lower visual field. The stimulus area was changed to allow for equal motion trajectories in all four directions. Two displacements were used, $\frac{1}{4}\lambda$ and 3.5λ, to isolate the first and second-order mechanism, respectively. Previous results (see figures 2.2, 2.3, Baker and Hess (1998) and Ledgeway and Hess (2000)) show that the responses at these displacements are dominated

by the first and second-order mechanism, respectively.

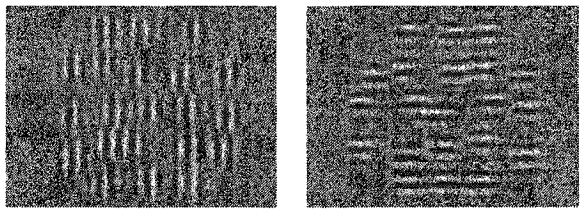

(a) (b)

Figure 2.4: Spatial layout of the visual stimuli. Stimulus configuration for horizontal motion (A) and vertical motion (B). The stimuli were presented with the center at a 20 deg eccentricity from the fixation point (ranging from 11 to 29 deg) in the left, right, upper and lower visual field.

In pilot studies at this eccentricity a perceptual difference between centrifugal and centripetal motion was noticed. Centrifugal motion was vividly perceived, but centripetal motion appeared incoherent with no net direction motion component. This anisotropy provided a cue in a direction-discrimination task, i.e. when subjects do not perceive any motion away from the center, they could conclude that it is going in the other direction. To eliminate this possibility, a two-interval two-alternative forced-choice task was designed, i.e. two judgements were required from the subject. Each trial consisted two intervals. One of these intervals contained the actual stimulus of a given coherence, the other a 0% coherent stimulus. The coherent stimulus could contain any of seven coherence levels (including 0% coherence, providing "catch trials" to reveal any internal or observer bias). In the first forced-choice judgement, subjects indicated which interval contained the coherent moving stimulus. In each session, the direction of motion was either vertical (up-down) or horizontal (left-right). In the second forced-choice judgement, the subjects indicated the direction of motion, i.e. in a session where the direction of motion was vertical, an up-down discrimination was required, and a left-right discrimination was required in a session where the motion-direction was horizontal. Two displacements, each varying across the seven coherence levels, were interleaved in each session. Due to the two judgements which were required in each trial, chance level is at 75% errors.

Two experienced psychophysical observers were used as subjects, one of whom was naive to the purpose of the study. The subjects used their dominant (right) eyes, they were instructed to fixate at a provided fixation-point. Both observers had normal or corrected to normal visual acuity.

2.3.2 Results

Both first-order ($\frac{1}{4}\lambda$) and second-order (3.5λ) motion stimuli were interleaved in the same session. Furthermore, a 0% coherence trial, was interleaved to assess any internal, or observer, "bias". In the 0% coherence trial, both first and second-order motion were present without a net motion direction. For the coherence judgment no bias was found (see figure 2.5 A & B). In figure 2.5 C & D the judged directions, averaged over all four positions, for centrifugal, centripetal and clockwise (90 deg) and counterclockwise (270 deg), are plotted just for the 0% coherence trials. Both observers chose centrifugal motion significantly more than centripetal motion, even though no net motion was present. This result is consistent with the study of Georgeson and Harris (1978), who reported an apparent centrifugal drift with counter-phase gratings.

The internal bias found in figure 2.5 predicts anisotropies in motion-direction judgements which would be a function of observer performance. Thus on the basis of the internal bias alone anisotropies in either motion mechanism would be predicted as observer performance decreases. These anisotropies would be a function of observer performance, no anisotropies would be found at 0% error and a maximal anisotropy reflecting the internal bias at 75% error (chance level). The relationship between the internal bias and observer performance relates to signal-to-noise within the observer. Therefore we assume a linear relationship between the internal bias and the subject's performance:

$$PE_b = C_b \frac{PE}{C}, \tag{2.2}$$

i.e. PE is what the percent error should be if no bias was present. PE_b represents the percent error predicted on the basis of the internal bias, C is chance level (75% in this case) and C_b is the error rate which is produced by the subject based on the internal preference, as measured

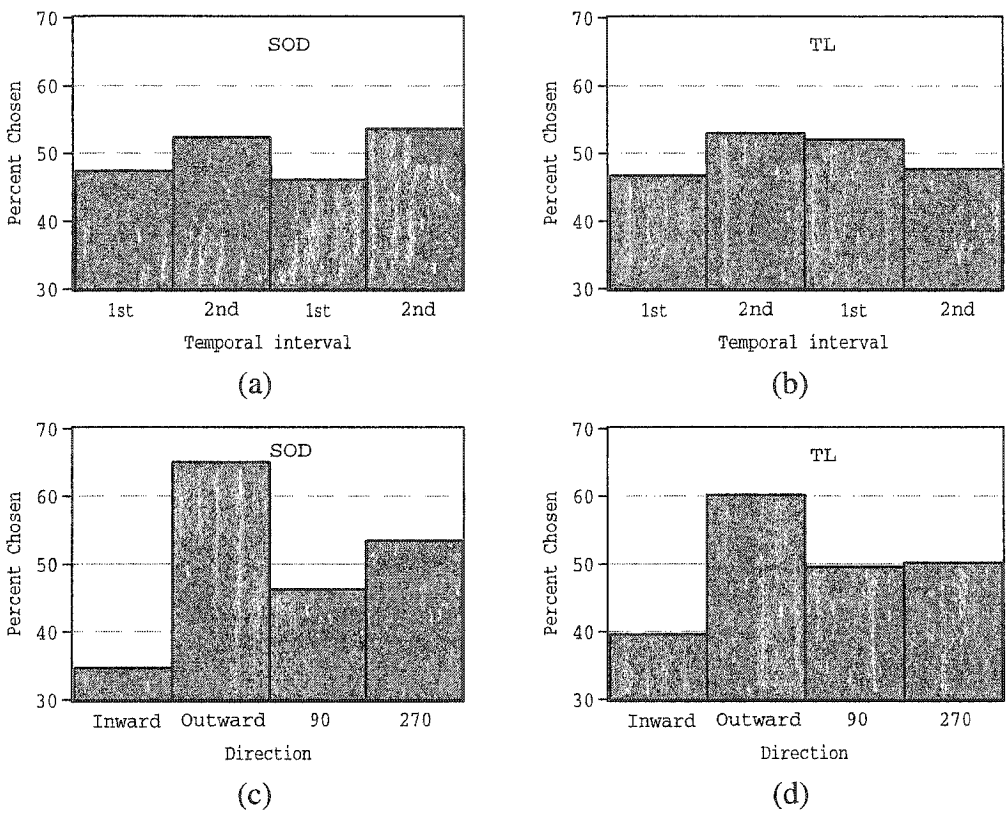

Figure 2.5: A 0% coherence trial was intermixed in the trials, i.e. both presentations were of 0% coherence. The data shown here is the average of all four positions. In the first two graphs (A and B) the relative intervals judged to contain the coherent stimulus are shown for two subjects. They are plotted for the 1st or 2nd interval when the stimulus was moving centrifugal/centripetal (first two bars) or clockwise/counterclockwise (last two bars). No clear preference is present. In C and D the judgements of direction of motion are shown, revealing internal biases for centrifugal versus centripetal motion for two subjects (n=640 (SOD) and n=320 (TL)).

in figure 2.5. The chance level is 75% because the percent errors are a combination of the detection and discrimination tasks.

The data collected in each of the four positions in the visual field are shown in figure 2.6 (vertical motion) and 2.7 (horizontal motion). All these figures show a rising error rate with declining coherences. The data of perceptual judgements to the second-order motion

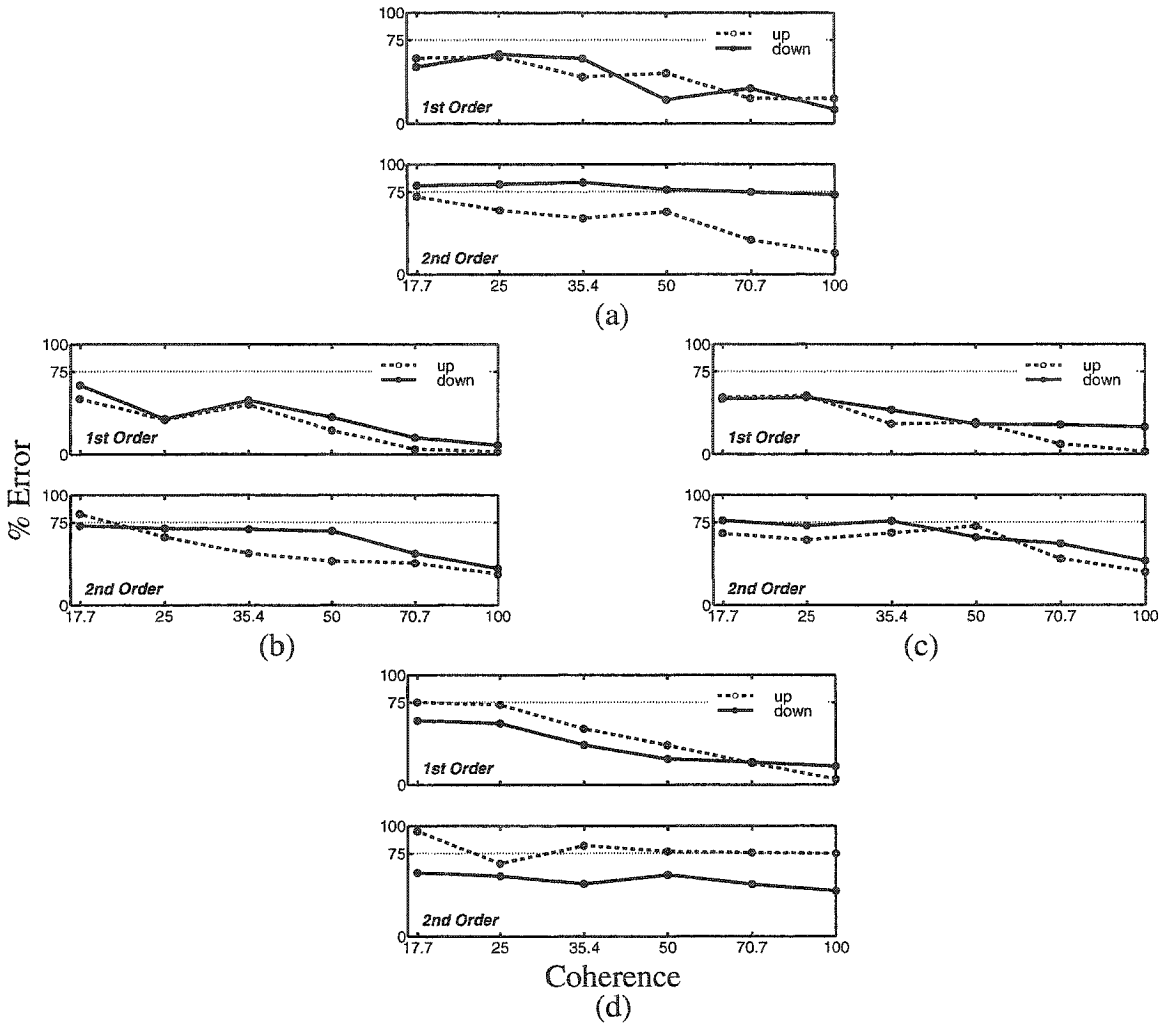

Figure 2.6: (a) Upper visual field, (b) left visual field, (c) right visual field, and (d) lower visual field. The psychometric functions for vertical motion at four different positions in the visual field for one subject (n=40). Percentage errors in a coherence and direction discrimination task are plotted as a function of coherence for both first (top graph-parts) and second-order (bottom graph-parts) motion. Data of motion in the upward direction is represented with open circles and dashed lines. The downward motion results are plotted with closed circles and solid lines.

stimuli show higher error percentages than to the first-order stimuli at comparable coherences, consistent with the data in figure 2.2.

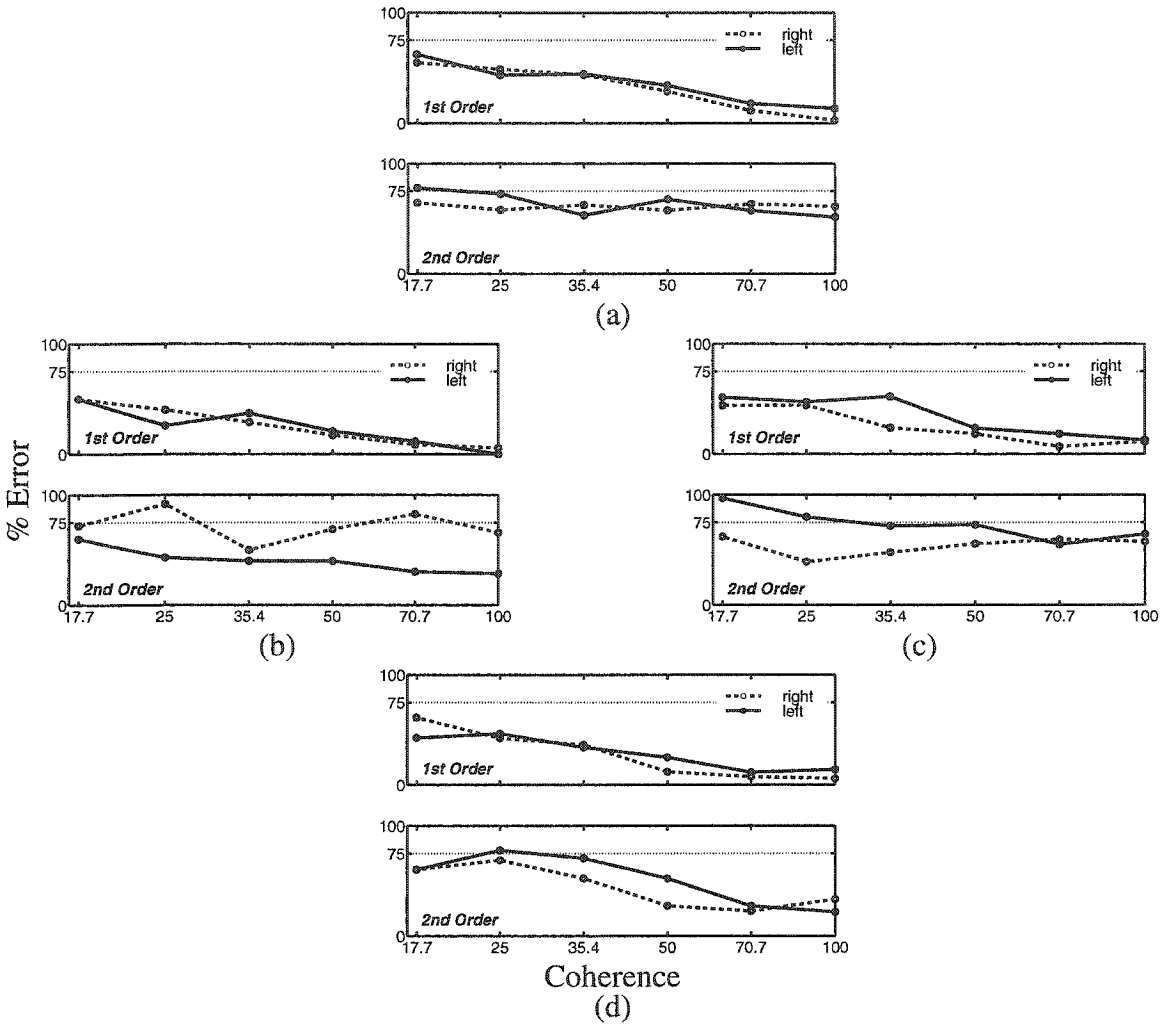

Figure 2.7: Same as figure 2.6, but for horizontal motion.

For vertical motion (figure 2.6), the second-order data show different error rates measured in the upper and lower visual fields (A,D), but not for the left and right fields (B,C). A similar result is present for the horizontal motion directions in the left and right field (figure 2.7 B,C), but not for the upper and lower fields (A,D). In both cases no similar systematic differences are seen for first-order motion. All these differences for second-order motion are consistent with a common centrifugal/centripetal organization. To reveal any centripetal/centrifugal anisotropies, the data from the different parts of the visual field (see figures 2.6 and 2.7) were selectively averaged based on their directions relative to the fixation

point, e.g. data for centrifugal motion directions in the four visual positions were averaged. Similarly the data in the four positions for centripetal, clockwise and counterclockwise motion were averaged. The data shown in figure 2.8 is the resultant of different parts of the visual field, averaged based on their directions relative to the fixation point and thus more clearly depict the data of figures 2.6 and 2.7.

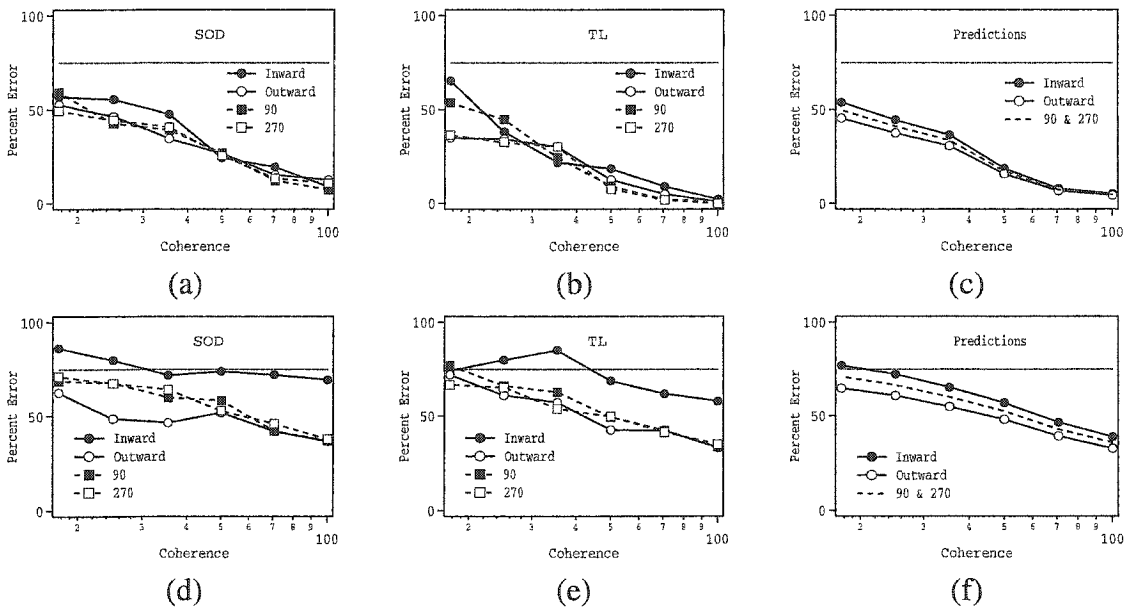

Figure 2.8: The psychometric functions at a 20 deg eccentricity for two subjects, and predictions based on the internal bias. Percentage errors in a coherence and direction discrimination task are plotted as a function of coherence for first-order motion (A, B & C) and second-order motion (D, E & F). Standard errors of the mean of each point were smaller than the size of the symbols (n=160 and n=80 for observers SOD and TL, respectively). Centrifugal motion is represented with a solid line and open circles, centripetal motion with a solid line and filled circles, clockwise and counterclockwise motion are represented with a dashed line and open and solid squares, respectively. In C and F the dashed line represents the average of the clockwise and counterclockwise percent errors of observers TL and SOD. The percent errors in C and F for centripetal and centrifugal motion are calculated according to equation 2.2. The thin line represents chance performance (75%).

The left and the middle columns of the resulting figure (2.8) shows the percent error as a function of coherence for first (A-B) and second-order (D-E) motion. In each graph the data for four different directions relative to the fixation point are plotted separately, i.e. centripetal, centrifugal, clockwise (90 deg) and counterclockwise (270 deg) around the fixation point. The last two directions served as a control, since on they would be unlikely to show a difference. In this figure are also plotted (C & F) the anisotropies predicted purely from the internal bias (equation 2.2). The input to the equation (PE) was the measured value of average percent error for clockwise and counterclockwise motion for both observers. C_b was estimated from figure 2.5, C was 75%.

All figures show a rising error rate with declining coherence. The data of the second-order motion stimuli show higher error rates than for the first-order stimuli at comparable coherences consistent with the data in figure 2.2. The perceptual judgements to the first-order stimuli reaches error rates at lower coherence levels similar to the detection of second-order motion at higher coherence levels.

Figure 2.8 (A & B) does not show any large or systematic differences between the different motion directions for first-order motion, or a large deviation from the anisotropies predicted by the internal bias (C). Thus we conclude that no measurable first-order anisotropies or bias was evident.

For perceptual judgements to second-order motion (figure 2.8 D & E), however, a centrifugal bias was found across a range of coherence levels. It could be argued that this anisotropy is mediated by the internal bias revealed in figure 2.5. However, this anisotropy was larger than predicted by the internal bias alone (figure 2.8 F). Furthermore, if the second-order anisotropy was purely due to the internal bias then the anisotropies should vary as a function of subjects' performance (and thus also with coherence). Figure 2.8 D & E show that the anisotropies are present over a large range of coherences and the anisotropies do not seem to vary as a function of the coherence. Therefore we would argue that the internal bias cannot explain the second-order anisotropy. Together with the absence of an anisotropy in the responses to first-order stimuli even at comparable error rates, figure 2.8 rather suggests the opposite, i.e. the internal bias, found at 0% coherence, could be largely mediated by an

anisotropy of the second-order motion mechanism.

The first and second-order mechanism were selectively activated by the same stimulus but with different displacements. Motion at these displacements with the same temporal properties is thus at different effective velocities. The difference between first and second-order motion might be due to this velocity difference rather than due to the two types of motions per se. If this is so then the bias found would be expected to disappear if the two velocities were similar.

Figure 2.9 A and B show the perceptual judgements to second-order motion at a large range of displacements. The orientation of the Gabors were changed by 90 deg on alternative exposures to eliminate the contribution of first-order motion to the perceptual judgements (Ledgeway and Hess, 2000; Baker and Hess, 1998; Boulton and Baker, 1994). The total displacements between alternate (like-orientations) exposures were multiples of $\frac{1}{2}\lambda$, so the direction of motion could not be determined by a first-order mechanism correlating every other exposure. The centrifugal bias is present at all displacements, suggesting that the anisotropies of the second-order mechanism is not velocity dependent. At the velocity of the first-order motion stimuli, i.e. a displacement of $\frac{1}{4}\lambda$, the responses to second-order motion reaches D_{min}, i.e. the minimal displacement needed to detect motion (Braddick, 1974; Nakayama, 1981; Baker and Braddick, 1985). In order to bring the first-order motion into the velocity range of the second-order stimuli, a control experiment was performed at a lower spatial frequency (λ of 3 deg) and with exposure times of 50ms (figure 2.9 C & D). This manipulation increased the velocity four-fold. The σ to λ ratio of the micropatterns and the relative density of the micropattern distribution was kept constant. The coherence was decreased to 50% to achieve comparable performance (percent errors). Two displacements were used, $\frac{1}{4}$and $\frac{3}{8}\lambda$. These displacements are plotted in figure 2.9 B at their corresponding velocities (displacements of 1 and $1\frac{1}{2}\lambda$). No anisotropies were seen similar in size to those for the second-order mechanism. Therefore we conclude that the difference between first and second-order motion, and the anisotropies of the second-order stimuli, are not velocity dependent.

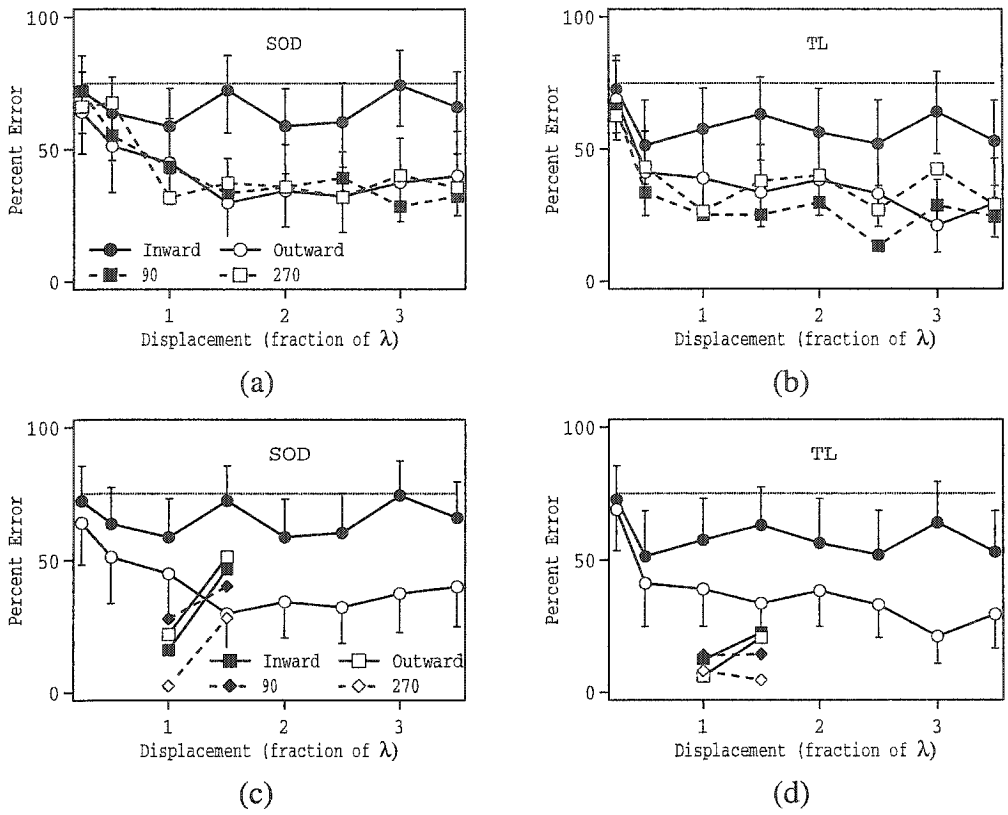

Figure 2.9: Percent error in a coherence and direction discrimination task is plotted as a function of the displacement size for two subjects (n=40 for observer SOD). (A & B) The orientation of the Gabors were changed by 90 deg on alternate exposures thus eliminating contributions from the first-order mechanism. Centrifugal motion is represented with a solid line and open circles, centripetal motion with a solid line and filled circles, and clockwise and counterclockwise motion are represented with a dashed line and open and solid squares, respectively. The errorbars indicate the upper or lower part of the 95% confidence interval for centripetal and centrifugal motion. The dotted line represents chance performance (75%). (C & D) The same data as figure A & B are plotted for centripetal and centrifugal motion, and the results of a first order control experiment at comparable velocities are plotted as well. Centrifugal and centripetal first-order motion are represented as solid lines with open and closed squares respectively. Clockwise and counterclockwise are shown as dashed lines with open and closed diamonds, respectively.

2.3.3 Conclusion

Second-order motion, unlike first-order, exhibits a bias for centrifugal directions, suggesting a role for the second-order mechanism in optic flow processing and providing a dissociation between first and second-order motion processing.

2.4 General discussion

Using contrast-defined second-order motion a variety of studies suggest that second-order motion can be perceived in peripheral vision under the appropriate spatio-temporal conditions (Smith et al., 1994; Solomon and Sperling, 1995; Smith and Ledgeway, 1997; Wang et al., 1997; Gurnsey et al., 1998). In our first experiment we confirmed these findings using limited-lifetime Gabor patterns which allowed a comparison of first and second-order motion with the same stimulus. A significant though weaker contribution of the second-order motion mechanism was found.

In the second experiment a centrifugal bias was found for second-order but not first-order motion mechanisms. Since the performance to centrifugal motion is similar to rotational motion directions, this centrifugal bias seems to be mediated by a reduced sensitivity to centripetal motion rather than a elevated sensitivity to centrifugal motion. Optic flow patterns due to self motion with independent head and eye movement contain both translational and rotational components (Harris, 1994b,a; Hildreth and Royden, 1998). The second-order mechanism is best at detecting the centrifugal and rotational components, thus the anisotropies described would suggest a role for the second-order system in optic flow processing. This result is in agreement with the results of Gurnsey et al. (1998) who found a contribution of first and second-order motion mechanisms to vection (illusory self motion induced by image flow).

The trials at 0% coherence indicate that a centrifugal bias exists when no net first or second-order motion is present. This is consistent with the results of Georgeson and Harris (1978), though they used a pure first-order stimulus. The intrinsic bias implies that a

centrifugal bias would be more prominent at lower coherence levels. At similar coherence levels the first-order motion mechanism do not show such a bias whereas the second-order one does. Therefore the result indicates that the intrinsic bias may be largely mediated by the second-order motion mechanism.

Edwards and Badcock (1993) and Raymond (1994) both found a centripetal preference using random dot stimuli, a result opposite to the one described here. Raymond (1994) collected data at smaller eccentricities (up to 12.5 deg). Edwards and Badcock (1993) collected data at similar eccentricities to this study (16 to 24 deg), and reported a decline or loss of the observed centripetal bias. Thus the difference between their results and the data described here might be related to the eccentricity at which the data is collected. Neither study distinguishes between first and second-order motion, however, that does not explain the opposite bias found. The difference in results might be explained based on the internal bias described by Georgeson and Harris (1978) and this study. Edwards and Badcock (1993) and Raymond (1994) measured detection thresholds in a temporal coherence-judgement two-alternative forced-choice method, i.e. the minimal amount of motion needed to detect global motion in 79% and 71%, respectively, of the cases. The control interval contained incoherent motion. The internal centrifugal bias described by Georgeson and Harris (1978) and in this paper is present in incoherent motion. Therefore, the difference in perceived motion of low-coherence centrifugal movement and incoherent motion, with centrifugal bias, is less than the difference between centripetal motion and incoherent motion. Thus the difference in perceived motion, or motion energy, would result in lower thresholds for identifying coherent centripetal motion. Therefore lower thresholds centripetal motion might be elicited by a centrifugal bias. Thus, even though they describe lower thresholds for centripetal motion, these results do not necessarily disagree with our data.

Seiffert and Cavanagh (1998) suggested that, for their stimulus, second-order motion is detected by a mechanism tracking the change of position of features over time. Ledgeway and Hess (2000) demonstrated that two mechanisms underlie the perception of the kind of second-order motion described here. They implicated that both low-level and high-level second-order mechanisms, such as feature tracking, mediate the perceptual judgements. We

cannot say at present which of these two second-order mechanisms is responsible for the reported bias.

To conclude, we have used limited-lifetime Gabor stimuli to identify both first and second-order mechanisms in peripheral vision. Anistropies in motion directions were found for second but not first-order motion. The second-order motion mechanism, but not the first-order one, mediates a bias for centrifugal motion. In ecological conditions we are more exposed to centrifugal (expanding) flow patterns due to our forward motion relative to the world. The second-order centrifugal bias suggests a role for the second-order mechanism in optic flow processing.

Chapter 3

Automatic volumetric segmentation of human visual retinotopic cortex

In the previous chapter a psychophysical experiment was described, which contributed evidence for two motion mechanisms by reporting a divergent behavior in peripheral vision. A cortical specialization for these mechanisms has been proposed, involving early visual areas, but remains controversial. An important prerequisite to any functional assessment (e.g. next chapter) is the accurate identification and delineation of early visual areas. Here a novel methodology is presented to automatically segment early visual areas ("In Press" in *NeuroImage*: Dumoulin et al., 2003), which will be used in subsequent parts of this thesis (chapter 4).

Abstract

Previous identification of early visual cortical areas in humans with phase-encoded retinotopic mapping techniques have relied on an accurate cortical surface reconstruction. Here a 3D retinotopic mapping technique is demonstrated that does not require a reconstruction of the cortical surface. The visual field sign identification is completely automatic and the method directly supplies volumes for a region-of-interest analysis, facilitating the application of cortical mapping to a wider population. A validation of the method is provided by simulations and comparison to cortical surface-based methodology.

3.1 Introduction

The cortex contains many separate regions that are involved in different processes and their localization aids functional studies of cortical neuronal mechanisms. For example, the localization of cortical areas allow the possibility of using a volume (or region) of interest (VOI/ROI) analysis and thereby improving signal-to-noise ratio (SNR) due to intra- and inter-subject averaging. This offers an advantage over previous stereotaxic based averaging methods, by ensuring that voxels are averaged only within the same functional visual areas.

All early visual cortical areas contain a complete retinotopic map of the visual field (see figure 3.1 for a schematic diagram). These areas can be distinguished on the basis of a number of differences in their retinotopy. For example, the visual field representation can be mirror or non-mirror symmetric (Sereno et al., 1994, 1995), and the borders can occur at either the horizontal or vertical meridia (Holmes, 1945; Fox et al., 1987; Felleman and Van Essen, 1991; Horton and Hoyt, 1991; Rosa et al., 1993; Shipp et al., 1995; DeYoe et al., 1996; Engel et al., 1997; Hasnain et al., 1998).

A method that has been developed to take advantage of the retinotopic organization of early visual areas is phase-encoded retinotopic mapping. This method was made possible by the finding that time-delays (or phase-lags) of the cortical activity elicited by slowly expanding circular patterns depend on visual field location (Engel et al., 1994). Sereno et al. (1995) were the first to map visual areas using this phase-encoded method and both expanding rings and rotating wedge stimuli. By combining these maps on a cortical surface, Sereno et al. (1995) were able provide an objective criterion of the visual borders by the identification of visual field signs of areas V1, V2, V3, VP and V4v using a nomenclature previously established from research in non-human primates (Felleman and Van Essen, 1991; Rosa et al., 1993). This procedure did not require a significance threshold, and could be implemented in an automatic way. These results were replicated by DeYoe et al. (1996) and Engel et al. (1997), also utilizing a cortical surface-based analysis but manually distinguishing the borders based on polar-angle information. Further phase-encoded mapping studies

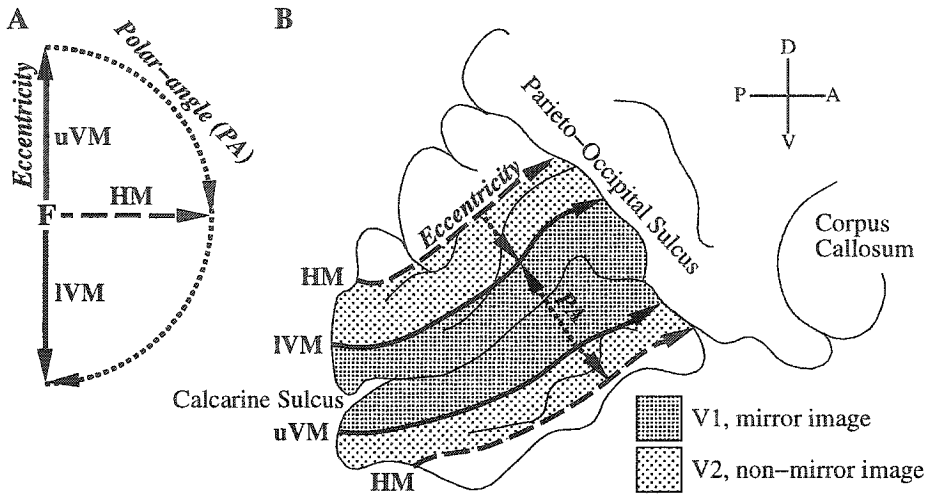

Figure 3.1: Schematic diagram of the form of Engel et al. (1997) of the right visual field (A) and cortical representations of areas V1 and V2 on the left hemisphere (B). (A) Illustrates the right part of the visual field where the fixation (F), upper and lower part of the vertical meridian (uVM, lVM) and horizontal meridia (HM) are indicated. (B) Schematic drawing of the medial view of the left occipital lobe. The locations of anatomical structures have been indicated for orientation purposes. Drawn are the retinotopic maps of areas V1 and V2 with the corresponding the eccentricity and polar-angle axis and HM and VM representations.

with modifications of the stimulus revealed visual areas V3A (DeYoe et al., 1996; Tootell et al., 1997, 1998c), V3B (Smith et al., 1998; Press et al., 2001), V7 (Tootell et al., 1998a,c; Mendola et al., 1999; Press et al., 2001; Tootell and Hadjikhani, 2001), V8 (Hadjikhani et al., 1998), a putative homologue of the lateral intraparietal area, LIP (Sereno et al., 2001), and retinotopic organization in human MT/V5 (Huk et al., 2002).

Both versions of the above phase-encoded retinotopic mapping method rely upon a reconstructed cortical surface derived from anatomical MRI data. Potentially, this could cause problems because not only could there be errors in the surface reconstruction, but also because of the different spatial resolutions of anatomical and functional images. Furthermore, even if the cortical surface is accurately reconstructed, there is a problem of interpolating a 3D volume onto a 2D surface, especially if a given voxel intersects twice with the

surface or not at all.

Here we present a volumetric method that extracts early retinotopically mapped visual areas in a completely automatic way. More importantly, it does not require an explicit reconstruction of the cortical surface, thereby bypassing any potential problems to do with surface reconstruction thus greatly simplifying the analysis. Assuming the primary goal of the visual area identification is to define a VOI, then this new algorithm achieves this without the intermediate cortical surface reconstruction/resampling step.

3.2 Methods

3.2.1 Magnetic resonance imaging

The magnetic resonance images were acquired with a Siemens Magnetom Vision 1.5T MRI. The experiments were conducted with a surface-coil (circularly polarized, receive-only) centered over their occipital pole. Head position was fixed by means of a foam headrest and a bite-bar.

T1-weighted anatomical MR images (aMRI) were acquired prior to the functional scans. This aMRI utilized a 3-D gradient echo (GE) sequence (TR=22ms, TE=10ms, flip angle = 30 deg.) and yielded 80 256x256 sagittal slices images 1x1x2mm voxels.

Multislice T2*-weighted GE echo-planar imaging (EPI) functional MR images (TR/TE = 3/51ms, flip angle = 90deg., #slices = 25, slice thickness = 4mm) were acquired with a 64x64 acquisition matrix and a 256x256 rectangular field of view, providing a voxel resolution of $4mm^3$. The slices were either taken parallel or perpendicular to the calcarine sulcus. For each dynamic scan, 128 measurements (time frames) were acquired, giving a total scanning time of approximately 6.5 minutes. Six to eight dynamic scans were performed in each session.

In a separate session T1-weighted aMRI images were acquired with a head-coil (circularly polarized, transmit and receive), also with a 3-D GE sequence, yielding 170 256x256 sagittal images comprising $1mm^3$ voxels.

Seven subjects were used (1 female; mean age: 34, age range: 25–48). All observers had normal or corrected to normal visual acuity. All studies were performed with the informed consent of the subjects and were approved by the Montréal Neurological Institute Research Ethics Committee.

3.2.2 Visual stimuli

The visual stimuli were generated on a Silicon Graphics O2 computer with OpenGL-based software and displayed with an LCD projector (NEC Multisync MT820). The stimuli were presented on a rear-projection screen placed in the bore, which was viewed by means of a mirror mounted above the eyes of the subject. The total visual display subtended 34 degrees.

In the center of each stimulus was a fixation triangle, subtending 0.2 deg., randomly changing during the scan to point either left or right. After each functional time-frame, i.e. every 3 seconds, the subjects indicated the direction of the triangle by means of a mouse-press. This task ensured fixation of the subjects and controlled their attention.

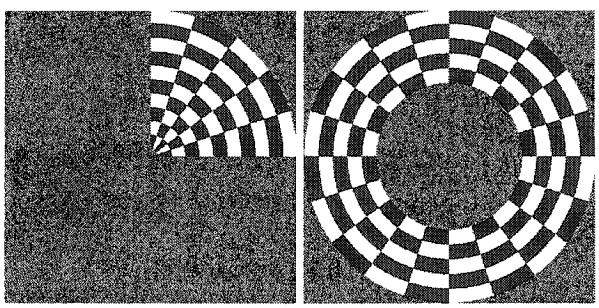

(a) (b)

Figure 3.2: Spatial layout of the visual stimuli used. Stimuli used for phase-encoded retinotopic mapping of polar-angle (A) and eccentricity (B). The checks in the wedge and annulus were contrast reversing at 8Hz. The entire wedge and annulus were rotating and expanding, respectively, at a rate of 0.03Hz

Standard stimuli were used to create polar-angle and eccentricity maps of the visual cortex (Engel et al., 1994; Sereno et al., 1995; DeYoe et al., 1996; Engel et al., 1997). Typically, two versions of each stimuli are used moving in opposite directions to cancel out the

hemodynamic phase-lag. Since our method is independed of any global phase-lag, we only used one direction. This may slightly move the borders if the hemodynamic phase-lag is locally different around the borders of the areas. Rotating wedge and expanding annulus sections of a radial dynamic checkerboard were used for the phase-encoded retinotopic mapping (Figure 3.2 A & B). Both stimuli completed a full cycle in 12 time frames (0.03Hz) giving a total of 10 cycles per scanning run. The checkerboard had a contrast of 100%, which was contrast reversing at 4Hz. The wedge subtended 90 degrees.

3.2.3 Data analysis

Anatomical images

The global T1-weighted aMRI scans were corrected for intensity non-uniformity (Sled et al., 1998; Arnold et al., 2001) and automatically registered (Collins et al., 1994) in a stereotaxic space (Talairach and Tournoux, 1988) using a stereotaxic model of 305 brains (Evans et al., 1992). The surface-coil aMRI, acquired in the same session as the functional images, was aligned with the head-coil aMRI, thereby allowing an alignment of the functional data with a head-coil MRI and subsequently stereotaxic space. This alignment was performed with an automated script combining correction for the intensity gradient in the surface-coil aMRI (Sled et al., 1998) and intra-subject registration (Collins et al., 1994). A validation of this method was described in a previous study (Dumoulin et al., 2000). The aMRIs were classified into gray-matter, white-matter and CSF (Kollokian, 1996; Zijdenbos et al., 1998), after which two cortical surfaces were simultaneously reconstructed at the inner and outer edge of the cortex (MacDonald et al., 2000). The surface-normals of the cortical models were smoothed to produce an 'unfolded' model of the cortical sheet (MacDonald et al., 2000). All processing steps were completely automatic and all the data are presented in a stereotaxic space (Talairach and Tournoux, 1988; Collins et al., 1994).

Preprocessing of functional images

The first 8 time-frames of each functional run were discarded due to start-up magnetization transients in the data. All remaining scans in each functional run were normalized for spatial slice-intensity variations by multiplying each slice by a constant factor across all time-frames. The functional data were blurred with an isotropic 3D Gaussian kernel (full-width-half-maximum (fwhm) = 6mm) to attenuate high frequency noise, and to get a more robust minimization of the motion correction algorithm (Woods et al., 1992, 1998). Two of the subjects' (SD and CB) functional runs contained high amplitude spurious spikes, these spikes interfere with the VFS computation and were removed by a median filter (width 3 time-points) in the time domain. The functional scans were corrected for subject motion within and between scans using the AIR package (Woods et al., 1992, 1998; Jiang et al., 1995).

Volumetric visual field sign identification

A flow chart illustrating the method of volumetric visual field sign identification is shown in figure 3.3. The data were analyzed in a stereotaxic space (Talairach and Tournoux, 1988; Collins et al., 1994), at a high resolution ($1mm^3$) using an average of all preprocessed functional runs. A slice through the left hemisphere (y=-10) in stereotaxic space is shown for the volumes created at different stages. At the top of the flow chart, the input images are shown: the T1-weighted anatomical MRI and two average preprocessed fMRIs of responses to each of the two stimuli used (see figure 3.2).

The power spectrum of each voxel's time-series was computed using a discrete Fourier transform and used in the construction of four preliminary maps, i.e. two phase-maps, a magnitude-map and a *t*-statistical map (see figure 3.3 row 2). The phase-maps were created by taking the phase of the fundamental frequency (i.e. 10cycles/scan) of the fMRI response. The phases of the fundamental frequency varied as a function of polar-angle when the stimulus was the rotating wedge and as a function of eccentricity when subjects viewed expanding annuli. For the creation of the magnitude-map and the *t*-statistical map data of the two fMRI scans were combined. Magnitude-maps were generated by dividing the am-

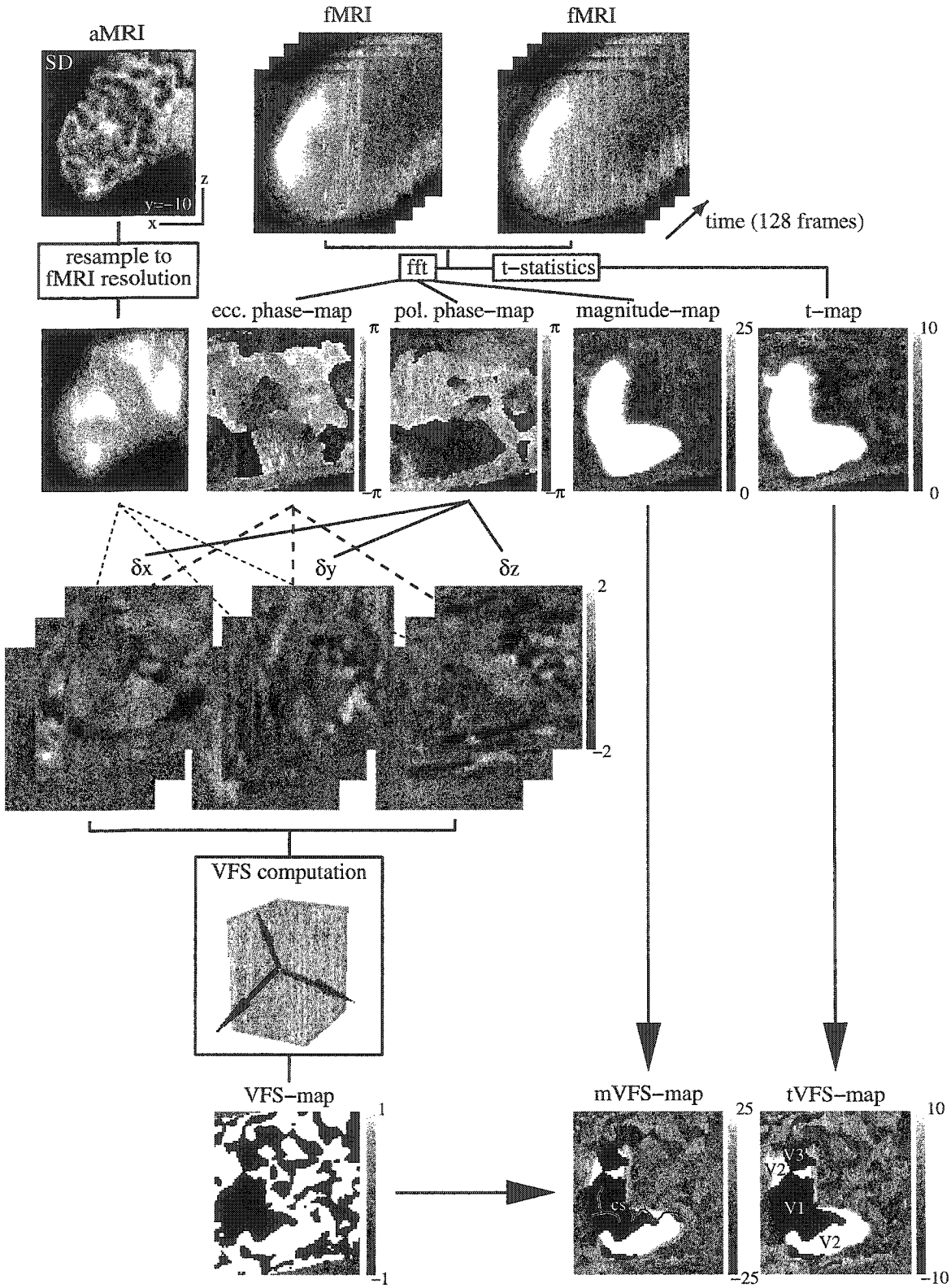
aMRI
SD
y=-10
z
x
fMRI
fMRI
time (128 frames)
resample to fMRI resolution
fft
t-statistics
ecc. phase-map
pol. phase-map
magnitude-map
t-map
π
−π
25
0
10
0
δx
δy
δz
2
−2
VFS computation
VFS-map
1
−1
mVFS-map
tVFS-map
25
−25
10
−10
V3
V2
V1
V2
cs

Figure 3.3: A flow chart describing the method with examples of slices through volumes created by the different processing steps. On the top of the flow chart the three input MR images are shown (aMRI and two fMRI scans), bottom-right shows two output images (mVFS and tVFS). On the input anatomical scan and the mVFS-map the calcarine sulcus (CS) is indicated with black and white lines for orientation purposes. On the tVFS-map the different visual areas are labeled.

plitude of the fundamental component of the fMRI response by the average amplitude of frequencies assumed to contain noise (typically 40-60cycles/scan). T-statistical maps were created using a Spearman rank order test for each voxel, where the phase of the design matrix is taken from the corresponding phase-map. Both the magnitude-map and the t-statistical map provide types of signal-to-noise maps which are used to weight the data.

To define for each voxel a 3D-vector orthogonal to the rate of change in the phase-maps, the δx, δy and δz partial directional derivatives were computed. The δx, δy and δz partial derivatives of the phase-maps were created by convolving the volumes with the partial derivative of a Gaussian kernel (typically, fwhm = 3mm). Due to the circular nature of phase, the phase-maps contain π to $-\pi$ reversals, and the derivative vector for these voxels will point orthogonal to the π/-π change which is opposite to the actual phase-change. To avoid these π/-π artifacts other sets of phase-maps are created from the original set by shifting the phase (typically by 0.5π). Thus in the resulting phase maps (typically 4) the π/-π shift occurs at a different location. The π/-π artifacts can be identified on a voxel by voxel basis due to their opposite polarities when comparing the derivatives of the phase-maps. Selective averaging (or by taking the median) of the partial derivative sets for each voxel removes the π/-π artifacts, resulting in one partial derivative set for polar-angle and eccentricity (see figure 3.3, row 3).

To prevent aliasing due to the resolution differences of the aMRI and the fMRI datasets, the anatomical MRI was resampled to the resolution of the functional images (see figure 3.3 column 1). Partial derivative volumes were also generated from the anatomical MRI (after resampling); these derivative vectors identify the cortical surface normals (see

figure 3.3, row 3).

The relative directions of these three orthogonal derivative vectors (polar-angle, eccentricity and cortex) identify the visual field sign (VFS) of each voxel (figure 3.3, row 4; an example of the three vectors within a voxel) resulting in a VFS-map (figure 3.3, row 5; -1 for mirror image, 1 for non-mirror image, and 0 if the the field sign could not be determined). More specifically, for each voxel the derivative vectors for eccentricity and polar angle were projected onto the plane defined by the anatomical normal vector, which should be tangential to the cortex. After which the vector cross product was computed of the tangential gradient vectors for eccentricity and polar angle, the sign of the cross product is the visual field sign (Sereno et al., 1994).

To create a weighted map of the VFS computation, the VFS-map is multiplied by either the magnitude map or the t-statistical map. The absolute value in the resulting maps (mVFS or tVFS, respectively) indicate the SNR or statistical certainty of the VFS computation (see figure 3.3 last row) and are very similar. Before this multiplication all values below 0 are set to 0 in the t-statistical map to prevent VFS reversals.

3.2.4 Simulations

To validate the data analysis, simulated data-sets were used to test the method in a controlled environment and assess the dependence on different variable values. To evaluate the results of the analysis objectively, besides a visual inspection, a correlation coefficient (r_{xy}) of the predefined and reconstructed VFS maps was computed:

$$r_{xy} = \frac{\sum_{i=1}^{n}(x_i y_i)}{\sqrt{\sum_{i=1}^{n} x_i^2 \sum_{i=1}^{n} y_i^2}} \tag{3.1}$$

where x is the predefined VFS-map from which the data were simulated, y is the mVFS-map reconstructed by the method. The magnitude of the signal in the reconstructed maps may vary due to resampling to a lower resolution and spatial smoothing. Only voxels with a predefined field sign and their corresponding voxels in the mVFS-maps were included

in the r_{xy}-computation. The relevant values of r_{xy} range between 0 (no correlation between the two maps) and 1 (exact reconstruction of the predefined-map).

A simple spherical model was constructed at a $1mm^3$ resolution with a single sulcus (see Figure 3.4 A). The dimensions of the model were chosen to be roughly similar to the occipital lobe with the calcarine sulcus in a stereotaxic space (Talairach and Tournoux, 1988; Collins et al., 1994). In this model retinotopically mapped regions were defined with different field signs. Simulated fMRI-data were generated from the predefined map, at a spatial ($4mm^3$) and temporal (3 sec) resolution of the actual fMRI scans (see Figure 3.4 E, after blurring). Each functional time-series had a mean value, determined by the anatomical model, added to this voxel were Gaussian noise and, if present, an fMRI signal. The fMRI signal of a particular phase was computed by convolving the block design with a hemodynamic response model (Boynton et al., 1996). The variance of the zero-mean Gaussian noise was 2/3 the maximum simulated fMRI signal amplitude. The resulting signal-to-noise ratio in the simulated data as indicated by the magnitude-maps was about 30% worse than the real data. Thus the simulated data represented a worst case scenario. The simulated data-sets were analyzed the same way as the real fMRI data.

3.3 Results

3.3.1 Simulations

Results of the simulation are shown in figure 3.4. The slices are taken through the middle of the spherical model, orthogonal to the sulcus. Panel A shows the anatomical model. The functional data were simulated according to the visual field layouts of panels B to D (VFSs are either 1 or -1). The volume in panel B simulates the textbook layout of cortical areas V1 and V2, while panels C & D represent more complex versions of cortical area layouts. A slice through one time-frame of a preprocessed (blurred) functional data-set of lower spatial resolution is shown in panel E. Panels F to H show the resulting visual field sign map multiplied by the computed magnitude map (image values range between -7.5 and 7.5).

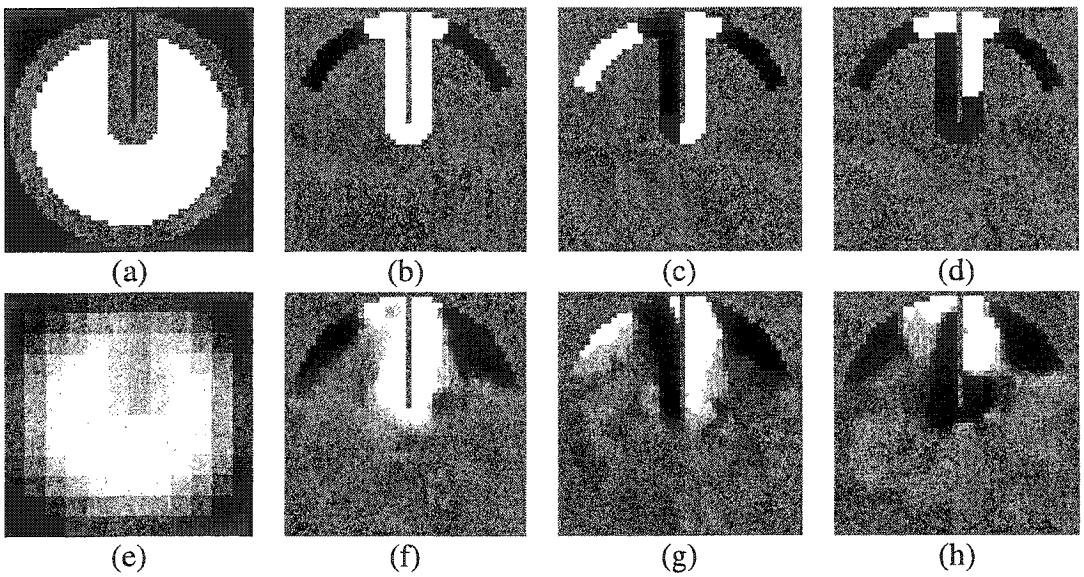

Figure 3.4: Slices from volumes created during simulations. A, anatomical volume. B-D, three simulated visual field sign maps used to generate the functional data. E, a lower resolution preprocessed functional time-frame. F-H, corresponding reconstructed mVFS-maps.

Notice that all areas and corresponding visual field signs were accurately reconstructed. The average correlation coefficient and standard deviation (see equation 3.1) for reconstructed mVFS-maps as shown in panels F to H was 0.89 ± 0.03, 0.82 ± 0.03 and 0.70 ± 0.00, respectively (n=4). The decreasing values are due to an increasing amount of borders between predefined areas. Even though the relative topography of all areas are accurately reconstructed, the exact border locations may vary due to partial volume effects and spatial smoothing of the data, degrading the correlation coefficient.

The different spatial resolution for the anatomical and functional data sets could interfere with the identification of the visual field signs. Take, for instance, a functional voxel with a specific polar and eccentricity angle located in a narrow or small sulcus, which is accurately represented in an aMRI. When analyzed at the spatial resolution of the aMRI data, parts of this voxel will fall on opposite banks of the sulci and one location will be a mirror image of the other. Therefore they will be assigned different field signs and may be interpreted as different visual areas. This problem is illustrated in Figure 3.5. Panels A & B

show the anatomical volume with a small sulcus and the predefined VFS-map, respectively. Panel C displays the resulting mVFS-map showing the incorrectly labeled lower side of the sulcus. In panel D this problem is solved by matching the functional and anatomical spatial resolutions. This is a problem that could also occur with methods that depend on a cortical surface reconstruction even if the cortical surface is accurately reconstructed.

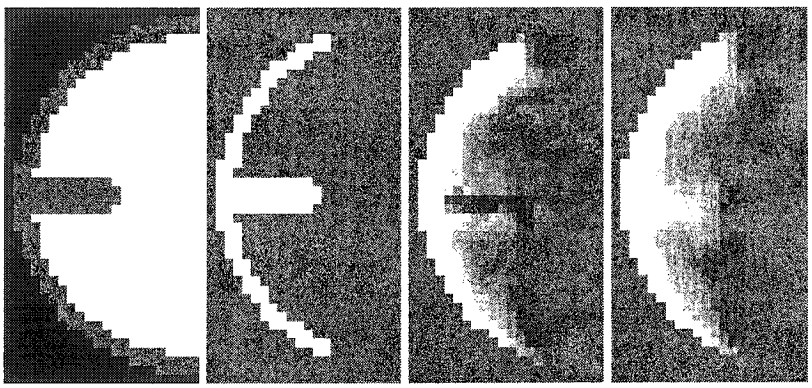

Figure 3.5: Simulated volumes, Figure A & B show a slice through the anatomical volume and predefined VFS-map, respectively. Figure C & D show the reconstructed VFS-map without and with matching the spatial resolution of the functional and anatomical data.

3.3.2 Volumetric visual field sign identification

Examples of slices through resulting VFS maps are shown in figure 3.6 and 3.7. In both cases the VFS-maps are weighted by the corresponding t-statistical maps, i.e. the absolute value indicates the statistical accuracy of the VFS calculation (tVFS). In both figures, neighboring areas with different field signs can be distinguished, and are identified based on (1) their field sign, (2) what part of the visual field is represented, (3) their relative organization and (4) their anatomical locations, e.g. V1 is known to be at least partially located within the calcarine sulcus (Stensaas et al., 1974; Rademacher et al., 1993; Gilissen et al., 1995; Gilissen and Zilles, 1996). Thus the tVFS segmentation of the visual cortex is completely automatic, but not the identification of the visual areas which has to be done manually. The

locations of the calcarine sulcus (CS) and parieto-occipital sulcus (POS) are indicated in the sagittal slices of figure 3.6.

Inspection of figure 3.6 provides a validation of the method described here. In the calcarine sulcus a large region of negative field sign (mirror image) is present, around which regions opposite field sign can be distinguished corresponding to the known layout of areas V1 and V2 (Holmes, 1945; Stensaas et al., 1974; Clarke and Miklossy, 1990; Horton and Hoyt, 1991; Rademacher et al., 1993; Gilissen et al., 1995; Gilissen and Zilles, 1996; Wong and Sharpe, 1999; Amunts et al., 2000). In a similar fashion other areas can be distinguished.

For comparison with conventional methods, the tVFS maps are shown on reconstructed unfolded cortical surfaces (MacDonald et al., 2000) in the middle columns of figure 3.7. The cortical surface was extracted halfway between the gray-matter CSF border and the white-matter gray matter border. Besides the tVFS-maps the corresponding polar-angle phase-maps are also shown on the unfolded cortical surfaces (left and right columns). The colors of the phase-maps correspond to the locations in the visual field as shown in the insets; furthermore the intensity of the colors in the phase-maps are also weighted by the t-statistical maps in an identical scale as the tVFS-maps. The black-white dashed lines are the borders of visual areas as derived from the tVFS-maps.

Results in figure 3.7 are comparable to those from surface-based methods (Sereno et al., 1995; DeYoe et al., 1996; Engel et al., 1997). The alternation of visual field signs is in accordance with the known layout of the visual areas. Besides tVFS-maps, the polar-angle phase-maps are shown in identical views. The representations of the polar-angle maps provide results similar to the methods of DeYoe et al. (1996) and Engel et al. (1997), where on these kinds of representations the borders were identified manually. The borders on the phase-maps in figure 3.7 are derived from the corresponding tVFS-maps and fall at the horizontal and vertical meridia, as they are known to occur. For a more quantitative comparison, the VFS were computed on the flattened surfaces (see figure 3.8). The correlation coefficient and standard deviation (see equation 3.1) between surface and volumetric computed tVFS-maps on the surfaces was 0.50 ± 0.07 (n=6, for the subjects in figure 3.7) and 0.64 ± 0.07 after smoothing (fwhm=4mm) of the surface-based tVFS-map (Chung et al., 2001). Even

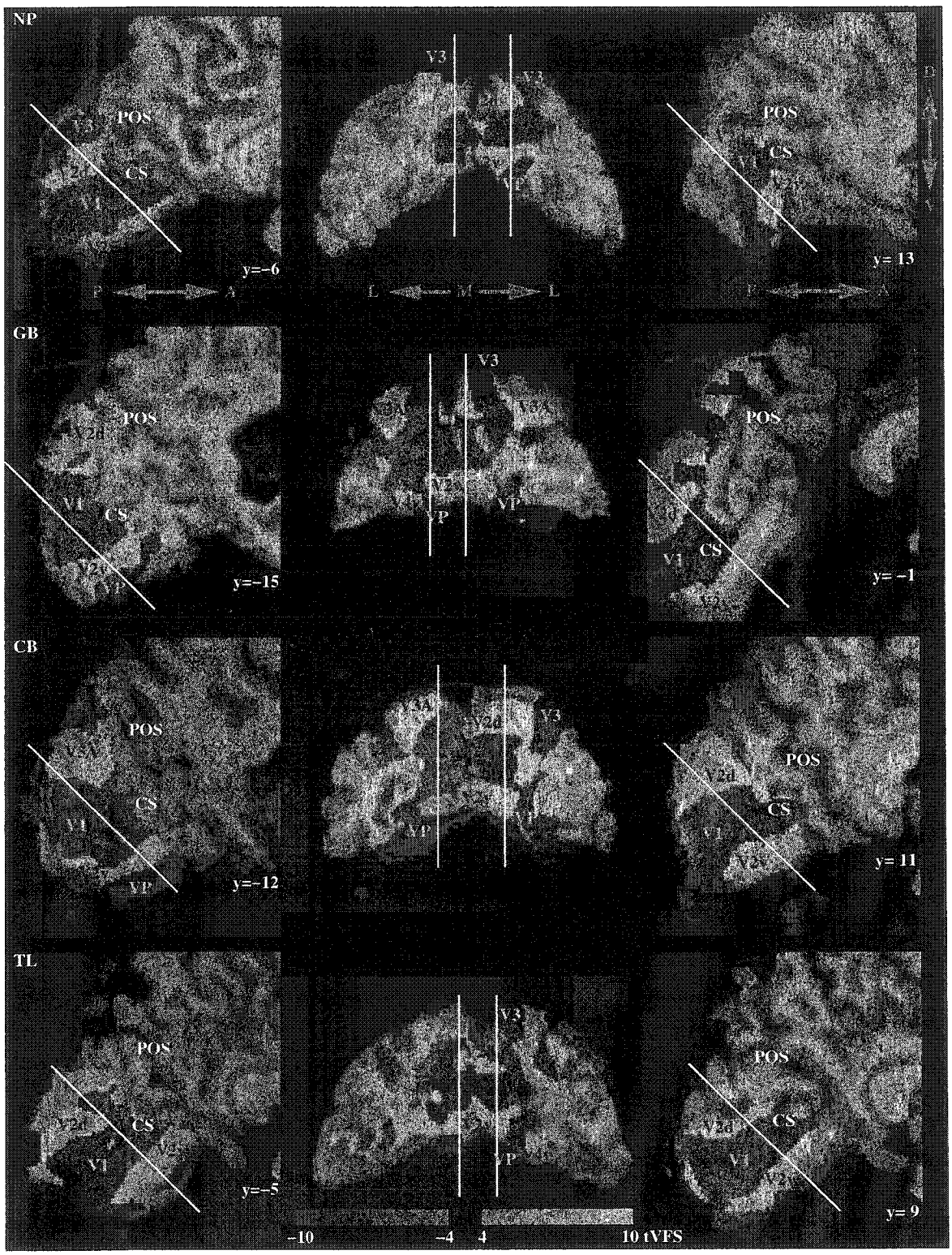
NP
GB
CB
TL
POS
CS
V1
V2d
V2v
V3
V3A
VP
y=-6
y= 13
y=-15
y=-1
y=-12
y= 11
y=-5
y= 9
-10
-4
4
10 tVFS

Figure 3.6: Visual Field Sign (VFS) maps are shown overlaid on the corresponding anatomical images for four subjects in a stereotaxic space, weighted by the corresponding *t*-statistical maps (tVFS). For each subject two sagittal slices through each hemisphere and an oblique slice are shown. The location of the slices is indicated with the white lines; for the sagittal slices the Talairach coordinates are given. Blue and yellow correspond to opposite field signs, mirror and non-mirror image respectively. Different visual areas can be identified and are labeled in the volumes. CS and POS indicate the location of the calcarine sulcus and parieto-occipital sulcus respectively.

though the relative topography of all areas are accurately reconstructed, the surface-based tVFS-maps differ due to a dependence on the cortical surface reconstruction, resampling and processing, and due to resolution differences between the cortical surface and functional data (see figure 3.5).

The visual field sign pattern is in accordance with previous studies identifying visual areas (Sereno et al., 1995; DeYoe et al., 1996; Engel et al., 1997; Tootell et al., 1997; Smith et al., 1998). In all subjects visual area V1, V2, V3/VP, V4v and V3A could be identified. The part of the visual field represented in these areas matched with previous studies (see figure 3.7). Parts of visual areas V3B, V7 and V8 could be identified only in some of the subjects (14/14, 13/14 and 9/14 hemispheres, respectively). In the V3B only a representation of one (lower) quadrant of the visual field could be identified, for V7 both an upper and a lower field representation was found. In our results, V4v only contains a (upper visual field) quadrant representation, and V8 contains a hemifield representation in agreement with (Hadjikhani et al., 1998), for a debate about a different naming scheme and the relationship to macaque V4 see Zeki et al. (1998) and Tootell and Hadjikhani (1998).

A large variability in the location of areas and the borders between them was observed for the different subjects, and even between hemispheres of a given subject. In imaging data in stereotaxic space (Talairach and Tournoux, 1988; Collins et al., 1994) variability may be due to gross anatomical variations, differences in the topographic relationship of gross anatomy and functional areas, and methodological issues (Steinmetz et al., 1989,

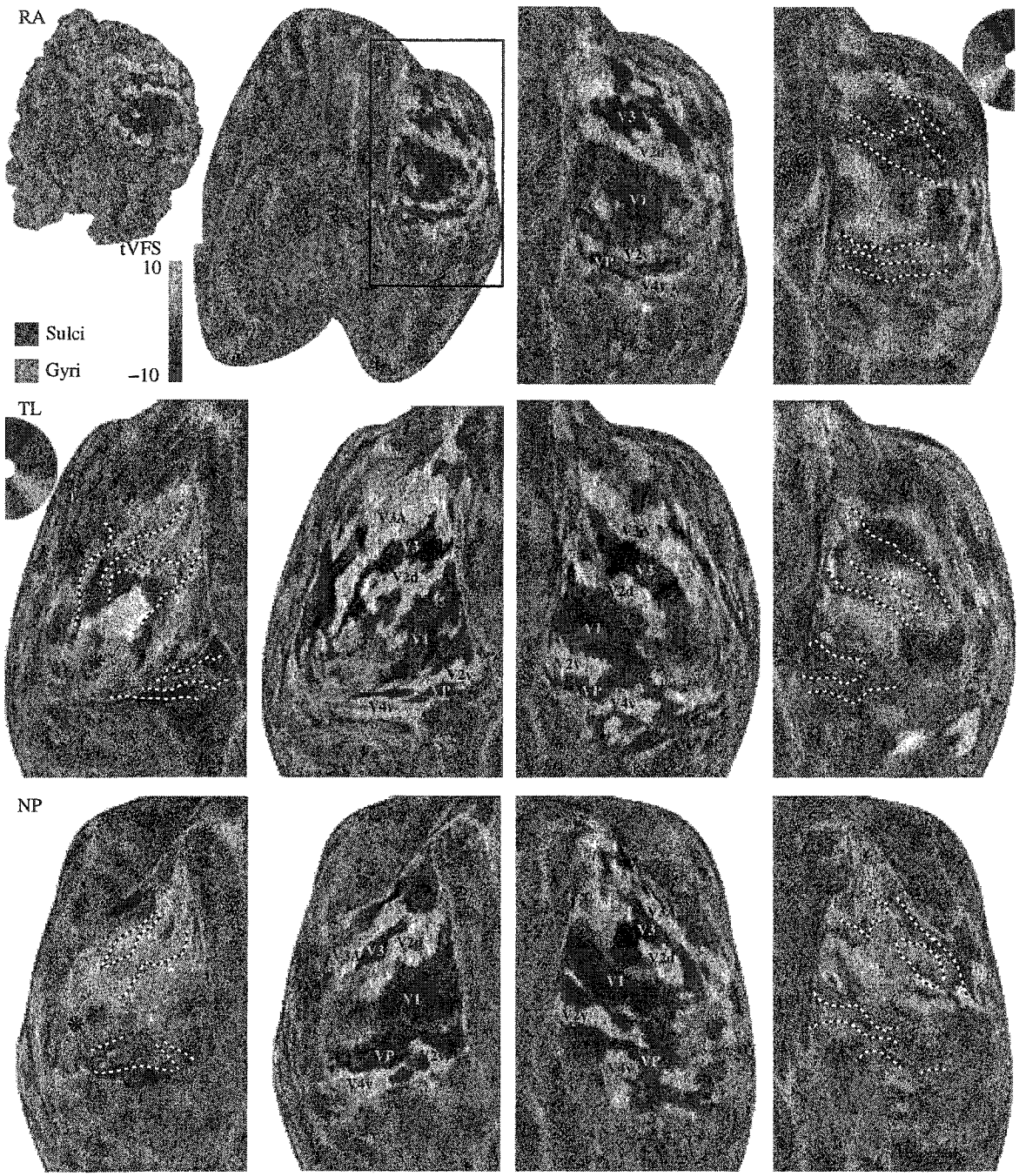
RA
tVFS
10
Sulci
Gyri
−10
TL
NP

Figure 3.7: tVFS images are shown overlaid on the corresponding unfolded cortical surfaces of three subjects. For the first subject (RA) the whole folded and unfolded cortical surfaces are shown to facilitate orientation on the other enlarged views. Sulci are colored darker gray then the gyri. For subject RA only the right hemisphere is shown, for the other subjects both hemispheres are presented. Beside the surfaces overlaid with the tVFS-maps, the same surfaces are shown overlaid with colored polar-angle phase-maps are in identical views. The intensity of the phase-maps are weighted by the *t*-statistical maps identical to the tVFS-maps. The black and white dashed lines indicate borders between visual areas derived from the tVFS-maps. The asterisk indicates the cortical representation of the fovea.

1990; Steinmetz and Seitz, 1991; Rademacher et al., 1993; Hunton et al., 1996). To quantify this variability a correlation coefficient, r_{xy} (see equation 3.1) was computed for voxels of the mVFS-maps falling within an average anatomical occipital lobe mask in stereotaxic space (Talairach and Tournoux, 1988; Collins et al., 1994). The mVFS-maps were used 1) to weight the data according to signal strength, because the occipital lobe mask will contain more than the identified visual areas, and 2) for consistency with the further interpretations where either the tVFS- or mVFS-maps are used. The average correlation coefficient (r_{xy}) and standard deviation between pairs of individual subjects (n=7) is 0.11±0.06 (n=21).

To estimate how much of this variation is due to the method, r_{xy} was also computed over different runs of the same subject (subjects TL and RA, table 3.1). Taking one run reduces the amount of signal and the average r_{xy} and standard deviation comparing the grand average of that subject with each individual run is 0.70±0.09 (n=7, average occipital lobe mask). The next step compares single fMRI runs of the same subject, using data acquired in identical and different slice positions. Different slice positions because 1) the slices were moved within a scanning session or 2) the runs were acquired in a different scanning sessions altogether, as would occur with different subjects. Computing r_{xy} by comparing single runs the r_{xy} was 0.61±0.06 (n=3) and 0.35±0.03 (n=6), for the same and different slice positions respectively. These values suggest that the position of the sampling grid (slice positions) is the primary origin of variability within a subject. In each of the individual runs all areas were

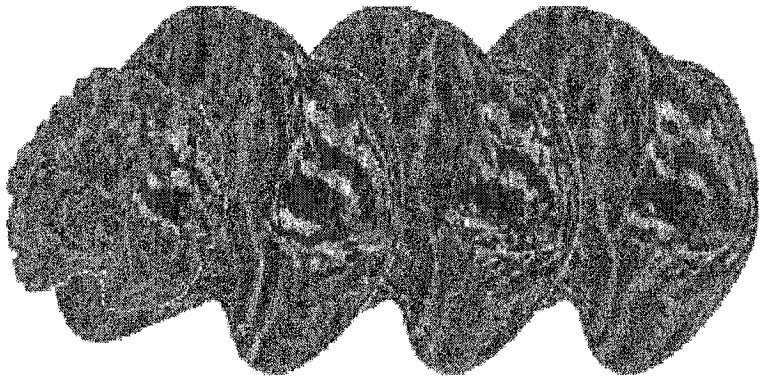

Figure 3.8: A comparison of volumetric VFS computation with a surface-based VFS computation. Three unfolded tVFS-maps are displayed on the corresponding cortical surface of one subject (TL) in a view similar to Figure 3.7. The whole folded cortical surface is shown to facilitate orientation on the other unfolded surfaces. The left unfolded surface shows the tVFS-map resulting from the volumetric VFS computation. The right tVFS-maps are resulting from a surface-based VFS computation, where the far right one has been smoothed (fwhm=4mm).

accurately reconstructed, suggesting that the lowered r_{xy} values result from variations in the exact border locations and size of the areas, as is also supported by the simulation results. This is verified quantitatively by blurring (fwhm 2, 4 and 6mm) the mVFS-maps, attenuating the border-contribution to the r_{xy}-computation and thus resulting in stronger correlations (table 3.1). Please note that the r_{xy} values depend on the volume of interest (VOI/ROI) over which the r_{xy} was computed. Here the VOI was an average anatomical map of the occipital cortex so one VOI could be used for different subjects. If only identified areas V1 to V3A and V4v were used for the within subjects comparison an increase of the r_{xy} values was observed (see table 3.1).

This within subject variability is less (larger r_{xy} values) than the variability between subjects (r_{xy}=0.11$\pm$0.06), notwithstanding that each subject's maps are of a higher quality (SNR) in the between subjects comparison. Given these two arguments, the data suggests that the methodological variations, as indicated by the within subject comparison, are rela-

Comparison	fwhm	avg. occ. lobe mask	indiv. V1 to V4v mask
average vs.	0	0.70±0.09	0.79±0.06
single runs (n=7)	2	0.78±0.05	0.85±0.04
	4	0.83±0.04	0.89±0.03
	6	0.86±0.03	0.91±0.03
single runs,	0	0.61±0.06	0.76±0.04
identical slice pos. (n=3)	2	0.71±0.06	0.85±0.04
	4	0.77±0.05	0.89±0.04
	6	0.81±0.04	0.91±0.03
single runs,	0	0.35±0.03	0.48±0.03
different slice pos. (n=6)	2	0.45±0.04	0.58±0.04
	4	0.53±0.04	0.66±0.04
	6	0.60±0.04	0.72±0.04

Table 3.1: Correlation coefficients comparing mVFS-maps of the same subject for three conditions using two masks. The results suggest that different slice positions is the primary origin of intra-subject variability. The different levels of spatial smoothing (fwhm) suggest a high reproducibility of the global topography of visual areas.

tively small and cannot explain the between subject variation. Therefore we conclude that the between subject variation is primarily due to variations in gross anatomy and variations in the relation between gross anatomy and functional areas.

In the previous analysis T1-weighted aMRI were used, but white-matter only images can be used as well; making the analysis independent of the anatomical scan parameters. In the latter case the white matter was automatically identified using the classifier INSECT (Kollokian, 1996; Zijdenbos et al., 1998). Results for both input anatomical images were very similar (r_{xy}=0.86 for subject RA).

3.4 Discussion

Volumetric retinotopic mapping can be used to identify retinotopically mapped visual areas. This method is automatic, does not require a cortical surface reconstruction and directly supplies volumes for a region of interest analysis.

All early retinotopic areas up to and including V3A and V4v could be identified reliably in all subjects (n=7). The layout of the cortical areas are in agreement with previous fMRI (Sereno et al., 1995; DeYoe et al., 1996; Engel et al., 1997; Tootell et al., 1997; Smith et al., 1998), positron emission tomography (Fox et al., 1987; Hasnain et al., 1998, 2001), lesion studies (Holmes, 1945; Horton and Hoyt, 1991; Wong and Sharpe, 1999) and cytoarchitectonic maps of Brodmann's area 17 and 18 (Clarke and Miklossy, 1990; Amunts et al., 2000).

In most subjects, parts of V3B, V7 and V8 could also be identified. These areas are at the limit of the current methodology and therefore may be only partially identified if at all, as evidenced by inconsistent descriptions of several studies (Smith et al., 1998; Tootell et al., 1998a,b; Press et al., 2001). Press et al. (2001) found an upper and lower visual field representation for both V3B and V7. Smith et al. (1998) could only determine a lower field representation for area V3B, while Tootell et al. (1998a,b) could only measure a lower field representation for area V7. Here we can confirm both an upper and lower field representation for V7, however for V3B only a representation of the lower visual field was found.

A high variability in the location of the visual areas was found between subjects in a stereotaxic space. This is not surprising since various studies have described variations in functional and anatomical patterns in striate and extra-striate cortex (Stensaas et al., 1974; Steinmetz et al., 1990; Steinmetz and Seitz, 1991; Watson et al., 1993; Rademacher et al., 1993; Gilissen et al., 1995; Aine et al., 1996; Gilissen and Zilles, 1996; Roland et al., 1997; Hasnain et al., 1998; Amunts et al., 2000; Dumoulin et al., 2000; Hasnain et al., 2001). The variability found here can mainly be attributed to variations in gross anatomy and variations in the relationship between gross anatomy and functional areas, rather than methodological differences.

Surface-based analysis, display and 2D coordinate systems have been proposed (Drury et al., 1996; Van Essen and Drury, 1997; Van Essen et al., 1998, 2000; Fischl et al., 1999a,b). Indeed cortical surfaces are now widely used for display purposes, including this study. Our method does not argue against surface-based methods. It provides a methodological simplification for retinotopic mapping applications, especially for volume-of-interest analysis, by avoiding potential problems with cortical surface reconstruction and resampling. The data can still be presented on a cortical surface but the analysis is not limited by it, i.e. the analysis does not depend on its accurate, resolution-matched, reconstruction.

The method described here provides an automatic volumetric segmentation of early visual areas, which is comparable to conventional surface-based methods. Offering the advantage of not requiring any manual interference and directly supplying VOIs thereby facilitating the application of cortical mapping to a wider population. Furthermore, due to its completely automatic analysis and decreased processing time by bypassing cortical surface reconstruction, this method offers the possibility of near real-time retinotopic mapping (for example, see near real-time creations of phase-maps in Voyvodic 1999).

Chapter 4

Cortical specialization for processing first- and second-order motion

THIS chapter (*Submitted* for publication) describes a study investigating a possible cortical specialization for first- and second-order mechanisms. Such a cortical specialization is controversial in both neurological (Greenlee and Smith, 1997; Vaina et al., 1999) and brain imaging (Smith et al., 1998; Somers et al., 1999) studies. The stimulus construction and psychophysical procedures are identical to those previously described in chapter 2. Besides standard stereotaxic based analysis, a more powerful volume-of-interest analysis in early visual areas (Dumoulin et al., 2000, 2003, chapter 3) is performed.

Abstract

Distinct mechanisms underlying the visual perception of luminance- (first-order) and contrast-defined (second-order) motion have been proposed from electrophysiological, human psychophysical and neurological studies; however a cortical specialization for these mechanisms has proven elusive. Here human brain imaging (fMRI) combined with psychophysical methods was used to assess cortical specializations for processing these two kinds of motion. A common stimulus construction was employed, controlling for differences in spatial and temporal properties, psychophysical performance and attention. Distinct cortical regions have been found preferentially processing either first- or second-order

motion, both in occipital and parietal lobes, producing the first physiological evidence in humans to support evidence from psychophysical studies, brain-lesion sites and computational models. These results provide evidence for the idea that first-order motion is computed in V1 and second-order motion in later occipital visual areas, and additionally suggest a functional dissociation between these two kinds of motion beyond the occipital lobe.

4.1 Introduction

Our visual world contains both luminance- (first-order) and contrast-defined (second-order) information (Schofield, 2000). Separate mechanisms for processing first- and second-order stimuli, both stationary and moving, have been demonstrated by electrophysiological and psychophysical studies (for reviews see Smith, 1994; Baker, 1999; Clifford and Vaina, 1999; Baker and Mareschal, 2001; Chubb et al., 2001; Lu and Sperling, 2001). The idea of separate neuronal substrates is also supported by reports describing a double dissociation of deficits for either first- (Greenlee and Smith, 1997; Vaina et al., 1998, 1999, 2000) or second-order motion (Plant et al., 1993; Plant and Nakayama, 1993; Vaina and Cowey, 1996; Greenlee and Smith, 1997; Braun et al., 1998; Vaina et al., 1999) perception in brain-damaged subjects. Comparing the location of lesions affecting first- and second-order motion perception, Greenlee and Smith (1997) reported extensive overlap in a standard space (Seeger, 1978) whereas Vaina et al. (1996; 1998; 1999; 2000) found separate sites in medial and lateral occipital lobe, respectively. Models of motion detection, derived from these psychophysical, electrophysiological and neurological studies, propose parallel mechanisms at separate cortical sites, i.e. extraction of first- and second-order information at early (V1) and later cortical stages, respectively (Chubb and Sperling, 1988; Wilson et al., 1992; Clifford and Vaina, 1999). Thus separate mechanisms have been proposed for processing first- and second-order motion but direct evidence for such cortical specializations has proven elusive.

Previous human brain imaging attempts have implicated a variety of areas in processing both first- and second-order stimuli (Smith et al., 1998; Somers et al., 1999), with some responding more to second-order motion (Smith et al., 1998). These previous stud-

ies employed differently constructed first- and second-order stimuli, as is common in psychophysical experiments where only certain stimulus attributes can be used for a given task. However, in the brain imaging data, differential responses can be elicited by differences in processing at any level, e.g. stimulus, task or attentional. In particular, second-order stimuli necessarily contain first-order carriers whereas the first-order stimuli did not contain any second-order structure. Thus the previous experiments might have been biased towards detecting responses to second-order attributes, which could explain why no cortical regions were selectively activated by first-order motion. In addition, attentional modulation can substantially affect neuroimaging responses (Beauchamp et al., 1997; O'Craven et al., 1997; Somers et al., 1999), and could potentially confound the interpretation of the results (Huk et al., 2001). Therefore a careful control of attention is a prerequisite 1) to avoid activations elicited by differential attentional requirements of the experimental conditions, and 2) to minimize attentional tracking proposed to occur in second-order motion (Seiffert and Cavanagh, 1998; Derrington and Ukkonen, 1999).

Here a single kind of stimulus is used (Figure 4.1), constructed of Gabor micropatterns in limited-lifetime stochastic motion to avoid attentional tracking (Baker and Hess, 1998). This stimulus contains both first- and second-order structure within the same image, related to the luminance-carrier and contrast-envelope of the Gabor micropatterns, respectively. Stimulus parameters, as delineated in previous psychophysical experiments (Boulton and Baker, 1993a,b, 1994; Bex and Baker, 1997; Baker and Hess, 1998; Clifford et al., 1998; Bex and Baker, 1999; Clifford and Vaina, 1999; Ledgeway and Hess, 2000; Dumoulin et al., 2001), were manipulated 1) to force the subjects' direction-discrimination by either first- or second-order mechanism, and 2) to equate the stimulus conditions for their psychophysical performance. The stimuli were presented in the MR scanner as they would be in a psychophysical experiment, and the subjects were required to perform a psychophysical task. This task 1) verified similar psychophysical performances for the different conditions within the MR environment, 2) focused and maintained the subjects' attention on the motion of the stimulus, and 3) allowed for a more direct comparison of the brain imaging and psychophysical data. Using this single stimulus paradigm with its inbuilt controls for dif-

ferences in spatial and temporal stimulus properties, we show cortical specializations for processing either type of motion, in both the occipital and parietal lobe.

4.2 Materials and methods

4.2.1 Subjects

Eight experienced psychophysical observers were used as subjects (all male, mean age: 36, age range: 25-51), four of whom were naive to the purpose of the study. The subjects were instructed to fixate at a provided fixation-point and trained prior to the scanning session to familiarize them with the task and to equate the stimulus conditions. All observers had normal or corrected to normal visual acuity.

Gabor micropattern stimulus

The visual stimuli (Fig. 4.1) were generated using the VideoToobox (Pelli, 1997) on a Macintosh G4 Powerbook, and displayed on a LCD projector (NEC Multisync MT820). The stimuli were presented on a rear-projection screen placed in the bore, which was viewed by means of a mirror mounted above the eyes of the subject. The total visual display subtended 15 degrees (horizontal and vertical) at the viewing distance of 1m. The projector intensity non-linearity was measured using a photometer (United Detector Technology, S370), and corrected using internal look up tables. The monitor was operated using its green video input only.

The stimuli contained non-overlapping Gabor micropatterns each consisting of a 1D sinewave carrier enclosed by a 2D Gaussian envelope:

$$L(x,y) = L_0 \left[1 + C^{-\left(\frac{x^2}{2\sigma_x^2} + \frac{y^2}{2\sigma_y^2}\right)} \sin\left(\frac{2\pi x}{\lambda} + \phi\right) \right] \tag{4.1}$$

where L_0 is the mean luminance, C is the contrast, σ is the sigma of the gaussian envelope, λ and ϕ the wavelength and phase of the carrier luminance sinewave. The orientation of

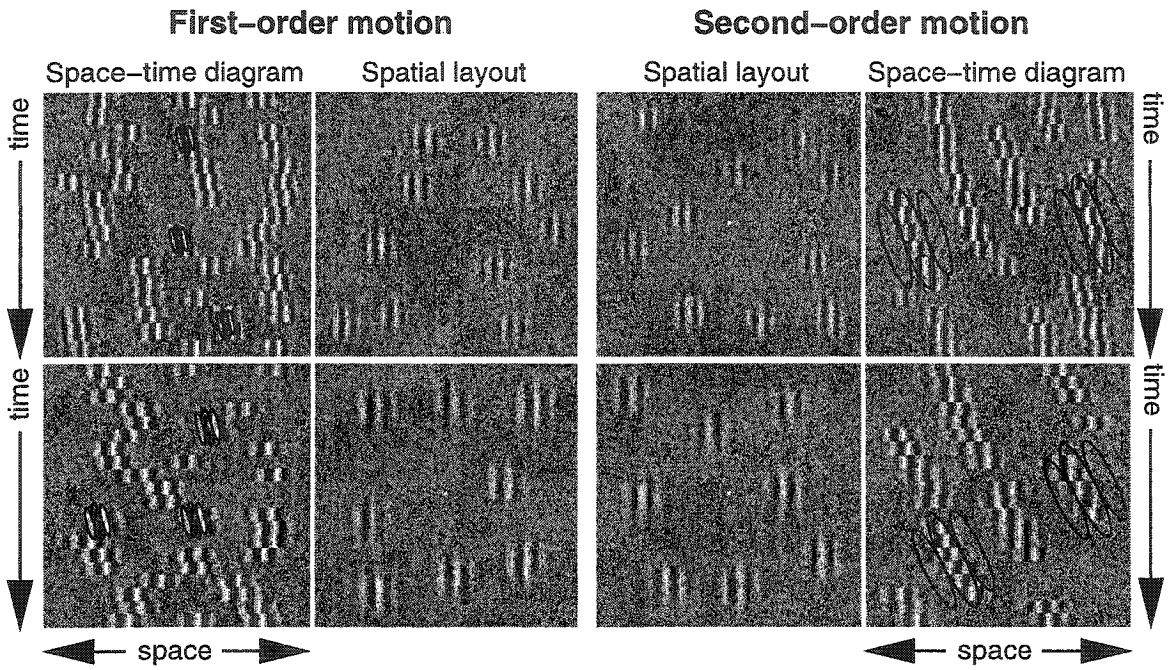

the Gabors was perpendicular to their direction of motion, i.e. vertical. Each stimulus presentation lasted 1600ms. Two kinds of Gabor micropatterns were used, which only differed in their motion trajectories. One set of micropatterns moved coherently in fixed displacements, the others were randomly replotted. The average probability of a micropattern moving coherently was determined by the coherence level. The Gabors had a limited-lifetime, after which they were re-plotted in a random position, and it was freshly determined whether each would move coherently or not for the next set of displacements. Micropatterns falling in a central circular zone of radius 4 deg were not plotted to avoid attentional tracking. The net direction of motion of the Gabor patterns was either to the left or to the right. For a more detailed description of the limited-lifetime Gabor stimuli see Baker and Hess (1998) and Ledgeway and Hess (2000). The subjects performed a two-alternative forced-choice direction-discrimination task and their responses were recorded.

Two different versions of this stimulus were used with different spatial (λ=1.4deg and 1.9deg) and temporal properties (16 exposures of 100ms and 20 exposures of 80ms). In both conditions the envelope size (σ) was 3/4λ and the contrast (C) was 30%. To force the

Figure 4.1: Spatial layout and space-time diagrams of the four conditions of the visual stimulus. The top and bottom rows differ only in stimulus parameters controlling velocity. The central four panels show four representative spatial layouts, flanked by corresponding examples of space-time diagrams having an overall direction of motion (displacement direction) to the right. The left four panels are examples of the first-order stimulus conditions whereas the right four panels illustrate second-order stimulus configurations. The spatial and temporal properties of both first- and second-order stimulus conditions are virtually identical. A few hypothetical filters are drawn on top of the space-time diagrams illustrating that on the left panels first-order mechanisms underlie the perceptual judgments, whereas in the right panels the overall direction of motion can only be determined by second-order mechanisms. In the first-order configurations (left side) a displacement of quadrature phase, a lifetime of 1 and a lower coherence (50%) was used, parameters known to favor processing by first-order mechanisms. In the second-order conditions (right side) the carrier-phase was randomized on each exposure, forcing the perceptual judgments by a second-order mechanism. The first- and second-order conditions have slightly different velocities (different displacements with identical temporal properties). As a control condition, the spatial and temporal properties of the top and bottom stimulus versions were chosen in such a way that the second-order (top-right) condition has the same velocity as the first-order (bottom-left) condition, allowing for a velocity-matched control. The contrast of the Gabor micropatterns is higher than in the actual stimulus (30%) for illustration purposes.

detection of the direction of motion by the first-order mechanism a displacement of $1/4\lambda$, a lifetime of 1 with a fixed carrier-phase (ϕ=0) and a lower coherence level were used. To ensure that a second-order mechanism is mediating the subject's directional judgments, the carrier-phase was randomized on each exposure ($-\pi < \phi < \pi$) at a displacement of $1/2\lambda$. These conditions are known to force the detection of the direction of motion by either mechanism (Baker and Hess, 1998; Ledgeway and Hess, 2000; Dumoulin et al., 2001), which was verified during initial psychophysics. Both coherence and lifetime were adjusted for each subject in order to equate the psychophysical direction-discrimination of the first- and second- order conditions, but were kept constant during the experiment. Both lifetime and coherence parameters vary the stimulus signal-to-noise ratios (SNR) to equate the psychophysical performance (and thus perceptual SNR), with the aim to achieve similar neuronal load. Thus at least perceptually the stimuli did not contain different SNR levels. Typically, a coherence level of 50% and 90% and a lifetime of 1 and 5 was used for the first- and second-order conditions, respectively. Thus stimulus parameters were varied to force the detection of the direction of motion by either mechanism (displacement, lifetime and carrier-phase) and to equate the subjects' psychophysical performances (lifetime and coherence). A subset of the four conditions provide a control to assess the effect of displacement (velocity) manipulation (see figure 4.1), and a separate coherence control experiment investigated the effect of the coherence manipulation.

Presentations of a mean-luminance block (21s) and two blocks containing the limited-lifetime Gabor stimuli (each 30s) were repeated four times. Thus each block of the four Gabor stimulus conditions was shown twice in random order, giving a total of 4 first- and 4 second-order blocks. Stimulus presentations lasted 1.6s and were time-locked to the acquisition of fMRI time-frames, i.e. every 3 seconds. In the remaining 1.4 seconds the subjects' responses were recorded. The subjects continually performed a two-alternative forced-choice (2AFC) psychophysical task, i.e. a left-right direction-discrimination task when the motion stimuli were presented and a black-white fixation-dot polarity task during blank periods. All subjects reported the tasks to be challenging, including the fixation-dot polarity task. The latter one can be attributed to 1) time-constraints, 2) the stimulus design,

i.e. in the blank periods both stimulus and response period contained a fixation-dot of random polarity, and 3) the response requirements, i.e. the left and right response buttons did not map on to the black-white judgment as intuitively as in the left-right motion judgment.

4.2.2 Mapping stimuli

The visual stimuli used for identification of visual cortical areas were generated on a Silicon Graphics O_2 computer with OpenGL-based software and displayed with an LCD projector (NEC Multisync MT820). The total visual display subtended 34 degrees. Standard stimuli were used to create polar-angle and eccentricity maps of the visual cortex (Engel et al., 1994; Sereno et al., 1995; DeYoe et al., 1996; Engel et al., 1997; Dumoulin et al., 2003). Rotating wedge and expanding annulus sections of a radial checkerboard were used for the phase-encoded retinotopic mapping. Both stimuli completed a full cycle in 12 time frames (0.03Hz) giving a total of 10 cycles per scanning run. The contrast of the checkerboard was 100%, which was contrast reversing at 4Hz. The wedge subtended 90 degrees. Low contrast flickering stimuli (8Hz, 6%) contrasted with stationary patterns were used to localize hMT+ or V5-complex (Tootell et al., 1995b; Dumoulin et al., 2000).

4.2.3 Magnetic resonance imaging

The magnetic resonance images were acquired with a Siemens Magnetom Vision 1.5T MRI. The experiments were conducted with the subjects lying on their back with a surface-coil (circularly polarized, receive only) centered over their occipital poles. Head position was fixed by means of a foam head-rest and a bite-bar.

Multislice T2*-weighted gradient echo (GE) echo-planar imaging (EPI) functional MR images (TR/TE = 3000/51ms, flip angle = 90deg., #slices = 25 (contiguous), slice thickness = 4mm) were acquired using a surface-coil (receive only) with a 64x64 acquisition matrix and a 256x256mm rectangular field of view. The slices were taken parallel to the calcarine sulcus and covered the entire ocipital and parietal lobes and large dorsal-posterior parts of the temporal and frontal lobes. One hundred and ten measurements (time frames)

were acquired. Ten dynamic scans were performed in each session. T1-weighted anatomical MR images (aMRI) were acquired prior to the commencement of the functional scans. This aMRI utilized a 3-D GE sequence (TR=22ms, TE=10ms, flip angle = 30 deg., 256x256mm rFOV) and yielded 80 saggital images with a thickness of 2mm. The coherence control experiments were performed using identical MR parameters and setup using a Siemens Sonata 1.5T MRI.

In separate sessions T1-weighted aMRI images were acquired with a head-coil, also with a 3-D GE sequence, yielding 170 saggital images comprising $1mm^3$ voxels. Identification of the visual areas was also performed in another separate session with identical parameters except for the number of time frames acquired and total runs which were 128 and 6-10, respectively. All studies were performed with the informed consent of the subjects and were approved by the Montréal Neurological Institute Research Ethics Committee.

4.2.4 Processing of anatomical images

The anatomical MRI scans were corrected for intensity non-uniformity (Sled et al., 1998; Arnold et al., 2001) and automatically registered (Collins et al., 1994) in a stereotaxic space (Talairach and Tournoux, 1988). The surface-coil aMRI, taken with the functional images, was aligned with the head-coil aMRI, thereby allowing an alignment of the functional data with a head-coil MRI and subsequently stereotaxic space. This alignment was performed with an automated script combining correction for the intensity gradient in the surface-coil aMRI (Sled et al., 1998) and intra-subject registration (Collins et al., 1994). A validation of this method was described in a previous study (Dumoulin et al., 2000). The aMRIs were classified into gray-matter, white-matter and CSF (Kollokian, 1996; Zijdenbos et al., 1998), after which two cortical surfaces were automatically reconstructed at the inner and outer edge of the cortex (MacDonald et al., 2000). The surface-normals of the cortical models were smoothed to produce an 'unfolded' model of the cortical sheet (MacDonald et al., 2000). All processing steps were completely automatic and all the data are presented in a stereotaxic space (Talairach and Tournoux, 1988; Collins et al., 1994).

4.2.5 Preprocessing of functional images

The first 8 scans of each functional run were discarded due to start-up magnetization transients in the data. All remaining scans in each functional run were corrected for variations in spatial slice intensity and blurred with an isotropic 3D Gaussian kernel (full-width-half-maximum=6mm) to attenuate high frequency noise. The functional scans were corrected for subject motion within each fMRI scan and between scans with the AIR package (Woods et al., 1992; Jiang et al., 1995; Woods et al., 1998). Functional scans were excluded from further analysis if artifacts were found (e.g. large subject motion or spurious spikes) or if the subjects' psychophysical responses for any given condition contained more than 40% errors. In total 13 out of 108 fMRI-scans were excluded from further analysis, primarily due to imaging artifacts.

4.2.6 Identification of visual areas

Early visual cortical areas were identified using volumetric phase-encoded retinotopic mapping (Dumoulin et al., 2003). By combining eccentricity and polar-angle phase-maps with the anatomical MRI, the visual field signs of different visual areas could be segmented. Neighboring visual areas could be identified due to opposite field signs; i.e. V1, V2, V3/VP, V3a, V3b, V4v and V7 (Sereno et al., 1994, 1995; Dumoulin et al., 2003). Areas V3b and V7 could be identified lateral and anterior to area V3A, due to their change in field sign relative to this area. Therefore, only one border could be identified with certainty, i.e. the V3A border. Thus, only parts of these two areas are identified in all subjects, containing quadri-field and hemi-field representations, respectively (Dumoulin et al., 2003). Area MT (or V5) was identified using a low contrast flickering stimulus (Tootell et al., 1995b; Dumoulin et al., 2000). This activation region is usually termed hMT+ (or V5-complex) to indicate that parts of adjacent cortical areas might be included.

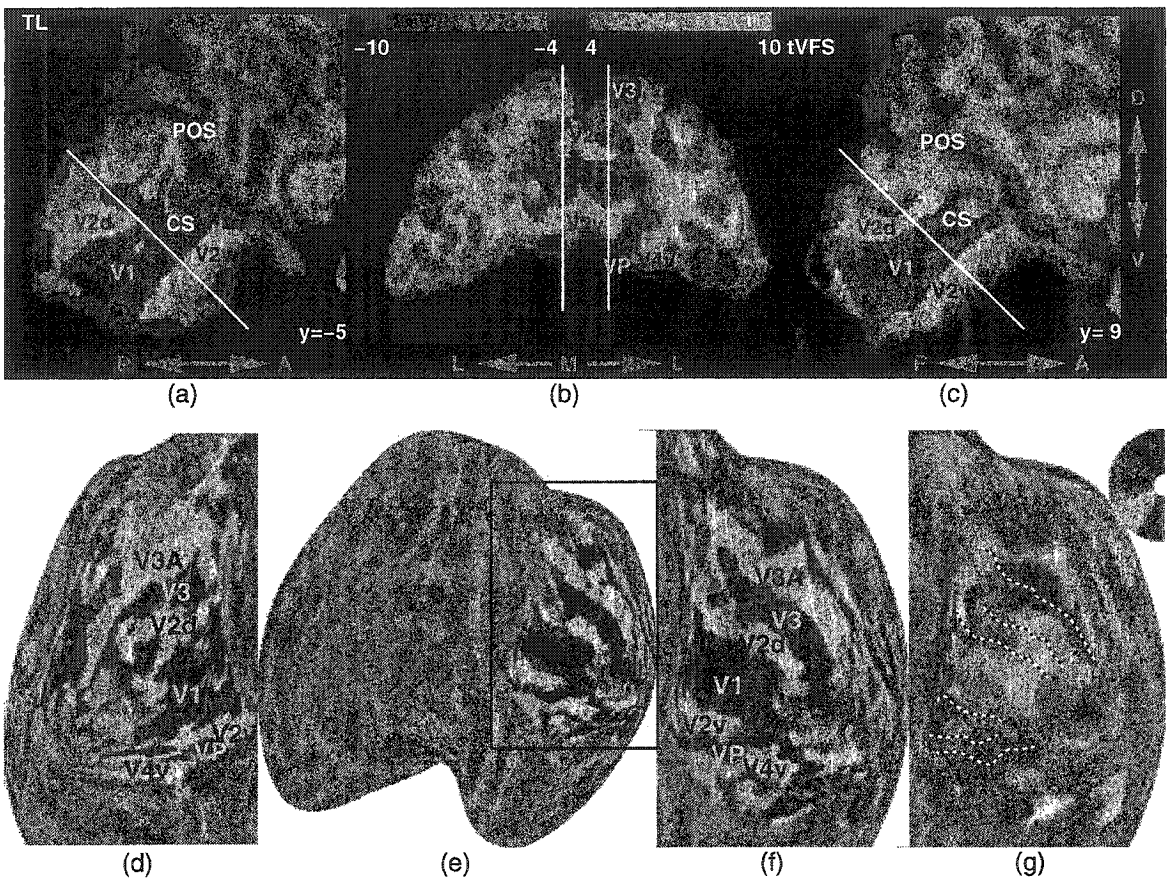

Figure 4.2: Example of volumetric visual area identification (Dumoulin et al., 2003) for one subject (TL). The top row (a-c) shows the volumetric visual field sign maps (VFS) weighted by *t*-statistical maps (tVFS). On the saggital slices (a,c) the parietal-occipital sulcus (POS) and calcarine sulcus (CS) have been identified. The bottom row shows the same data (same colormap range) on unfolded cortical surfaces of the left (d) and right (e,f) hemisphere. The bottom row also shows an example of the polar-angle phase map (g), where the borders of the areas are drawn based on the tVFS-changes. The polar-angle map is used in combination with the eccentricity map and the surface-normals to compute the VFS.

4.2.7 Statistical analysis

The fMRI data was analyzed using software developed by Worsley et al. (2002). This statistical analysis is based on a linear model with correlated errors. Runs, sessions and subjects were combined using a linear model with fixed effects and standard deviations taken from the previous analysis. A random effects analysis was performed by first estimating the the ratio of the random effects variance to the fixed effects variance, then regularizing this ratio by spatial smoothing with a 15mm fwhm gaussian filter. The variance of the effect was then estimated by the smoothed ratio multiplied by the fixed effects variance to achieve higher degrees of freedom. The resulting t-statistical images were thresholded for peaks and cluster sizes using random field theory (Worsley et al., 1996). In determining significant clusters and peaks in the first- versus second-order comparison, the search region was restricted to voxels within the brain which responded to the "stimulus" versus "blank" comparison (t=1.96 corresponding to an uncorrected p=0.05, however the results were robust over a range of thresholds $1<t<4$).

The volume-of-interest analysis of the identified visual areas (V1 to V7) was done in an identical fashion. Prior to the statistical analysis, time-series of voxels responding to motion stimuli within a VOI (left and right hemispheres) were averaged together, with exclusion of voxels displaying artifacts.

4.3 Results

The motion stimuli had virtually identical spatial and temporal properties (see Figure 4.1), and even though all conditions contain stochastic first- and second-order information, the correct net direction of motion can only be determined by one mechanism. Drawn on the space-time diagrams are hypothetical filters signaling the motion-direction of certain Gabor micropatterns. In the first-order configurations (Figure 4.1 left panels) the net direction of motion can correctly be determined by a standard (first-order) quasi-linear filter (Adelson and Bergen, 1985; Van Santen and Sperling, 1985) responding to the luminance-carrier;

previous psychophysical studies (Baker and Hess, 1998; Ledgeway and Hess, 2000; Dumoulin et al., 2001) indicate that in those conditions a second-order mechanism does not contribute to judgments of the net direction of motion. In the second-order conditions (Figure 4.1 right panels) the carrier-phase is randomized on different exposures, eliminating direction-discrimination based on first-order mechanisms. Here the mechanism signaling the correct direction of motion has been shown to be based on the contrast-envelope of the micropatterns, i.e. second-order information, because the average luminance in the different subfields of the filter are identical (Baker and Hess, 1998; Bex and Baker, 1999; Ledgeway and Hess, 2000; Dumoulin et al., 2001).

The average psychophysical data for all subjects is shown in Figure 4.3 for the different conditions. The percent error and standard deviations for first- and second-order motion conditions were 7.3 ± 10.5 and 8.9 ± 9.7, respectively. The results show that 1) the subjects were able to do the tasks, 2) the tasks were challenging enough to engage their full attention (rarely 0% errors performance occurred) and 3) the psychophysical performances for the conditions were not significantly different ($p>0.2$).

The first fMRI statistical analysis aimed at identifying cortical regions involved in processing *all* stimulus aspects. Since any first- and second-order differences would be expected to occur in these cortical regions, any further statistical comparisons will be restricted to this region. This statistical comparison, i.e. motion versus blank conditions, indicates a widespread activation (Figure 4.4, thin black lines). In early visual areas, this activation region corresponds to the cortical representation of the eccentric locations where the Gabor stimulus was presented, as it should. This statistical map is very similar to t-statistical maps comparing each individual stimulus configuration to the blank-periods (correlation: r_{xy}=0.85), which therefore allows the further statistical analysis to be restricted by the combined statistical map. Furthermore, this result indicates that similar areas are involved in processing any version of the stimulus, which is in agreement with previous studies investigating first- and second-order motion (Smith et al., 1998; Somers et al., 1999). This is not surprising since this is a highly unspecific comparison and the blank-periods do not provide a resting baseline. That is, it is an unspecific comparison because we are comparing stim-

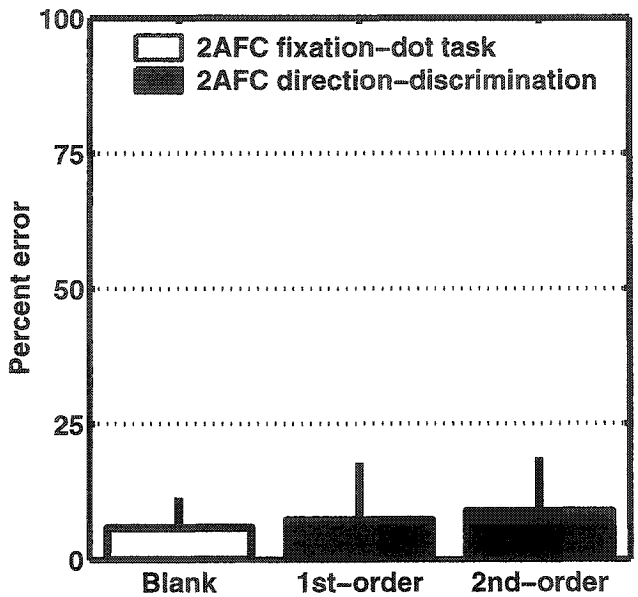

Figure 4.3: Subjects' psychophysical performance during the MR scans. Percent error and standard deviations of the subjects' performance during the fMRI scans are plotted for three conditions. All tasks comprised psychophysical two-alternative forced choice (2AFC) judgments. During the blank periods, the subjects judged the fixation-dot polarity (black-white). When the Gabor-stimuli, either first- or second-order version, were presented the subjects performed a direction-discrimination (left-right) task. The results show that the subjects were able to do either task and that the responses to first- and second-order stimulus conditions were statistically indistinguishable ($p>0.2$), indicating that the conditions were equated for their psychophysical performance.

ulus "present" versus "absent". Therefore, this activation distribution is not motion specific. And furthermore, any stimulus version always contained both first- and second-order noise. Lastly, it does not represent a resting baseline because these activation patterns are also produced by changes in "more eccentric" versus "foveal" spatial-attention (Watanabe et al., 1998; Tootell et al., 1998a; Gandhi et al., 1999; Smith et al., 2000; Sasaki et al., 2001). In summary, comparing "stimuli" versus "blank" is a highly unspecific comparison where all aspects contribute to, and thus can only be used for, the identification of cortical areas processing *any* stimulus aspects.

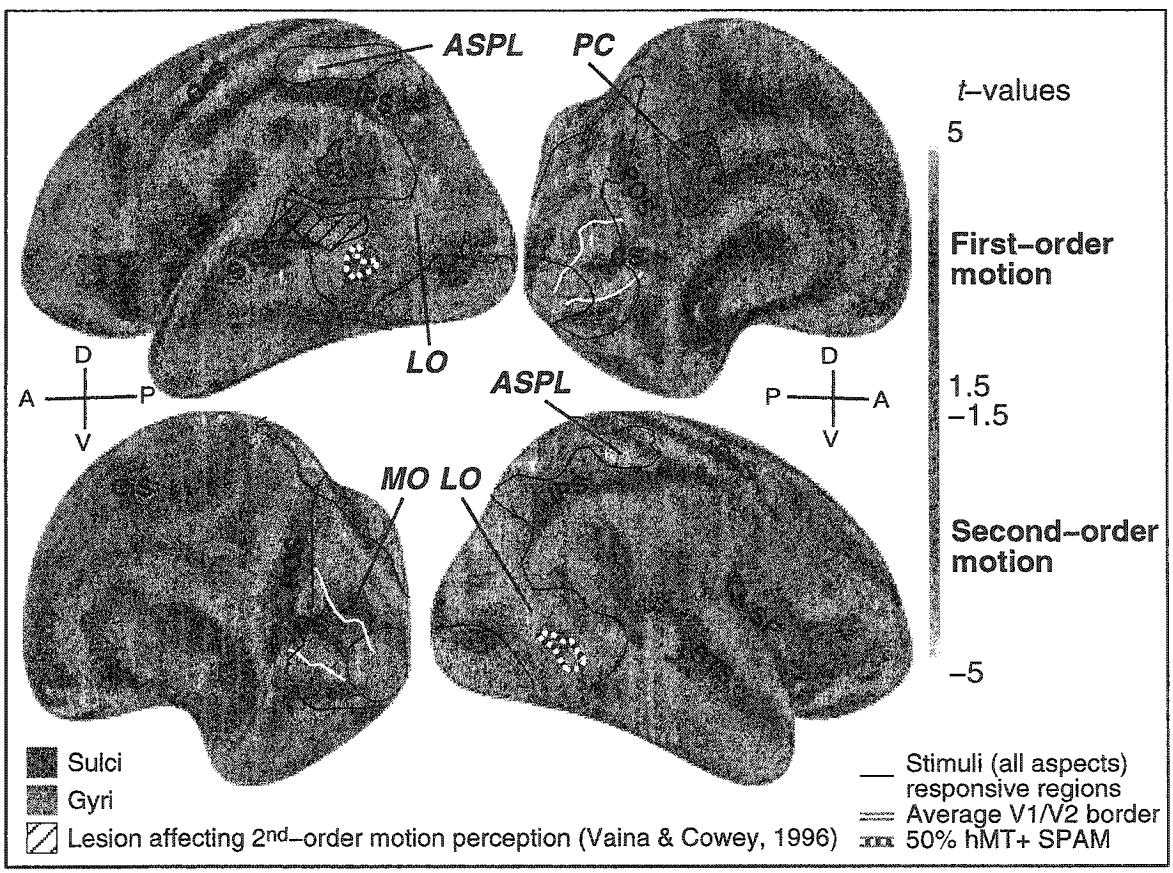

The second statistical analysis compared first- versus second-order motion responses. This statistical comparison was constrained to the cortical regions found to process any of the stimulus attributes, thereby increasing statistical sensitivity. To identify the cortical regions involved in any processing steps related to motion stimuli the *t*-statistical map

Figure 4.4: Average *t*-statistical map (n=8) comparing first- and second-order motion conditions displayed on their average unfolded cortical surfaces. The oblique lateral and medial views (left and right) of the left hemisphere are shown in the top row whereas the oblique medial and lateral views (left and right) of the right hemisphere are shown in the bottom row. On their averaged surfaces major anatomical structures can be identified (MacDonald et al., 2000) and some are labeled to facilitate orientation on the surfaces. On the lateral views the Central Sulcus (CeS), Sylvian Fissure (SF), Superior Temporal Sulcus (STS) and Intra-Parietal Sulcus (IPS) are labeled. On the medial side the locations of the Cingulate Sulcus (CiS), Parietal-Occipital Sulcus (POS) and Calcarine Sulcus (CS) are indicated. Relevant regions are indicated (for *t* and p-values see Table 4.1). Significant stronger responses to second-order motion is found both in the anterior superior parietal lobule (*ASPL*) and in lateral occipital regions (*LO*). Areas responding more to first-order motion are found in the precuneus (*PC*) and medial occipital cortex (*MO*). The *MO*-activation show a trend that is disclosed significantly in the VOI-analysis (Figure 4.5). Regions responding to *all* stimulus and task aspects are delineated with black lines (corresponding to t=1.96, uncorrected p=0.05); in early visual areas this indicates the eccentricity range where the stimuli were presented. On the medial views the average V1/V2 border is indicated with white lines. The average location of hMT+ is indicated by black-white iso-probability lines (50%) of the hMT+ statistical probabilistic anatomical map (SPAM) on the lateral views. The hMT+ iso-probability lines suggest that the main second-order *LO*-activation peak is most likely not MT. Also, the lesion location of subject FD is indicated, who was selectively impaired in second-order motion perception, (Vaina and Cowey, 1996).The lesion data was provided by Dr. Vaina.

was thresholded (Figure 4.4 thin lines, correspond to t=1.96). To not, a priori, exclude certain regions due to an overly restricted search region, this threshold was generously chosen (t=1.96 corresponding to an uncorrected p-value of 0.05). However, the final results did not critically depend upon, and were robust over, a wide range of thresholds (1<t-threshold<4). The results of this statistical analysis are shown in Figure 4.4. Significant t-statistical clusters and peaks (p<0.05) in the resulting t-map were determined (Worsley et al., 1996) and are identified in Figure 4.4, and Table 4.1. Cortical specializations for processing first- and second-order motion were found both in occipital and parietal lobes.

	Brain region	P-value	T-peak (P-value)	Coordinates x	y	z
1st-order:	Left precuneus (*PC*)	0.01	4.03(0.21)	-8	-52	30
	Right medial occipital lobe (*MO*)	0.14	3.26(>0.7)	14	-94	14
2nd-order:	Right lateral occipital lobe (*LO*)	0.00	5.23(0.00)	44	-78	8
	Left lateral occipial lobe (*LO*)	0.00	4.80(0.01)	-32	-74	20
	Right anterior superior parietal lobule (*ASPL*)	0.00	6.08(0.00)	36	-44	54
	Left anterior superior parietal lobule (*ASPL*)	0.01	6.18(0.00)	-32	-46	50

Table 4.1: Brain regions where a significant difference (p<0.05, except *MO*) in processing either stimulus condition was found, p-values are indicated for the clusters and the peak t-statistical value (corrected for multiple comparisons Worsley et al., 1996, 2002) with corresponding x, y and z stereotaxic-coordinates (Collins et al., 1994; Talairach and Tournoux, 1988). *MO* is shown in the table as well, beause it does reach significance (p=0.00) when taking predictions into account from current models (Wilson et al., 1992) and lesion data (Vaina et al., 1998, 2000); furthermore the *MO* activations reveal a trend which is significant in the VOI analysis (figure 4.5).

In the parietal lobe, cortical specializations for processing first- and second-order motion were found in the left precuneus (*PC*) and bilateral anterior superior parietal lob-

ule (*ASPL*) within the dorsal part of the intraparietal sulcus (IPS). These *ASPL* regions are known to respond to motion stimuli (Sunaert et al., 1999) and also to attentional tasks such as motion tracking (Culham et al., 1998, 2001a; Jovicich et al., 2001). In the same contiguous *ASPL* cluster in the right hemisphere, a visually distinct peak (t=5.14, p=0.00, xyz-coordinates=18,-66,54) was found more posterior within the middle superior parietal lobule (*MSPL*).

In the occipital lobe, a clear segregation of regions preferentially responding to each of the two types of motion was found. Responses driven more by second-order motion are apparent in higher visual areas at the edge and beyond the early retinotopically mapped visual cortex. Several peaks reach significance, all in the lateral occipital cortex (*LO*), in the vicinity of area hMT+. Drawn on top of the activation maps are the statistical probability anatomical map (SPAM) of area hMT+ taken from the five subjects in whom it was identified. The hMT+ SPAM suggests that the largest peak found to preferentially process second-order motion stimuli is slightly posterior to hMT+, and not hMT itself (indicated in Figure 4.4). Stronger fMRI (but not significant) responses elicited by first-order motion stimuli are located in the early visual areas (medial occipital cortex, *MO*). They are mentioned, however, because they are of interest, since activations would be predicted in V1 and V2 based on current models (Wilson et al., 1992) and lesion studies (Vaina et al., 1998). When this V1/V2 prediction is taken into account, this *MO*-cluster does reach significance (p=0.00). These occipital specializations (*MO* and *LO*) are in agreement with the lesion sites described by Vaina et al. (1996; 1998; 1999; 2000, as illustrated in figure 4.4), which were associated with selective deficits of first- and second-order motion perception.

To further identify the origin of the fMRI peaks in the occipital lobe (Figure 4.4), a volume-of-interest (VOI) analysis was performed in five subjects on the first seven visual areas: V1 to V7 including hMT+ (Figure 4.5).Areas V3b and V7 are included in this analysis because they may partially overlap with the *LO*-cluster, even though they are incompletely localized. However, including or excluding areas V3b and V7 in the VOI analysis does not alter our results or conclusions in any way. The complete *MO*-cluster was covered by these visual areas, which was not the case for the *LO*-cluster. The unidentified parts of the *LO*-

cluster were processed as a separate VOI, and most likely consist of several visual areas. This VOI is termed as LO– to indicate that identified visual areas have been removed from this VOI. Thus all occipital activations found in the stereotaxic-analysis were processed in the VOI-analysis.

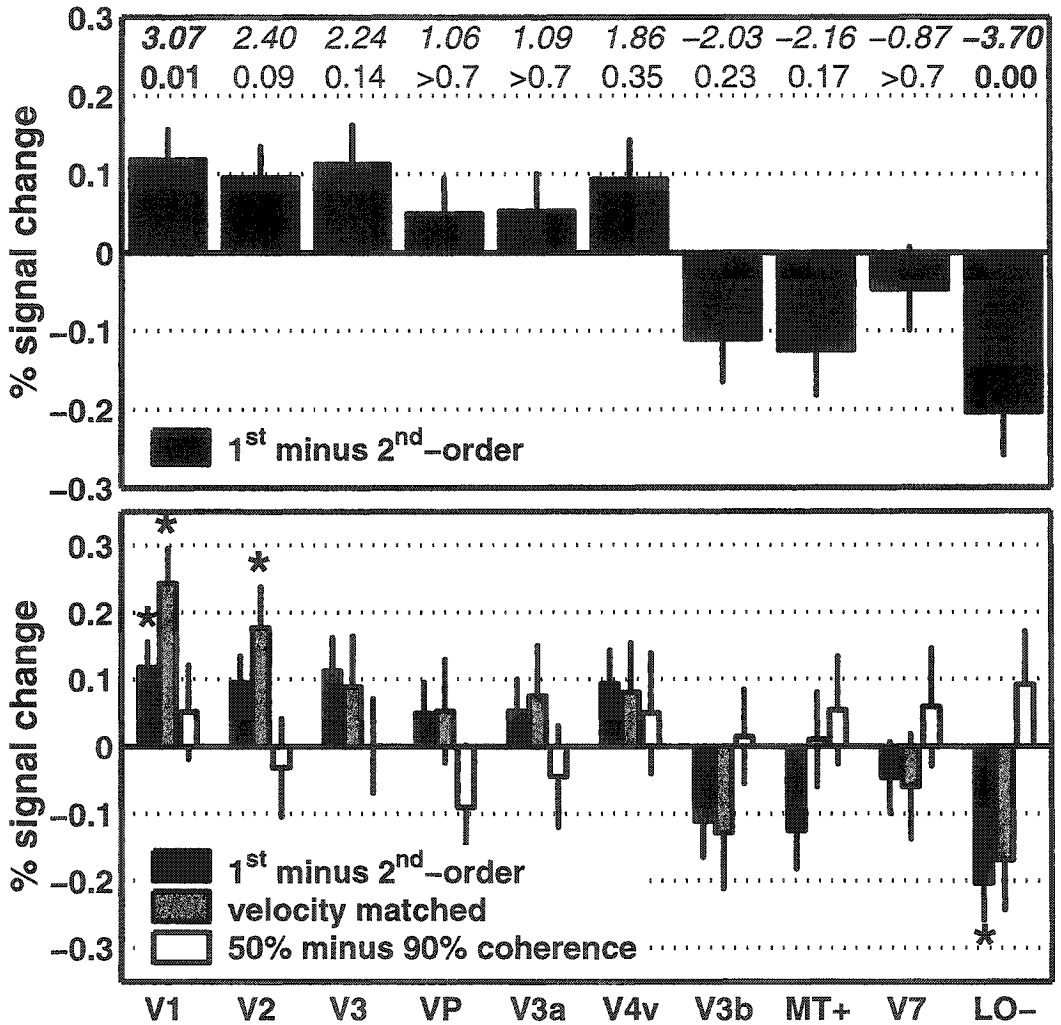

The VOI results (Figure 4.5, top panel) provide evidence for a stronger involvement of early visual areas (V1 and V2) in processing first-order motion, a trend that decreases and eventually reverses in higher visual areas. Significant differential activations are found in VOIs V1 and LO–. These results suggest that V1 (and V2: p=0.09) are responsible for the *MO* activation, and because no significant activation was determined for hMT+ (p=0.17),

Figure 4.5: Comparison of activation to first- and second-order motion in occipital visual areas. The *LO*-activation that was not covered by the identified visual areas is plotted as area LO–. Average fMRI percent signal changes and standard deviations for comparing first- and second-order stimulus conditions are plotted for the identified visual areas. The top part shows the results for each visual area comparing first- versus second-order motion (see figure 4.4). The results reveal the general trend that first-order motion is processed relatively more in early visual areas, a trend that disappears and then reverses in higher visual areas. The *t*-statistical (top) and corresponding Bonferroni-corrected p-values (bottom) comparing first- and second-order stimulus conditions for each area are shown as well. These *t*- and p-values indicate a significantly ($p<0.05$) stronger response to first-order motion in V1 and significantly stronger response to second-order in the undefined *LO* regions (LO–). These MR signal changes are relatively small, which can be attributed to the following facts. Firstly, all stimulus conditions contain first- and second-order noise, only the net-direction of motion can be determined by one mechanism. Secondly, this is a *relative* difference since all areas respond to all stimuli (but to a different degree). The bottom part shows the same results (black) with the results for two control conditions (gray & white). Significant values ($p<0.05$, corrected) are indicated with stars. The first control (gray bars) addressed whether the activation pattern can be explained by velocity differences present between the first- and second-order conditions. To this aim first- and second-order conditions were compared where the velocities were equal (see figure 4.1). The pattern is similar to the original results indicating that velocity-differences cannot explain the first- and second-order activation pattern. The second comparison, white bars, shows a control for coherence, which was used to equate the psychophysical performances for the first- and second-order conditions. In this control condition coherence was varied for a first-order stimulus version, taking coherence levels used in the first- and second-order comparison. A different pattern is found than for the first- and second-order activations illustrating that different coherence levels cannot explain the patterns found.

also confirm the previous suggestion that the main *LO*-activation peak is not hMT+.

The bottom panel shows the same VOI results with two control conditions, illustrating that the results can not be accounted for in terms of the different stimulus parameters (displacement and coherence) used. Firstly, the results might be explained by the velocity differences between first- and second-order conditions (due to different displacements, see Figure 4.1). Though a net velocity difference existed amongst our four stimulus configurations, one particular pair of first- and second-order conditions were velocity-matched. A comparison of these two conditions alone revealed a similar activation pattern (data shown for VOI analysis, figure 4.5, bottom panel, gray bars), indicating that velocity differences cannot account for the observed activation pattern, and furthermore may even have decreased activations in the early visual areas. A second possibility is that first- and second-order stimuli may have different stimulus signal-to-noise (SNR) levels due to the different coherences and lifetimes used. The different stimulus SNR levels were used to equate the conditions for their psychophysical performance (and thus perceptual SNR), with the aim to achieve similar neuronal load. Thus perceptually the stimuli did not contain different SNR levels, which is arguably more important than stimulus SNR levels. Nevertheless, control experiments were performed, using first-order motion, comparing the same coherence levels (50% and 90%) as used in the first- and second-order conditions. This data revealed a different and non-significant activation pattern (data shown for VOI analysis, figure 4.5, bottom panel, white bars). Based on this result the possibility of a coherence-confound seems very unlikely. We conclude that the different pattern of cortical activation produced by first- and second-order motion suggests a relative cortical specialization for the processing of these two different types of visual motion.

The coherence control indicates no significant differences of 50% versus 90% coherent motion, including area hMT+ (slightly stronger response to 50% coherent motion, if anything). This differs from that expected from previous fMRI and multi-unit electrophysiology studies (Heeger et al., 1999; Rees et al., 2000; Braddick et al., 2000; Singh et al., 2000; Braddick et al., 2001) that find a stronger response to coherent motion in hMT+ (but for an opposite result see McKeefry et al., 1997). This can be attributed to, firstly, stimulus

construction, i.e. the stimulus is constructed differently than in the previous studies, being narrow-band in both orientation and spatial frequency. Secondly, subjects were able to correctly detect the direction of motion in both conditions, indicating that perhaps the coherence differences, both suprathreshold, were not large enough to replicate the previous studies (using 0-100%). Thirdly, direction-discrimination for the 50% coherence condition is slightly harder, thereby requiring more attention which will increase hMT+ activation (O'Craven et al., 1997).

A methodological implication of these results is that a VOI analysis alone may lead to misinterpretations when neighboring areas are not processed. More specifically, taken with the *t*-statistical maps in Fig. 4.4, the bias of hMT+ to second-order motion (significant when uncorrected p-values are used) could be explained by a smearing of the activity of the adjacent area (*LO*-peak) due to blurring, resampling and partial volume effects, an interpretation which might be missed if the neighboring cortex was not also analyzed.

4.4 Discussion

Here we have shown relative cortical specializations using fMRI for first- and second-order mechanisms in both occipital and parietal cortex. We also have shown that these differences cannot be accounted for in terms of the parameters chosen to equate psychophysical performance and to force the observers' perceptual judgments by either mechanism (figure 4.5). These results differ from Smith et al. (1998) and Somers et al. (1999), where no cortical specialization (Somers et al., 1999) or some areas responding more to second-order motion were found. These differences can be explained by our different approach, where subjects were performing a psychophysical task in the scanner while controlling for differences in spatial and temporal properties, psychophysical performance and attention. Due to the nature of the stimulus construction, all stimulus conditions contained both first- and second-order structure; consequently only a *relative* cortical specialization could be determined, i.e. all areas responded to all stimulus conditions but to a different degree.

Our results are complementary to electrophysiological and psychophysical studies suggesting different mechanisms for processing first- and second-order motion (for reviews see Smith, 1994; Baker, 1999; Clifford and Vaina, 1999; Baker and Mareschal, 2001; Chubb et al., 2001; Lu and Sperling, 2001). In particular, our results are largely in agreement with single-unit recordings, where neurons responding to first- and second-order motion have been reported in relatively early (V1 and V2, e.g. Zhou and Baker, 1993; Chaudhuri and Albright, 1997; Mareschal and Baker, 1998a) and late (MT and neighbors, e.g. Albright, 1992; Geesaman and Andersen, 1996; O'Keefe and Movshon, 1998; Churan and Ilg, 2001) visual areas. This is in agreement with our finding that all areas responded to both first- and second-order stimuli. In agreement with our findings, electrophysiological studies describe a smaller proportion of neurons responding to second-order stimuli in early (area 17, 18) visual areas, where the response is weaker than to first-order stimulus versions (Zhou and Baker, 1993; Chaudhuri and Albright, 1997; Mareschal and Baker, 1998a). Lastly, neurons in area MT and neighbors have been suggested to be "form-cue-invariant" (Albright, 1992; Geesaman and Andersen, 1996) or at least to a larger degree than V1 (O'Keefe and Movshon, 1998), i.e. responses to both first and second-order motion. Consistent with this notion hMT+ did respond to both stimuli, though differing from these single-unit recordings by a stronger, but not significantly ($p=0.17$), response to second-order motion.

Our results are in broad agreement with studies of brain-damaged subjects, where lesion sites in occipital and parietal lobes differentially affect first- or second-order motion perception (Plant et al., 1993; Plant and Nakayama, 1993; Vaina and Cowey, 1996; Greenlee and Smith, 1997; Braun et al., 1998; Vaina et al., 1998, 1999, 2000). Lesions in the lateral parietal lobe have been reported to mainly affect second-order motion perception (Greenlee and Smith, 1997; Braun et al., 1998); in agreement with these results we find stronger second-order activations in the lateral parietal lobe. Particularly in the occipital lobe, our locations of cortical specializations agree remarkably well with the lesion sites of Plant and Nakayama (1993), Greenlee and Smith (1997), and especially with the results of Vaina et al. (1996; 1998; 1999; 2000) which provides a neurological "double dissociation". Plant and Nakayama (1993) and Vaina et al. (1996; 1999) describe lesions in the lateral occipital lobe

(roughly corresponding to the *LO* region found in this study, see figure 4.4), which selectively affects second-order motion perception. With occipital-temporal lesions in roughly similar locations, second-order direction-discrimination was found to be more impaired by Greenlee and Smith (1997). Vaina et al. (1998; 1999; 2000) describes other subjects with lesions in the vicinity of V2, to be severely impaired in first-order but not second-order motion perception; this location corresponds closely to the stronger activation to first-order motion in our studies in the early visual areas V1 and V2 (p=0.09, see figure 4.5).

Finally, relatively higher visual areas are involved in second-order motion perception suggesting a more complex analysis, as predicted by current models, such as the filter-rectify-filter (FRF) model (Chubb and Sperling, 1988; Wilson et al., 1992; Clifford and Vaina, 1999). Thus these results provide human imaging evidence for distinct first- and second-order motion mechanisms within and beyond the occipital lobe, that converges with psychophysical and electrophysiological studies, brain lesion sites and current models.

Besides a volume-of-interest analysis on the early visual areas, a stereotaxic analysis was performed (Talairach and Tournoux, 1988; Collins et al., 1994); revealing a cortical specialization in the parietal lobe. The *ASPL* region is known to be involved in motion processing (e.g. Sunaert et al., 1999), but the *PC* cluster remains more surprising. Not much is known about cortical areas in the medial parietal lobe (in human or non-human primates — Culham and Kanwisher, 2001), but our results would implicate some areas of the medial parietal lobe in motion processing, especially first-order motion.

In view of the involvement of parietal areas, which have been implicated in motion tracking (Culham et al., 1998, 2001a; Jovicich et al., 2001), it is worth asking whether the results imply a higher-level process (e.g. feature tracking) rather than a low-level mechanism (e.g. FRF model), as a substrate of second-order motion perception (Seiffert and Cavanagh, 1998; Derrington and Ukkonen, 1999)? We would argue against a role of high-level feature tracking in our particular second-order motion task for the following reasons. Firstly, while psychophysical studies using similar Gabor stimuli have demonstrated both kinds of contribution, the stimulus parameters used here should strongly favor the low-level mechanism (Bex and Baker, 1999; Ledgeway and Hess, 2000). Secondly, in the motion tracking studies

it is controversial whether those areas are driven by the attentional aspects of the task (Culham et al., 2001a; Jovicich et al., 2001). Thirdly, the other areas of the cortical network previously implicated in the process of motion tracking (Culham et al., 1998, 2001a; Jovicich et al., 2001) were not activated or equally activated by both stimuli. Fourthly, early visual areas, such as V3 and V3A, involved in motion processing but not motion tracking, were equally activated by first- and second-order motion. And finally, similar parietal regions responding to attentional tracking also exhibit activation to general motion stimuli (Cornette et al., 1998; Sunaert et al., 1999). Taken together these statements argue against a role of attentional tracking in these second-order motion conditions.

If the occipital and not parietal activations are related to the extraction of first- and second-order motion, as predicted by the FRF model, how should the parietal activation be interpreted? Perhaps the first- and second-order pathways remain partly distinct, even after both kinds of motions have been extracted, suggesting a differential contribution to higher visual functions. Thus the parietal activations could suggest a functional specialization of each mechanism. For example, the superior parietal lobule has been implicated in processing more complex motion stimuli such as biological motion (Grèzes et al., 2001; Vaina et al., 2001) and optic flow (De Jong et al., 1994; Peuskens et al., 2001; Ptito et al., 2001, but see Beer et al., 2002). In the study of Peuskens et al. (2001) two visual motion sensitive areas were implicated in heading judgments: hMT+, including an adjacent area, and a dorsal intraparietal sulcus area, predominantly in the right hemisphere. This pattern is similar to that found for second-order motion activation in our study. Thus the parietal activations might indicate a functional specialization for second-order motion in optic flow analysis, a suggestion that has received recent psychophysical support (Gurnsey et al., 1998; Dumoulin et al., 2001).

Chapter 5

Concluding remarks

In this final chapter the general results of the different thesis-chapters are linked and discussed. The future implications of this research will be discussed in a broad scope. A brief overview of the relevant findings is provided first.

5.1 Brief overview and summary

Both chapters 2 and 4, using limited-lifetime Gabor stimuli (Baker and Hess, 1998), provided evidence for separate mechanisms for the extraction of first- and second-order motion. In addition, chapter 2 established the presence of second-order mechanisms in peripheral vision for this stimulus, an issue that has been controversial. The notion of distinct mechanisms was further strengthened by the finding of a different behavior in peripheral vision, i.e. a centrifugal bias for second- but not first-order motion (chapter 2), and distinct cortical activation patterns (chapter 4). Furthermore, both studies implicated, a contribution of the second-order mechanism to optic flow analysis, because 1) it is a possible explanation for the directional anisotropies (chapter 2), and 2) of the similarities between areas preferentially responding to second-order motion and brain regions involved in processing optic flow stimuli (chapter 4). The question why second-order might be involved in optic flow will be discussed in section 5.4.

A novel method was developed to segment early visual areas (chapter 3). The main advantage of this method is that it does not require a cortical surface reconstruction. The

implications of this method, especially regarding cortical surfaces, is discussed in section 5.2. Typically, the identified visual areas are used for a volume of interest (VOI) analysis (see chapter 4 and Barnes et al., 2003; Achtman et al., 2003). The relationship between a VOI analysis and a more standard stereotaxic analysis will be discussed in section 5.3. These two sections will be discussed first, and in a final section (5.5) possible future directions of this research will be discussed.

5.2 Cortical surfaces

In chapter 3, a retinotopic mapping method was introduced that does not require an explicit reconstruction of the cortical surface. The surface normals are taken directly from the aMRI volume rather than from the the explicitly reconstructed surface. Due to absence of a cortical surface reconstruction and no additional elaborate processing steps, this method provides a marked simplification of the analysis compared with precious surface-based methods (Sereno et al., 1995; DeYoe et al., 1996; Engel et al., 1997). In these paragraphs the use of cortical surfaces as they apply to visual area identification and functional imaging, as used in this thesis, are discussed.

In some cases, cortical surfaces are still required for visual area identification. The VFS identification (either volumetric or surface-based) requires three vectors: eccentricity, polar-angle and surface-normal. If one of them cannot be assessed then the VFS can not be computed. Either eccentricity or polar-angle maps may not be reconstructed because 1) that particular dimension was not retinotopically preserved in that visual area, or 2) it can not be acquired due to methodological limitations. For example, Sereno et al. (2001) only identified the polar-angle information (i.e. no eccentricity), requiring manual delineation on a cortical surface of a putative homologue of area LIP in humans. Similarly, Levy et al. (2001) was only able to determine an eccentricity map (i.e. no polar-angle) in human object areas. Thus, if one of the three vectors cannot be acquired, the visual area identification has to be performed manually on a explicitly reconstructed cortical surface.

As mentioned in chapter 3, the cortical surfaces are still used to *display* and *interpret* the data. Especially for the untrained eye, identification of the different visual areas is easier on the surfaces where all areas can be viewed simultaneously, and the striped alternating VFS pattern is clearly revealed. Cortical surfaces are also used to display and interpret the data in chapter 4 (figure 4.4). Like the retinotopic mapping, the t-statistical analysis is performed on the volumetric data, which is then displayed on an average unfolded surface, together with other data (identified areas).

If the visual area layout, as displayed on a cortical surface (either method) deviates from the typical organization; then this could be due to methodological issues, i.e. errors in surface reconstruction, or have a neurobiological basis, i.e. normal variations or pathological symptoms. In our method, the correctness of the surface-display can be assessed by comparison to the volumetric data, enabling identification of methodological errors related to the surface display. This verification would not be available in a surface-based analysis.

5.3 Stereotaxic and VOI analysis

5.3.1 VOI analysis

Commonly, visual area identification is a precursor to functional studies, where the areas are used for a VOI analysis (see sections 1.5, 1.6.2, and for examples see chapter 4 and Barnes et al., 2003; Achtman et al., 2003). For a VOI analysis, the final result of the retinotopic mapping should be a volume of functionally homogeneous voxels, which is directly supplied by our method without an intermediate cortical surface resampling step. The VOI analysis provides an improved SNR due to intra- and inter-subject averaging. In inter-subject averaging, VOIs can be averaged together directly rather than by stereotaxic averaging, i.e. averaging of similar coordinates after normalization for brain position, orientation and size (Collins et al., 1994; Talairach and Tournoux, 1988). Intra-subject averaging takes the mean response of a given area, with the underlying assumption of a homogeneous visual processing. The amount of SNR improvement due to intra-subject averaging depends on the size

of the area, i.e. the larger the area the more signal averaging can occur. The volume of the regions (in cm^3 and number of functional voxels) is shown in Table 5.1. In this table left and right hemispheres are averaged together, as well as the dorsal and ventral parts of V2 (as in chapter 4). These values indicate the volume of the regions as provided by the retinotopic mapping, i.e. these volumes do not represent surface areas but voxels whose response reflect activity of that particular visual area. These volume sizes will be smaller in the VOI analysis, due to resampling effects and exclusion criteria, i.e. exclusion of "noisy" voxels and narrowing to the relevant eccentricity range (see chapter 4). Large differences (up to factor 5 in relative proportions, last column) are found, hence demonstrating that the statistical power of the VOI analysis differs across visual areas, due to different amounts of intra-subject averaging.

Visual area	N	Stereotaxic-space (cm^3)	Native-space (cm^3)	# fMR voxels ($4mm^3$)	Rel. proportions
V1	7	15.6 ±2.4	13.2 ±1.9	206 ±29	1.00 ±0.14
V2	7	14.2 ±5.3	12.0 ±4.4	188 ±69	0.91 ±0.33
V3	7	3.7 ±0.7	3.2 ±0.7	50 ±11	0.24 ±0.06
VP	7	5.7 ±1.8	4.8 ±1.7	75 ±26	0.37 ±0.13
V3A	7	7.1 ±3.4	6.1 ±3.5	96 ±54	0.47 ±0.27
V4v	7	4.0 ±0.6	3.3 ±0.5	52 ±07	0.25 ±0.03
hMT+	5	3.1 ±2.5	2.6 ±2.1	41 ±32	0.20 ±0.15

Table 5.1: The mean and standard deviation of visual area volumes are given in stereotaxic (Collins et al., 1994; Talairach and Tournoux, 1988) and native space (cm^3). The last two columns show the number of fMR voxels ($4mm^3$) as used in the studies here (see chapters 3 and 4), and area volumes relative to area V1. Decreasing volumes are found for higher visual areas, i.e. V1>V2>V3/VP. The size of the area indicates the SNR improvement that may be achieved due to intra-subject averaging of voxels within the same area.

A large variation across subjects in the size of individual areas is found in agreement with histological (e.g. Andrews et al., 1997) and brain imaging studies (Dougherty et al., 2002). In addition, a decreasing volume was found for higher visual areas, i.e. V1>V2>V3/VP (on a relative scale: 1.00>0.91>0.61, see table 5.1). This result is in conflict with the results of Dougherty et al. (2002, V2(1.16)>V1(1.00)>V3/VP(0.84)), who measured visual areas sizes (mm^2) on a cortical surface. In histological studies, a larger volume of V1 (area 17) than V2 (area 18) is reported in humans by some (Amunts et al., 2000) but not others (Roland et al., 1997). In non-human primates, a larger V1 than V2 has been reported by several studies (Krubitzer and Kaas, 1990; Pessoa et al., 1992; Rosa et al., 1997). Thus, the sizes of the visual areas (table 5.1) are biologically plausible.

5.3.2 Stereotaxic *versus* VOI analysis

Identification of cortical areas allows for a volume-of-interest (VOI or ROI) analysis of those cortical areas (see previous section and chapters 3 and 4). That is, voxels within an identified area (VOI) are averaged within and across subjects without the need for a spatial normalization/alignment. A VOI analysis can increase the SNR as compared to standard stereotaxic methods (Talairach and Tournoux, 1988; Collins et al., 1994), where voxels of similar coordinates are averaged together, after spatial normalization/alignment. This has led a number of studies to only report a VOI analysis (e.g. Smith et al., 1998, as mentioned in chapter 4). Even though the VOI analysis is more powerful, I would argue it is complementary to stereotaxic methods, rather than replacing them, for the following reasons.

Firstly, only a few human visual areas have been identified compared to non-human primates — about half of the primate cerebral cortex responds to visual stimuli with about 30 identified visual areas (Felleman and Van Essen, 1991). Furthermore, only a few of the known human visual areas are localized in each study (e.g. first 5 to 7 visual areas in chapter 4 and Barnes et al., 2003; Achtman et al., 2003). Thus, performing a VOI analysis may limit the interpretation to those identified areas, whereas they may not necessarily be the only ones processing the stimulus. For example, one of the contributions of fMRI to motion vision

was to identify cortical areas processing motion in occipital and parietal lobes beyond the well described ones (see chapter 1 and the parietal activations in chapter 4). Even if those identified areas are assumed to be the primary areas involved, only a stereotaxic analysis, unlike the VOI analysis, is able to validate this assumption.

Secondly, a VOI analysis alone might fail to reveal alternative interpretations of the data. For instance, chapter 4 found area hMT+ to be more involved in processing second-order motion than any other identified area (see figure 4.5). Hence, a cortical locus for second-order processing in hMT+ might be postulated. This bias for processing second-order motion is also revealed in the stereotaxic analysis (figure 4.4). However, the peak of the second-order activations is slightly posterior to hMT+, suggesting that hMT+ is *not* the primary cortical region processing second-order motion. In an extreme case, one could even argue that the hMT+ second-order activation may be produced by partial volume and/or blurring effects of the more posterior activations. Either interpretation would have been missed if a stereotaxic analysis was not performed.

In conclusion, due to the relatively limited functional areas available for a VOI analysis, the stereotaxic and VOI analysis are complementary. Not performing a stereotaxic analysis may unnecessarily limit the interpretations of the data.

5.4 Optic flow

Optic flow includes motion patterns on the retina elicited by self motion, which can serve as a proprioreceptive sense. The results of chapters 2 and 4 suggest a role for the second-order mechanism in optic flow analysis, even though no actual optic flow stimuli were produced, i.e. flow patterns induced by subject movement. Three possible hypothesis are proposed addressing why second-order mechanisms are involved in optic flow analysis.

A possible explanation for these findings may be found in the stimulus statistics. That is, optic flow can be regarded as a second-order stimulus, since it potentially requires integration of differential motion vectors across the visual field. Hence, optic flow stimuli and our contrast-defined stimuli may be processed, in principal, by similar second-order

mechanisms. This hypothesis would predict that, the reported anisotropy (chapter 2) would be present for first-order defined optic flow stimulus versions as well, as then they can be regarded as second-order.

A second hypothesis is that local second-order information is used for extracting optic flow information, thus in effect a fourth-order stimulus. This argument is supported by results from Gurnsey et al. (1998), who found that both first- and second-order motions contribute to vection, i.e. induced perception of self-motion by image flow. On theoretical grounds, second-order structure provides information on a coarser scale (low-pass) than first-order structure (Schofield and Georgeson, 2003), and furthermore, would be more sensitive to object-borders rather than textures on the surfaces of those objects. Assuming that objects in our visual world provide landmarks useful for navigation, this could be a reason why second-order information may be used to extract optic flow. In agreement with these arguments, Warren et al. (2001) found that subjects' walking trajectories relied more on optic flow when objects were inserted in a virtual environment.

Heading judgments from optic flow are hypothesized to be based on an estimate of the focus of expansion (FOE; Gibson, 1954). However, eye- and head-movements distort the retinal heading motion vectors and can displace the FOE away from the heading direction, i.e. the FOE is now closer to the point of fixation (Regan and Beverley, 1982). In order to correctly detect the heading-direction from optic flow, the flow field due to our heading-direction has to be separated from the flow field elicited by our eye- and/or head-movements. Evidence exists that this problem can be solved by retinal motion vectors only (Perrone, 2001). As a third hypothesis, second-order mechanisms, in conjunction with first-order ones, may be used for flow field separation. Given that 1) the second-order mechanisms are less sensitive to motion towards the fovea (chapter 2, Dumoulin et al., 2001), and 2) second-order mechanisms require longer durations to detect the direction-of-motion (Derrington et al., 1993; Ledgeway and Hess, 2002), then the second-order mechanisms may respond differently to optic flow patterns contaminated with eye- and head-induced motion vectors, than the first-order ones. Therefore, two distinct response patterns may be acquired which could be used to dissociate the two different flow fields, e.g. two variables and two

equations. Thus, in this third hypothesis, the different properties of second-order mechanisms are used to segregate the optic flow field to correctly compute the heading direction.

5.5 Future work

As common with research, more questions were raised than answered, providing a number of new research directions. Logical development of these research projects would follow four lines.

Firstly, since optic flow has been closely linked with our second-order stimuli, it would be appropriate to use the limited-lifetime Gabor stimuli in a optic flow configuration. This may shed light on the questions if and why second-order motion is involved in optic flow analysis (see section 5.4). Furthermore, it would allow the relative contributions of first- and second-order motion to optic flow to be assessed within the same stimulus. It would also be interesting to know whether this directional anisotropy is present in other types of second-order stimuli as well.

Secondly, the retinotopic mapping method can be developed further. At the time of writing, the visual areas are automatically segmented but manually identified. The visual area identification step could be performed automatically by matching templates (e.g. Collins et al., 1995; Le Goualher et al., 1999; Brewer et al., 2002). Furthermore, the mapping stimulus could be optimized to more strongly activate higher-order visual areas which now only weakly respond to the flickering circular checkerboard parts (e.g. incorporating color, objects or motion in the wedges and circles: Hadjikhani et al., 1998; Levy et al., 2001; Huk et al., 2002).

Thirdly, a large variability of the location of cortical areas across subjects in a stereotaxic space (Collins et al., 1994; Talairach and Tournoux, 1988) was found, and it was determined that this was not due to methodological issues. This variability thus reflects misalignments in gross anatomy, and/or variations in the relationship between gross anatomy and functional areas. Since a close correspondence between V1 and the calcarine sulcus has been described by several studies (Stensaas et al., 1974; Rademacher et al., 1993; Gilis-

sen et al., 1995; Gilissen and Zilles, 1996), the prediction would be that the majority of the misalignment is due to variations in gross anatomy. Identification of gross anatomical structures with or without non-linear alignment may shed light on the origins of this variability and the nature of the relationship between gross anatomy and functional areas (see for example: Dumoulin et al., 2000).

Fourthly, the issue of a cortical specialization for first- and second-order motion has been addressed in chapter 4. Like previous studies (Smith et al., 1998; Somers et al., 1999), this was a "bottom-up" approach, where stimulus parameters were manipulated to force the detection of the direction of motion by either mechanism. While, the stimulus differences between first- and second-order versions were small and generally not noticed by the naive observers, they are nonetheless there. Therefore, control experiments were required (see figure 4.5) to assess the effects of these manipulations. A way around this would be to perform "top-down" experiments where the attention of the subjects is directed to either first- or second-order stimulus aspects of identical stimuli containing both first- and second-order motion, simultaneously (see for example: Corbetta et al., 1990).

Appendix A

Two-step statistical approach: search region and HRF-estimation

In chapter 4, a two-step statistical approach was used. This approach has several advantages, though the chapter mentions only one. Here the approach and advantages, in data interpretation and analysis, are described in detail.

A.1 Interpretation advantages

In chapter 4, a stimulus design was used with three different conditions: fixation, first- and second-order motion. Such a stimulus design with three conditions is quite common. That is, a third condition (C, i.e. fixation), besides the main two of interest (A & B, i.e. motion conditions), is inserted. This has several advantages, for example one can assess whether the difference found between A and B is due to an increase or decrease relative to the baseline condition (C). Please note that this is a relative baseline and not an absolute one, i.e. neuronal processing is present in the baseline condition. Furthermore, the baseline condition (C) contrasted with the conditions of interest (A & B) reveals a more complete, but less specific, activated brain pathway (Buckner et al., 1996).

Another advantage of such a design would be to validate the analysis. For instance, if the comparison (A versus B) would not have yielded any differential activation, it could have been because 1) they are processed to the same extent in the same cortical areas (for the

first- versus second-order comparison, chapter 4, as suggested by Greenlee and Smith, 1997; Somers et al., 1999), 2) a difference is present but at too small SNR to reach significance, or 3) an error occurred during any of the preprocessing or analysis steps. The advantage of the two-step stimulus design would be to dissociate between these possible explanations, i.e. in the first two cases the first statistical comparison (C versus AB; i.e. the average, or maximum, response of A & B) would still reveal large activations, whereas in the last case it would not (Buckner et al., 1996).

The disadvantage of inserting the third condition (C) is that this data does not address the primary question (A versus B), i.e. time and data needed for condition (C) are generally not used for the actual comparison of interest (A versus B). Thus, statistical power is sacrificed. However, in the next section two advantages of the approach are presented, potentially increasing statistical sensitivity for the comparison of interest (A versus B).

A.2 Analysis advantages

In chapter 4, a two-step statistical procedure was used. In short, the procedure first compared motion versus blank (AB versus C), after which the two motion conditions (A versus B) were compared. The first comparison (AB versus C) is known to elicit strong responses in occipital cortex, whereas it was uncertain whether the second comparison (A versus B) would reveal any activations.

A.2.1 Search region

This procedure has two general advantages for the statistical analysis, though the chapter mentions only one, i.e. the first comparison (C versus AB) narrows the search region for the second statistical comparison (A versus B). This is justified because cortical regions that do not respond to the stimulus (AB) would not respond differentially to the various stimulus versions either. Narrowing the search region allows the statistical threshold to be lowered thereby increasing statistical sensitivity (i.e. reduction of correction for multiple compar-

isons, Worsley et al., 1996, 2002).

If this procedure is used, care has to be taken to not a priori exclude regions from the second analysis (AB). This can be accomplished and verified in the following ways (see chapter 4). Firstly, to not a priori exclude certain regions, a low *un*corrected threshold for the comparison AB versus C was used. Secondly, the effect of this threshold was robust over a range of values. Thirdly, the results for the (AC) and (BC) comparisons were very similar, indicating that the AB versus C comparison contained all regions found in the individual (AC and BC) comparisons. This does not necessarily need to be the case (e.g. A>C>B), in which case the comparison of C versus AB should be a maximum response of A & B (i.e. the opposite of a conjunction analysis).

A.2.2 HRF estimation

As a second advantage, the first statistical analysis (C versus AB) allows a robust estimation of the average hemodynamic response function (HRF), due to the known robust response to all stimulus attributes. Since the statistical analysis, as performed here (Worsley et al., 2002), fits a linear prediction to the MR data, the more accurate the prediction (including HRF-model), the more powerful the statistical analysis (e.g. Friston et al., 1995a,b; Boynton et al., 1996; Glover, 1996; Cohen, 1997; Dale and Buckner, 1997; Rajapakse et al., 1998; Goutte et al., 2000; Miezin et al., 2000; Gössl et al., 2001; Bénar et al., 2002; Worsley et al., 2002; Handwerker et al., 2002). This may be especially relevant given that HRFs may differ between stimuli, subjects and brain regions (Buckner et al., 1996; Kim et al., 1997; Aguirre et al., 1998; Friston et al., 1998; D'Esposito et al., 1999b; Miezin et al., 2000; Duann et al., 2002). The derived HRFs for each subject can be seen in figure A.1.

To briefly explain this process, let $m(t)$ be the measured MR time series and $h(t)$ the HRF. In a linear system with additive noise ($n(t)$) the response to the stimulus sequence ($s(t)$) should be:

$$m(t) = s(t) * h(t) + n(t), \tag{A.1}$$

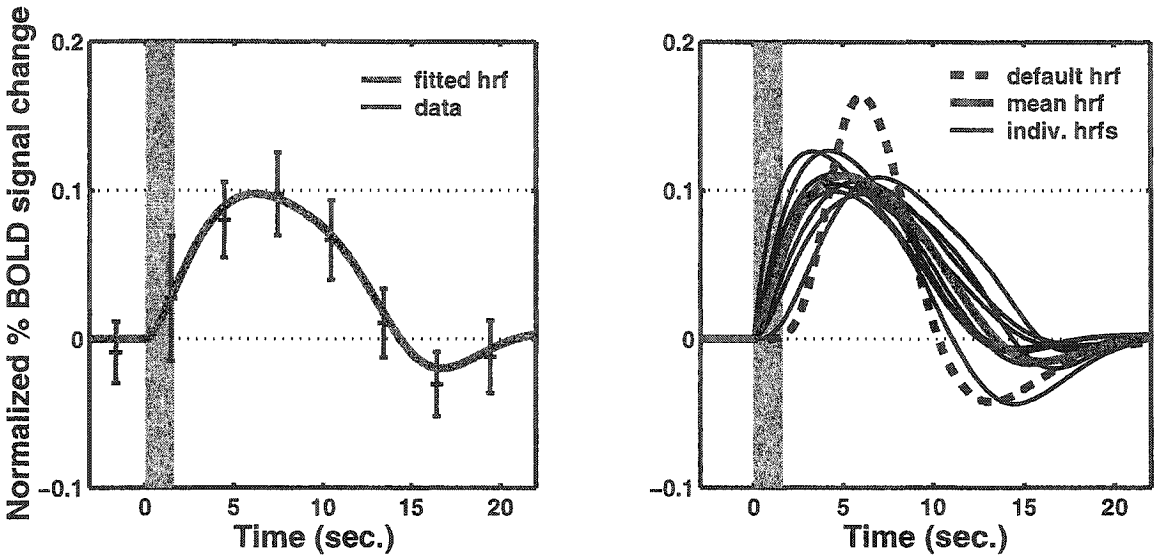

Figure A.1: Estimated hemodynamic response functions (HRF) by deconvolution of the average MR time series by the stimulus sequence. The gray bar indicates the onset and duration of the stimulus. Left panel illustrates the deconvolved MR data (mean and standard deviation) and fitted model of one subject (TL). The right panel shows the results of all eight subjects with the mean and default HRF (Glover, 1996; Worsley et al., 2002).

where $*$ denotes convolution. Given the high SNR of the signal, further improved by averaging runs ($\leq$10), blocks (4) and voxels ($\sim$5000), $n(t)$ approximates zero. Hence, the equation can be simplified to:

$$m(t) = s(t) * h(t). \tag{A.2}$$

Thus, the HRF can be estimated by deconvolution without the need for any temporal filtering. Typically, averaging blocks and voxels yielded a good estimate of the HRF, therefore the process was repeated for each run allowing a mean and standard deviation to be computed across runs (see figure A.1, left panel). The HRF was then modeled by the difference of two gamma functions (as used in Glover, 1996; Worsley et al., 2002), minimizing mean square error (mse).

The empirically derived HRFs differ from the default HRF used by Worsley et al. (2002), estimated for auditory stimuli by Glover (1996). This may reflect differences in

auditory-visual processing, scanning parameters, or task design, i.e. block versus event-related (see for similar design differences: Boynton et al., 1996). The HRFs describes the average HRF for each subject, i.e. due to the extensive averaging the HRF is a mean for the different stimulus conditions and cortical areas.

However, using the estimated HRF only altered the results minimally, and therefore the default HRF (Glover, 1996; Worsley et al., 2002) was used. This can mainly be attributed to the design of the experiment, which was a block design (block length: 30 sec). In such a design either model, default or estimated HRF, reach a steady-state during each block. Therefore, the differences between the HRF models are apparent primarily during the transitions of the blocks. This was verified with simulations (using default and mean HRF, see figure A.1). These simulations further revealed that a random reordering of the timing of different stimulus presentations, i.e. event-related design, would not only distribute the difference in predicted responses throughout the duration of the scan, but also increase the mean square difference between the two models (times 2.5). Thus, an accurate HRF-model would be more important in more stochastic (event-related) fMRI designs (e.g. Buckner et al., 1996; Josephs et al., 1997; Buckner, 1998; Rosen et al., 1998; Friston et al., 1999; D'Esposito et al., 1999a), rather than in a block-design as used here. Nevertheless, the feasibility of a simplified HRF-estimation in the two-step analysis is demonstrated.

References

Achtman, R. L., Dumoulin, S. O., Ledgeway, T., and Hess, R. F. (2003). Processing of global spatial structure in striate and extra-striate cortex: An fMRI study. *J. Neurophysiol.*, Submitted.

Adelson, E. A. and Bergen, J. R. (1985). Spatiotemporal energy models for the perception of motion. *J. Opt. Soc. Am. A*, 2: 284–299.

Aguirre, G. K., Zarahn, E., and D'Esposito, M. (1998). The variability of human BOLD hemodynamic responses. *Neuroimage*, 8: 360–369.

Aine, C. J., Supek, S., George, J. S., Ranken, D., Lewine, J., Sanders, J., Best, E., Tiee, W., Flynn, E. R., and Wood, C. C. (1996). Retinotopic organization of human visual cortex: departures from the classical model. *Cereb. Cortex*, 6(3): 354–61.

Albright, T. D. (1989). Centrifugal directional bias in the middle temporal visual area (MT) of the macaque. *Vis. Neurosci.*, 2: 177–188.

Albright, T. D. (1992). Form-cue invariant motion processing in the primate visual cortex. *Science*, 255: 1141–1143.

Allen, D. and Hess, R. F. (1992). Is the visual field temporally homogeneous? *Vision Res.*, 32(6): 1075–1084.

Allen, H. A. and Derrington, A. M. (2000). Slow discrimination of contrast-defined expansion patterns. *Vision Res.*, 40(7): 735–744.

Amunts, K., Malikovic, A., Mohlberg, H., Schormann, T., and Zilles, K. (2000). Brodmann's areas 17 and 18 brought into stereotaxic space — where and how variable?. *Neuroimage*, 11(1): 66–84.

Andrews, T. J., Halpern, S. D., and Purves, D. (1997). Correlated size variations in human visual cortex, lateral geniculate nucleus, and optic tract. *J. Neurosci.*, 17(8): 2859–2868.

Arnold, J. B., Liow, J.-S., Schaper, K. A., Stern, J. J., Sled, J. G., Shattuck, D. W., Worth,

A. J., Cohen, M. S., Leahy, R. M., Mazziotta, J. C., and Rottenberg, D. A. (2001). Qualitative and quantitative evaluation of six algorithms for correcting intensity nonuniformity effects. *Neuroimage*, 13(5): 931–943.

Ashida, H., Robin, N., Kaneko, H., Verstraten, F. A. J., and Ojima, S. (1997). Second-order motion has little effect on human postural control. *Investigative Ophthalmology and Visual Science*, 37: S743.

Bakan, P. and Mizusawa, K. (1993). Effect of inspection time and direction of rotation on a generalized form of the spiral aftereffect. *J. Exp. Psychol.*, 65: 583–586.

Baker, Jr., C. L. (1999). Central neural mechanisms for detecting second-order motion. *Curr. Op. Neurobiol.*, 9: 461–466.

Baker, Jr., C. L. and Braddick, O. J. (1985). Eccentricity-dependent scaling of the limits for short-range apparent motion perception. *Vision Res.*, 25: 803–812.

Baker, Jr., C. L. and Hess, R. F. (1998). Two mechanisms underlie processing of stochastic motion stimuli. *Vision Res.*, 38: 1211–1222.

Baker, Jr., C. L., Hess, R. F., and Zihl, J. (1991). Residual motion perception in a "motion-blind" patient, assessed with limited-lifetime random dot stimuli. *J. Neurosci.*, 11: 454–461.

Baker, Jr, C. L. and Mareschal, I., (2001). Processing of second-order stimuli in the visual cortex. In Casanova, C. and Ptito, M., editors, *Progress in brain research*. Elsevier Science, Amsterdam, pp. 1–21.

Ball, K. and Sekuler, R. (1980). Human vision favors centrifugal motion. *Perception*, 9: 317–325.

Bandettini, P. A., Wong, E. C., Hinks, R. S., Tikofsky, R. S., and Hyde, J. S. (1992). Time course EPI of human brain function during task activation. *Mag. Res. Med.*, 25: 390–397.

Bandettini, P. A. and Ungerleider, L. G. (2001). From neuron to BOLD: new connections. *Nat. Neurosci.*, 4(9): 864–866.

Bardy, B. G., Warren, W. H., and Kay, B. A. (1999). The role of central and peripheral vision in postural control during walking. *Percept. Psychophys.*, 61(7): 1356–1368.

Barnes, G. R., Dumoulin, S. O., Achtman, R. L., Beaudot, W. H. A., and Hess, R. F. (2003). Does contour integration represent a special case of figure/ground processing? *Vis. Neurosci.*, Submitted.

Baseler, H. A., Brewer, A. A., Sharpe, L. T., Morland, A. B., Jägle, H., and Wandell, B. A. (2002). Reorganization of human cortical maps caused by inherited photoreceptor abnormalities. *Nat. Neurosci.*, 5: 364–370.

Baseler, H. A., Morland, A. B., and Wandell, B. A. (1999). Topographic organization of human visual areas in the absence of input from primary cortex. *J. Neurosci.*, 19(7): 2619–2627.

Beauchamp, M. S., Cox, R. W., and DeYoe, E. A. (1997). Graded effects of spatial and featural attention on human area MT and associated motion processing areas. *J. Neurophysiol.*, 78: 516–520.

Beer, J., Blakemore, C., Previc, F. H., and Liotti, M. (2002). Areas of the human brain activated by ambient visual motion, indicating three kinds of self-movement. *Exp. Brain Res.*, 143(1): 78–88.

Belliveau, J. W., Kennedy, D. N., McKinstry, R. C., Buchbinder, B. R., Weisskoff, R. M., Kohen, M. S., Vevea, J. M., Brady, T. J., and Rosen, B. R. (1991). Functional mapping of the human visual cortex by magnetic resonance imaging. *Science*, 254: 716–719.

Bénar, C.-G., Gross, D. W., Wang, Y., Petre, V., Pike, B., Dubeau, F., and Gotman, J. (2002). The BOLD response to interictal epileptiform discharges. *Neuroimage*, 17: 1182–1192.

Benton, C. P., Johnston, A., McOwan, P. W., and Victor, J. D. (2001). Computational modeling of non-fourier motion: further evidence for a single luminance-based mechanism. *J. Opt. Soc. Am. A*, 18(9): 2204–2208.

Bex, P. J. and Baker, Jr., C. L. (1997). The effects of distractor elements on direction discrimination in random Gabor kinematograms. *Vision Res.*, 37: 1761–1767.

Bex, P. J. and Baker, Jr., C. L. (1999). Motion perception over long interstimulus intervals. *Percept. Psychophys.*, 61: 1066–1074.

Boulton, J. C. and Baker, Jr., C. L. (1991). Motion detection is dependent on spatial frequency not size. *Vision Res.*, 31: 77–87.

Boulton, J. C. and Baker, Jr., C. L. (1993). Dependence on stimulus onset asynchrony in apparent motion: evidence for two mechanisms. *Vision Res.*, 33: 2013–2019.

Boulton, J. C. and Baker, Jr., C. L. (1993). Different parameters control motion perception above and below a critical density. *Vision Res.*, 33: 1803–1811.

Boulton, J. C. and Baker, Jr., C. L. (1994). Psychophysical evidence for both a "quasi-linear" and a "nonlinear" mechanism for the detection of motion. In Lawton, T., editor, *Computational vision based on neurobiology*, volume 2054, pp. 124–133.

Boynton, G. M., Engel, S. A., Glover, G. H., and Heeger, D. J. (1996). Linear systems analysis of functional magnetic resonance imaging in human V1. *J. Neurosci.*, 16 (13): 4207–4221.

Braddick, O. (1974). A short-range process in apparent movement. *Vision Res.*, 14: 519–527.

Braddick, O. J., O'Brien, J. M., Wattam-Bell, J., Atkinson, J., and Turner, R. (2000). Form and motion coherence activate independent, but not dorsal/ventral segregated, networks in the human brain. *Curr. Biol.*, 10(12): 731–734.

Braddick, O. J., O'Brien, J. M., Wattam-Bell, J., Atkinson, J., and Turner, R. (2001). Brain areas sensitive to coherent visual motion. *Perception*, 30(1): 61–72.

Braun, D., Petersen, D., Schonle, P., and Fahle, M. (1998). Deficits and recovery of first- and second-order motion perception in patients with unilateral cortical lesions. *Eur. J. Neurosci.*, 10(6): 2117–2128.

Brewer, A. A., Press, W. A., Logothetis, N. K., and Wandell, B. A. (2002). Visual areas in macaque cortex measured using functional magnetic resonance imaging. *J. Neurosci.*, 22(23): 10416–10426.

Buckner, R. L. (1998). Event-related fMRI and the hemodynamic response. *Hum. Brain. Mapp.*, 6: 373–377.

Buckner, R. L., Bandettini, P. A., O'Craven, K. M., Savoy, R. L., Petersen, S. E., Raichle, M. E., and Rosen, B. R. (1996). Detection of cortical activation during averaged

single trials of a cognitive task using functional magnetic resonance imaging. *Proc. Natl. Acad. Sci. USA*, 93: 14878–14883.

Burr, D. C. and Ross, J. (2002). Direct evidence that "speedlines" influence motion mechanisms. *J. Neurosci.*, 22(19): 8661–8664.

Camhi, J. M., (1984). Visual worlds. In *Neuroethology: nerve cells and the natural behaviour of animals*. Sinauer Associates Inc., Sunderland, Mass., USA, pp. 109–156.

Cavanagh, P. (1992). Attention-based motion perception. *Science*, 257: 1563–1565.

Cavanagh, P. and Mather, G. (1989). Motion: the long and short of it. *Spat. Vis.*, 4: 103–129.

Chaudhuri, A. and Albright, T. D. (1997). Neuronal responses to edges defined by luminance vs. temporal texture in macaque area V1. *Vis. Neurosci.*, 14(5): 949–962.

Chubb, C., Olzak, L., and Derrington, A. (2001). Second-order processes in vision: introduction. *J. Opt. Soc. Am. A*, 18(9): 2175–2178.

Chubb, C. and Sperling, G. (1988). Drift-balanced random stimuli: a general basis for studying non-Fourier motion perception. *J. Opt. Soc. Am. A*, 5: 1986–2007.

Chun, M. M. and Marois, R. (2002). The dark side of visual attention. *Curr. Op. Neurobiol.*, 12: 184–189.

Chung, M. K., Worsley, K. J., Taylor, J., Ramsay, J., Robbins, S., and Evans, A. C. (2001). Diffusion smoothing on the cortical surface. *Neuroimage*, 13: S95.

Churan, J. and Ilg, U. J. (2001). Processing of second-order motion stimuli in primate middle temporal area and medial superior temporal area. *J. Opt. Soc. Am. A*, 18(9): 2297–2306.

Clarke, S. and Miklossy, J. (1990). Occipital cortex in man: organization of callosal connections, related myelo- and cytoarchitecture, and putative boundaries of functional visual areas. *J. Comp. Neurol.*, 298: 188–214.

Clifford, C. W. G., Freedman, J. N., and Vaina, L. M. (1998). First- and second-order motion perception in gabor micropattern stimuli: psychophysics and computational modelling. *Cogn. Brain Res.*, 6: 263–271.

Clifford, C. W. G. and Vaina, L. M. (1999). A computational model of selective deficits in first and second-order motion processing. *Vision Res.*, 39(1): 113–130.

Cohen, M. S. (1997). Parametric analysis of MRI data using linear systems methods. *Neuroimage*, 6: 93–103.

Collins, D. L., Neelin, P., Peters, T. M., and Evans, A. C. (1994). Automatic 3D intersubject registration of MR volumetric data in standardized Talairach space. *J. Comput. Assist. Tomogr.*, 18: 192–205.

Collins, D., Holmes, C., Peters, T., and Evans, A. (1995). Automatic 3D model-based neuroanatomical segmentation. *Hum. Brain. Mapp.*, 3(3): 190–208.

Corbetta, M., Miezin, F. M., Dobmeyer, S., Shulman, G. L., and Petersen, S. E. (1990). Attentional modulation of neural processing of shape, color, and velocity in humans. *Science*, 248(4962): 1556–1559.

Cornette, L., Dupont, P., Rosier, A., Sunaert, S., Van Hecke, P., Michiels, J., Mortelmans, L., and Orban, G. A. (1998). Human brain regions involved in direction discrimination. *J. Neurophysiol.*, 79(5): 2749–2765.

Courtney, S. M. and Ungerleider, L. G. (1997). What fMRI has taught us about human vision. *Curr. Op. Neurobiol.*, 7(4): 554–561.

Culham, J. C., Brandt, S. A., Cavanagh, P., Kanwisher, N. G., Dale, A. M., and Tootell, R. B. H. (1998). Cortical fMRI activation produced by attentive tracking of moving targets. *J. Neurophysiol.*, 80(5): 2657–70.

Culham, J. C., Cavanagh, P., and Kanwisher, N. G. (2001). Attention response functions: Characterizing brain areas using fmri activation during parametric variations of attentional load. *Neuron*, 32: 737–745.

Culham, J. C. and Kanwisher, N. G. (2001). Neuroimaging of cognitive functions in human parietal cortex. *Curr. Op. Neurobiol.*, 11: 157–163.

Culham, J. C., Verstraten, F. A. J., Ashida, H., and Cavanagh, P. (2001). Visual motion and the human brain: What has neuroimaging told us? *Acta Psychologica*, 107: 69–94.

Dale, A. M. and Buckner, R. L. (1997). Selective averaging of rapidly presented individual trial using fMRI. *Hum. Brain. Mapp.*, 5: 329–340.

De Jong, B. M., Shipp, S., Skidmore, B., Frackowiak, R. S., and Zeki, S. (1994). The cerebral activity related to the visual perception of forward motion in depth. *Brain*, 117

(5): 1039–1054.

Derrington, A. M., Badcock, D. R., and Henning, G. B. (1993). Discriminating the direction of second-order motion at short stimulus durations. *Vision Res.*, 33(13): 1785–1794.

Derrington, A. M., Badcock, D. R., and Holroyd, S. A. (1992). Analysis of the motion of 2-dimensional patterns: evidence for a second-order proces. *Vision Res.*, 32(4): 699–707.

Derrington, A. M. and Ukkonen, O. I. (1999). Second-order motion discrimination by feature-tracking. *Vision Res.*, 39(8): 1465–1475.

D'Esposito, M., Zarahn, E., and aguirre, G. K. (1999). Event-related functional MRI: implications for cognitive psychology. *Psychol. Bull.*, 125: 155–164.

D'Esposito, M., Zarahn, E., Aguirre, G. K., and Rypma, B. (1999). The effect of normal aging on the coupling of neural activity to the BOLD hemodynamic response. *Neuroimage*, 10: 6–14.

DeYoe, E. A., Bandettini, P., Neitz, J., Miller, D., and Winans, P. (1994). Functional magnetic resonance imaging (FMRI) of the human brain. *J. Neurosci. Methods*, 54: 171–187.

DeYoe, E. A., Carman, G. J., Bandettini, P., Glickman, S., Wieser, J., Cox, R., Miller, D., and Neitz, J. (1996). Mapping striate and extrastriate visual areas in human cerebral cortex. *Proc. Natl. Acad. Sci. USA*, 93: 2382–2386.

Di Russo, F., Martinez, A., Sereno, M. I., Pitzalis, S., and Hillyard, S. (2001). Cortical sources of the early components of the visual evoked potential. *Hum. Brain. Mapp.*, 15: 95–111.

Dougherty, R. F., Brewer, A. A., Wade, A. A., and Wandell, B. A. (2002). Measurements of human visual areas across individuals. *SFN abstract*, p. 658.12.

Drury, H. A., Van Essen, D. C., Anderson, C. H., Lee, C. W., Coogan, T. A., and Lewis, J. W. (1996). Computerized mappings of the cerebral cortex: a multiresolution flattening method and a surface-based coordinate system. *J. Cogn. Neurosci.*, 8: 1–28.

Duann, J. R., Jung, T. P., Kuo, W. J., Yeh, T. C., S, M., Hsieh, J. C., and Sejnowski, T. J. (2002). Single-trial variability in event-related bold signals. *Neuroimage*, 15(4):

823–835.

Dukelow, S. P., DeSouza, J. F. X., Culham, J. C., van den Berg, A. V., Menon, R. S., and Vilis, T. (2001). Distinguishing subregions of the human MT plus complex using visual fields and pursuit eye movements. *J. Neurophysiol.*, 86(4): 1991–2000.

Dumoulin, S. O., Baker, Jr, C. L., and Hess, R. F. (2001). Centrifugal bias for second-order but not first-order motion. *J. Opt. Soc. Am. A*, 18(9): 2179–2189.

Dumoulin, S. O., Bittar, R. G., Kabani, N. J., Baker, Jr, C. L., Le Goualher, G., Pike, G. B., and Evans, A. C. (2000). A new anatomical landmark for reliable identification of human area V5/MT: a quantitative analysis of sulcal patterning. *Cereb. Cortex*, 10 (5): 454–463.

Dumoulin, S. O., Hoge, R. D., Baker, Jr, C. L., Hess, R. F., Achtman, R. L., and Evans, A. C. (2003). Automatic volumetric segmentation of human visual retinotopic cortex. *Neuroimage*, 18: 576–587.

Edwards, M. and Badcock, D. R. (1993). Asymmetries in the sensitivity to motion in depth: a centripetal bias. *Perception*, 22: 1013–1023.

Engel, S. A. (1996). Looking into the black box: new directions in neuroimaging. *Neuron*, 17: 375–578.

Engel, S. A., Glover, G. H., and Wandell, B. A. (1997). Retinotopic organization in human visual cortex and the spatial precision of functional MRI. *Cereb. Cortex*, 7: 181–192.

Engel, S. A., Rumelhart, D. E., Wandell, B. A., Lee, A. T., Glover, G. H., Chichilnisky, E. J., and Shadlen, M. N. (1994). FMRI of human visual cortex. *Nature*, 369: 525.

Evans, A. C., Collins, D. L., and Milner, B. (1992). An MRI-based stereotaxic atlas from 250 young normal subjects. *Soc. Neurosci. Abstr.*, 18: 408.

Ewert, J.-P. (1974). The neural basis of viusally guided behavior. *Scientific Am.*, 230(3): 34–42.

Fahle, M. and Wehrhahn, C. (1991). Motion perception in the peripheral visual field. *Graefe's Arch. Clin. Exp. Ophthal.*, 229: 430–436.

Felleman, D. J. and Van Essen, D. C. (1991). Distributed hierarchical processing in the primate cerebral cortex. *Cereb. Cortex*, 1(1): 1–47.

Fennema, C. L. and Thompson, W. B. (1979). Velocity determination in scenes containing several moving objects. *Comput. Graph. Image Process.*, 9: 301–315.

Fischl, B., Sereno, M. I., and Dale, A. M. (1999). Cortical surface-based analysis. II: Inflation, flattening, and a surface-based coordinate system. *Neuroimage*, 9(2): 195–207.

Fischl, B., Sereno, M. I., Tootell, R. B., and Dale, A. M. (1999). High-resolution intersubject averaging and a coordinate system for the cortical surface. *Hum. Brain. Mapp.*, 8(4): 272–84.

Fox, P. T., Miezin, F. M., Allman, J. M., Van Essen, D. C., and Raichle, M. E. (1987). Retinotopic organization of human visual cortex mapped with positron- emission tomography. *J. Neurosci.*, 7(3): 913–922.

Friston, K. J., Fletcher, P., Josephs, O., Holmes, A., Rugg, M. D., and Turner, R. (1998). Event-related fMRI: characterizing differential responses. *Neuroimage*, 7: 30–40.

Friston, K. J., Frith, C. D., Frackowiak, R. S. J., and Turner, R. (1995). Characterizing dynamic brain responses with fMRI: A multivariate approach. *Neuroimage*, 2: 166–172.

Friston, K. J., Frith, C. D., Turner, R., and Frackowiak, R. S. J. (1995). Characterizing evoked hemodynamics with fMRI. *Neuroimage*, 2: 157–165.

Friston, K. J., Zarahn, E., Josephs, O., Henson, R. N. A., and Dale, A. M. (1999). Stochastic designs for event-related fMRI. *Neuroimage*, 10: 607–619.

Gandhi, S. P., Heeger, D. J., and Boynton, G. M. (1999). Spatial attention affects brain activity in human primary visual cortex. *Proc. Natl. Acad. Sci. USA*, 96: 3314–3319.

Geesaman, B. J. and Andersen, R. A. (1996). The analysis of complex motion patterns by form/cue invariant MSTd neurons. *J. Neurosci.*, 16: 4716–4732.

Georgeson, M. A. and Harris, M. G. (1978). Apparent foveofugal drift of counterphase gratings. *Perception*, 7: 527–536.

Gibson, J. J. (1954). The visual perception of objective and subjective movement. *Psychological Review*, 61: 304–314.

Gilissen, E., Iba-Zizen, M.-T., Stievenart, J.-L., Lopez, A., Trad, M., Cabanis, E. A., and Zilles, K. (1995). Is the length of the calcarine sulcus associated with the size of the

human visual cortex? a morphometric study with magnetic resonance tomograpy. *J. Brain Res.*, 36(4): 451–459.

Gilissen, E. and Zilles, K. (1996). The calcarine sulcus as an estimate of the total volume of the human striate cortex: a morphometric study of reliability and intersubject variability. *J. Brain Res.*, 37(1): 57–66.

Glover, G. H. (1996). Deconvolution of impulse response in event-related BOLD fMRI. *Neuroimage*, 9: 416–429.

Goldstein, E. B., (1999). Perceiving movement. In *Sensation and perception*. Brooks/Cole Publishing, Pacific Grove, USA, pp. 273–308.

Gössl, C., Fahrmeir, L., and Auer, D. P. (2001). Bayesian modeling of the hemodynamic response function in BOLD fMRI. *Neuroimage*, 14: 140–148.

Goutte, C., , Nielsen, F. A., and Hansen, L. K. (2000). Modeling the haemodynamic response in fMRI using smooth filters. *IEEE Trans. Med. Imag.*, 19(12): 1188–1201.

Greenlee, M. W. and Smith, A. T. (1997). Detection and discrimination of first- and second-order motion in patients with unilateral brain damage. *J. Neurosci.*, 17: 804–818.

Grèzes, J., Fonlupt, P., Bertenthal, B., Delon-Martin, C., Segebarth, C., and Decety, J. (2001). Does perception of biological motion rely on specific brain regions? *Neuroimage*, 13(5): 775–785.

Gros, B. L., Blake, R., and Hiris, E. (1998). Anisotropies in visual perception: a fresh look. *J. Opt. Soc. Am. A*, 15: 2003–2011.

Gurnsey, R., Fleet, D., and Potechin, C. (1998). Second-order motions contribute to vection. *Vision Res.*, 38: 2801–2816.

Habak, C. and Faubert, J. (2000). Larger effect of aging on the perception of higher-order stimuli. *Vision Res.*, 40: 943–950.

Habak, C., Casanova, C., and Faubert, J. (2002). Central and peripheral interactions in the perception of optic ow. *Vision Res.*, 42: 2843–2852.

Hadjikhani, N., Liu, A. K., Dale, A. M., Cavanagh, P., and Tootell, R. B. H. (1998). Retinotopy and color sensitivity in human visual cortical area V8. *Nat. Neurosci.*, 1(3): 235–41.

Handwerker, D. A., Ollinger, J. M., Curtis, C. E., and D'Esposito, M. (2002). Effects of regional and subject variability of the hemodynamic response function on modeling fMRI signals. *SFN abstract*, p. 506.6.

Harris, L. R., (1994). Visual motion caused by movements of the eye, head and body. In Smith, A. T. and Snowdon, R. J., editors, *Visual detection of motion*. Academic Press, London, pp. 397–435.

Harris, L. R. and Smith, A. T. (1992). Motion defined exclusively by second-order characteristics does not evoke optokinetic nystagmus. *Vis. Neurosci.*, 9: 565–570.

Harris, M. G., (1994). Optic and retinal flow. In Smith, A. T. and Snowdon, R. J., editors, *Visual detection of motion*. Academic Press, London, pp. 307–332.

Hasnain, M. K., Fox, P. T., and Woldorff, M. G. (1998). Intersubject variability of functional areas in the human visual cortex. *Hum. Brain. Mapp.*, 6(4): 301–15.

Hasnain, M. K., Fox, P. T., and Woldorff, M. G. (2001). Structure–function spatial covariance in the human visual cortex. *Cereb. Cortex*, 11(8): 702–16.

Hawken, M. J. and Gegenfurtner, K. R. (2001). Pursuit eye movements to second-order motion targets. *J. Opt. Soc. Am. A*, 18(9): 2282–2296.

He, S. and MacLeod, D. I. A. (1998). Contrast-modulation ficker: dynamics and spatial resolution of the light adaptation process. *Vision Res.*, 38: 985–1000.

Heeger, D. J. and Ress, D. (2002). What does fMRI tell us about neuronal activity? *Nat. Rev. Neurosci.*, 3: 141–151.

Heeger, D. J., Boynton, G. M., Demb, J. B., Seidemann, E., and Newsome, W. T. (1999). Motion opponency in visual cortex. *J. Neurosci.*, 19(16): 7162–7174.

Hess, R. F., Ledgeway, T., and Dakin, S. (2000). Impoverished second-order input to global linking in human vision. *Vision Res.*, 40(24): 3309–18.

Hess, R. F. and Ziegler, L. R. (2000). What limits the contribution of second-order motion to the perception of surface shape? *Vision Res.*, 40: 2125–2133.

Hess, R. H., Baker, Jr., C. L., and Zihl, J. (1989). The "motion-blind" patient: Low-level spatial and temporal filters. *J. Neurosci.*, 9: 1628–1640.

Hildreth, E. C. and Royden, C. S., (1998). Visual motion caused by movements of the

eye, head and body. In Watanabe, T., editor, *High-level motion processing: computational, neurobiological, and psychopysical perspectives*. MIT Press, Cambridge, pp. 269–293.

Holliday, I. A. and Anderson, S. J. (1994). Different processes underlie the detection of second-order motion at low and high temporal frequencies. *Proc. Roy. Soc. Lond.*, 257: 165–173.

Holmes, G. (1945). The organization of the visual cortex in man. *Proc. Roy. Soc. Lond.*, 132: 348–361.

Horton, J. C. and Hoyt, W. F. (1991). Quadrantic visual field defects: a hallmark of lesions in extrastriate (V2/V3) cortex. *Brain*, 1114: 1703–1718.

Huk, A. C., Dougherty, R. F., and Heeger, D. J. (2002). Retinotopy and functional subdivision of human areas MT and MST. *J. Neurosci.*, 22: 7195–7205.

Huk, A. C., Rees, D., and Heeger, D. J. (2001). Neuronal basis of the motion aftereffect reconsidered. *Neuron*, 32: 161–172.

Hunton, D. L., Miezin, F. M., Buckner, R. L., van Mier, H. I., Raichle, M. E., and Petersen, S. E. (1996). An assessment of functional-anatomical variability in neuroimaging studies. *Hum. Brain. Mapp.*, 4(2): 122–139.

Jiang, A., Kennedy, D. N., Baker, J. R., Weiskoff, R. M., Tootell, R. B. H., Woods, R. P., Benson, R. R., Kwong, K. K., Brady, T. J., Rosen, B. R., and Belliveau, J. (1995). Motion detection and correction in functional MR imaging. *Hum. Brain. Mapp.*, 3: 224–235.

Johnson, A. P. and Baker, Jr, C. L. (2003). Response of first- and second-order filters to natural images. *VVS abstract*, p. Submitted.

Johnston, A., McOwan, P. W., and Buxton, H. (1992). A computational model of the analysis of some first-order and second-order motion patterns by simple and complex cells. *Proc. Roy. Soc. Lond.*, 250: 297–306.

Josephs, O., Rees, G., Turner, R., and Friston, K. J. (1997). Event-related fMRI. *Hum. Brain. Mapp.*, 5: 243–248.

Jovicich, J., Peters, R. J., Koch, C., Braun, J., Chang, L., and Ernst, T. (2001). Brain areas

specific for attentional load in a motion-tracking task. *J. Cogn. Neurosci.*, 13(8): 1048–1058.

Kanwisher, N. and Wojciulik, E. (2000). Visual attention: insights from brain imaging. *Nat. Rev. Neurosci.*, 1: 91–100.

Kersten, D., Mamassian, P., and Knill, D. C. (1997). Moving cast shadows induce apparent motion in depth. *Perception*, 26(2): 171–192.

Kim, S.-G., Richter, W., and Uğurbil, K. (1997). Limitations of temporal resolution in functional MRI. *Mag. Res. Med.*, 37: 631–636.

Koenderink, J. J. (1986). Optic flow. *Vision Res.*, 26(1): 161–180.

Kollokian, V. Performance analysis of automatic techniques for tissue classification in magnetic resonance images of the human brain. Master's thesis, Dept. of Computer Science, Concordia University, Montreal, Canada, (1996).

Krubitzer, L. A. and Kaas, J. H. (1990). Cortical connections of MT in four species of primates: areal, modular and retinotopic pattern. *Vis. Neurosci.*, 5: 165–204.

Kwong, K. K. (1995). Functional magnetic resonance imaging with echo-planar imaging. *Magn. Res. Q.*, 11(1): 1–20.

Kwong, K. K., Belliveau, J. W., Chesler, D. A., Goldberg, I. E., Weisskoff, R. M., Poncelet, B. P., Kennedy, D. N., Hoppel, B. E., Cohen, M. S., Turner, R., Cheng, H., Brady, T. J., , and Rosen, B. (1992). Dynamic magnetic resonance imaging of human brain activity during primary sensory stimu. *Proc. Natl. Acad. Sci. USA*, 89: 5675–5679.

Landy, M. S., Dosher, B. A., Sperling, G., and Perkins, M. E. (1991). The kinetic depth effect and optic flow—ii. first- and second-order motion. *Vision Res.*, 31: 859–876.

Le Goualher, G., Procyk, E., Collins, D. L., Venugopal, R., Barillot, C., and Evans, A. C. (1999). Automated extraction and variability analysis of sulcal neuroanatomy. *IEEE Trans. Med. Imag.*, 18: 206–217.

Ledgeway, T. and Hess, R. F. (2000). The properties of the motion-detecting mechanisms mediating perceived direction in stochastic displays. *Vision Res.*, 40(26): 3585–97.

Ledgeway, T. and Hess, R. F. (2002). Failure of direction identification for briefly presented second-order motion stimuli: evidence for weak direction selectivity of the mecha-

nisms encoding motion. *Vision Res.*, 42(14): 1739–1758.

Ledgeway, T. and Smith, A. T. (1994). Evidence for separate motion-detecting mechanisms for first- and second-order motion. *Vision Res.*, 34: 2727–2740.

Ledgeway, T. and Smith, A. T. (1994). The duration of the motion aftereffect following adaptation to first-order and second-order motion. *Perception*, 23: 1211–1219.

Levy, I., Hasson, U., Avidan, G., Hendler, T., and Malach, R. (2001). Center-periphery organization of human object areas. *Nat. Neurosci.*, 4(5): 533–539.

Logothetis, N. K., Guggenberger, H., Peled, S., and Pauls, J. (1999). Functional imaging of the monkey brain. *Nat. Neurosci.*, 2: 555–562.

Logothetis, N. K., Pauls, J., Augath, M., Trinath, T., and Oeltermann, A. (2001). Neurophysiological investigation of the basis of the fmri signal. *Nature*, 412: 150–157.

Lu, Z.-L. and Sperling, G. (1995). The functional architecture of human visual motion perception. *Vision Res.*, 35: 2697–2722.

Lu, Z. L. and Sperling, G. (2001). Three-systems theory of human visual motion perception: review and update. *J. Opt. Soc. Am. A*, 18(9): 2331–2370.

MacDonald, D., Kabani, N., Avis, D., and Evans, A. C. (2000). Automated 3-D extraction of inner and outer surfaces of cerebral cortex from MRI. *Neuroimage*, 12(3): 340–356.

Mareschal, I. and Baker, Jr., C. L. (1998). A cortical locus for the processing of contrast-defined contours. *Nat. Neurosci.*, 1: 150–154.

Mareschal, I. and Baker, Jr., C. L. (1998). Temporal and spatial response to second-order stimuli in cat area 18. *J. Neurophysiol.*, 80: 2811–2823.

Mareschal, I. and Baker, Jr., C. L. (1999). Cortical processing of second-order motion. *Vis. Neurosci.*, 16: 527–540.

Mateeff, S. and Hohnsbein, J. (1988). Perceptual latencies are shorter for motion towards the fovea than for motion away. *Vision Res.*, 28: 711–719.

Mateeff, S., Hohnsbein, J., Ehrenstein, W. H., and Yakimoff, N. (1991). A constant latency difference determines directional anisotropy in visual motion perception. *Vision Res.*, 31: 2235–2237.

Mateeff, S., Yakimoff, N., Hohnsbein, J., Ehrenstein, W. H., Bodanecky, Z., and Radil, T.

(1991). Selective directional sensitivity in visual motion perception. *Vision Res.*, 31: 131–138.

Mather, G. (1991). First-order and second-order visual processes in the perception of motion and tilt. *Vision Res.*, 31: 161–167.

Mather, G. and West, S. (1993). Evidence for second-order detectors. *Vision Res.*, 33: 1109–1112.

McCarthy, J., Pantle, A., and Pinkus, A. (1994). Detection and direction discrimination performance with flicker gratings in peripheral vision. *Vision Res.*, 36: 763–773.

McFarland, D., (1993). Ecology of the senses. In *Animal Behavior: Psychobiology, ethology and evolution*. Longman Scientific & Technical, Essex, England, pp. 251–264.

McKeefry, J., Watson, J. D. G., Frackowiak, R. S. J., Fong, K., and Zeki, S. (1997). The activity in human areas V1/V2, V3, and V5 during the perception of coherent and incoherent motion. *Neuroimage*, 5(1): 1–12.

Mendola, J. D., Dale, A. M., Fischl, B., Liu, A. K., and Tootell, R. B. H. (1999). The representation of illusory and real contours in human cortical visual areas revealed by functional magnetic resonance imaging. *J. Neurosci.*, 19(19): 8560–72.

Miezin, F. M., Maccotta, L., Ollinger, J. M., Petersen, S. E., and Buckner, R. L. (2000). Characterizing the hemodynamic response: Effects of presentation rate, sampling procedure, and the possibility of ordering brain activity based on relative timing. *Neuroimage*, 11: 735–759.

Morland, A. B., Baseler, H. A., Hoffmann, M. B., Sharpe, L. T., and Wandell, B. A. (2001). Abnormal retinotopic representations in human visual cortex revealed by fMRI. *Acta Psychol.*, 107: 229–247.

Nakayama, K. (1981). Differential motion hyperacuity under conditions of common image motion. *Vision Res.*, 21: 1475–1482.

Nakayama, K. (1985). Biological motion processing: a review. *Vision Res.*, 25: 625–660.

Nishida, S., Ashida, H., and Sato, T. (1994). Complete interocular transfer of motion aftereffect with flickering test. *Vision Res.*, 34: 2707–2716.

Nishida, S., Ledgeway, T., and Edwards, M. (1997). Dual multiple-scale processing for

motion in the human visual system. *Vision Res.*, 37: 2685–2698.

O'Craven, K. M., Rosen, B. R., Kwong, K. K., Treisman, A., and Savoy, R. L. (1997). Voluntary attention modulates fMRI activity in human MT-MST. *Neuron*, 18(4): 591–598.

Ogawa, S., Lee, T. M., Kay, A. R., and Tank, D. W. (1990). Brain magnetic resonance imaging with contrast dependent on blood oxygenation. *Proc. Natl. Acad. Sci. USA*, 87: 9868–9872.

Ogawa, S., Menon, R. S., Kim, S.-G., and Ugurbil, K. (1998). On the characteristics of functional magnetic resonance imaging of the brain. *Annu. Rev. Biophys. Biomol. Struct.*, 27: 447–474.

Ogawa, S., Tank, D. W., Menon, R., Ellermann, J. M., Kim, S., Merkle, H., and Ugurbil, K. (1992). Intrinsic signal changes accompanying sensory stimulation: Functional brain mapping with magnetic resonance imaging. *Proc. Natl. Acad. Sci. USA*, 89: 5951–5955.

Ohtani, Y. and Ejima, Y. (1997). Anisotropy for direction discrimination in a two-frame apparent motion display. *Vision Res.*, 37: 765–767.

O'Keefe, L. P. and Movshon, J. A. (1998). Processing of first- and second-order motion signals by neurons in area MT of the macaque monkey. *Vis. Neurosci.*, 15: 305–317.

Olavarria, J. F., DeYoe, E. A., Knierim, J. J., Fox, J. M., and van Essen, D. C. (1992). Neural responses to visual texture patterns in middle temporal area of the macaque monkey. *J. Neurophysiol.*, 68: 164–181.

Pantle, A. (1992). Immobility of some second-order stimuli in human peripheral vision. *J. Opt. Soc. Am. A*, 9: 863–867.

Pelli, D. and Zhang, L. (1991). Accurate control of contrast on microcomputer displays. *Vision Res.*, 31: 1337–1350.

Pelli, D. G. (1997). The Videotoolbox software for visual psychophysics: transforming numbers into movies. *Spat. Vis.*, 10: 437–442.

Perrone, J. A., (2001). A Closer Look at the Visual Input to Self-Motion Estimation. In Zanker, J. M. and Zeil, J., editors, *Motion vision – computational, neural, and eco-*

logical constraints. Springer Verlag, New York, pp. 169–179.

Pessoa, V. F., Abrahao, J. C. H., Pacheco, R. A., Pereira, L. C. M., Magalhaes-Castro, B., and Saraiva, P. E. S. (1992). Relative sizes of cortical visual areas in mormosets: functional and phylogenetic implications. *Exp. Brain Res.*, (459-462).

Peuskens, H., Sunaert, S., Dupont, P., Van Hecke, P., and Orban, G. A. (2001). Human brain regions involved in heading estimation. *J. Neurosci.*, 21(7): 2451–2461.

Plant, G. T., Laxer, K. D., Barbaro, N. M., Schiffman, J. S., and Nakayama, K. (1993). Impaired visual-motion perception in the contralateral hemifield following posterior cerebral-lesions in humans. *Brain*, 116: 1303–1335.

Plant, G. T. and Nakayama, K. (1993). The characteristics of residual motion perception in the hemifield contralateral to lateral occipital lesions in humans. *Brain*, 116: 1337–1353.

Pointer, J. S. and Hess, R. F. (1989). The contrast sensitivity gradient across the human visual field: with emphasis on the low spatial frequency range. *Vision Res.*, 29: 1133–1151.

Press, W. A., Brewer, A. A., Dougherty, R. F., Wade, A. R., and Wandell, B. A. (2001). Visual areas and spatial summation in human visual cortex. *Vision Res.*, 41: 1321–1332.

Ptito, M., Kupers, R., Faubert, J., and Gjedde, A. (2001). Cortical representation of inward and outward radial motion in man. *Neuroimage*, 14(6): 1409–1415.

Rademacher, J., Caviness, Jr., V. S., Steinmetz, H., and Galaburda, A. M. (1993). Topographical variations of the human primairy cortices: implications for neuroimaging, brain mapping, and neurobiology. *Cereb. Cortex*, 3: 313–329.

Rajapakse, J. C., Kruggel, F., Maisog, J. M., and Von Cramon, D. (1998). Modeling hemodynamic response for analysis of functional MRI time-series. *Hum. Brain. Mapp.*, 6: 283–300.

Raymond, J. E. (1994). Directional anisotropy of motion sensitivity across the visual field. *Vision Res.*, 34: 1029–1037.

Rees, G., Friston, K., and Koch, C. (2000). A direct quantitative relationship between the

functional properties of human and macaque V5. *Nat. Neurosci.*, 3(7): 716–723.

Rees, G., Kreiman, G., and Koch, C. (2002). Neural correlates of consciousness in humans. *Nat. Rev. Neurosci.*, 3: 261–270.

Rees, G. and Lavie, N. (2001). What can functional imaging reveal about the role of attention in visual awareness? *Neuropsychologia*, 39: 1343–1353.

Regan, D. and Beverley, K. I. (1982). How do we avoid confounding the direction we are looking and the direction we are moving? *Science*, 215: 194–196.

Reichardt, W., (1961). Autocorrelation, a principle for the evaluation of sensory information by the central nervous system. In Rosenblith, W. A., editor, *Sensory communication*. MIT Press, Cambridge, USA, pp. 303–317.

Robson, J. G. and Graham, N. (1981). Probability summation and regional variation in contrast sensitivity across the visual field. *Vision Res.*, 21: 409–418.

Rogers, B. and Graham, M. (1979). Motion parallax as an independent cue for depth perception. *Perception*, 8(2): 125–134.

Roland, P. E., Geyer, S., Amunts, K., Schormann, T., Schleicher, A., Malikovic, A., and Zille, K. (1997). Cytoarchitectural maps of the human brain in standard anatomical space. *Hum. Brain. Mapp.*, 5(4): 222–227.

Rosa, M. G. P., Fritsches, K. A., and Elston, G. N. (1997). The second visual area in the Marmoset monkey: visuotopic organization, magnification factors, architectonical boundaries, and modularity. *J. Comp. Neurol.*, 387: 547–567.

Rosa, M. G. P., Soares, J. G., Fiorani, Jr., M., and Gattass, R. (1993). Cortical afferents of visual area MT in the cebus monkey: possible homologies between new and old world monkeys. *Vis. Neurosci.*, 10(5): 827–855.

Rosen, B. R., Buckner, R. L., and Dale, A. M. (1998). Event-related functional MRI: past, present and future. *Proc. Natl. Acad. Sci. USA*, 95(3): 773–780.

Sasaki, Y., Hadjikhani, N., Fischl, B., Liu, A. K., Marrett, S., Dale, A. M., and Tootell, R. B. H. (2001). Local and global attention are mapped retinotopically in human occipital cortex. *Proc. Natl. Acad. Sci. USA*, 98(4): 2077–82.

Schofield, A. J. (2000). What does second-order vision see in an image? *Perception*, 29(9):

1071–1086.

Schofield, A. J. and Georgeson, M. A. (1999). Sensitivity to modulations of luminance and contrast in viusal white noise: separatte mechanisms with similar behaviour. *Vision Res.*, 39: 2697–2716.

Schofield, A. J. and Georgeson, M. A. (2003). Sensitivity to contrast modulation:the spatial frequency dependence of second-order vision. *Vision Res.*, 43: 243–259.

Scott, T. R., Lavender, A. D., McWirth, R. A., and Powell, D. A. (1966). Directional asymmetry of motion aftereffect. *J. Exp. Psychol.*, 71: 806–815.

Scott-Samuel, N. E. and Georgeson, M. A. (1999). Does early non-linearity account for second-order motion? *Vision Res.*, 39: 2853–2865.

Scott-Samuel, N. E. and Smith, A. T. (2000). No local cancellation between directionally opposed first-order and second-order signals. *Vision Res.*, 40: 3495–3500.

Seeger, W. *Atlas of topographical anatomy*. Springer, New York, (1978).

Seiffert, A. E. and Cavanagh, P. (1998). Position displacement, not velocity, is the cue to motion detection of second-order stimuli. *Vision Res.*, 38: 3569–3582.

Sereno, M. I. (1998). Brain mapping in animals and humans. *Curr. Op. Neurobiol.*, 8(2): 188–94.

Sereno, M. I., Dale, A. M., Reppas, J. B., Kwong, K. K., Belliveau, J. W., Brady, T. J., Rosen, B. R., and Tootell, R. B. H. (1995). Borders of multiple visual areas in humans revealed by functional magnetic resonance imaging. *Science*, 268(5212): 889–93.

Sereno, M. I., McDonald, C. T., and Allman, J. M. (1994). Analysis of retinotopic maps in extrastriate cortex. *Cereb. Cortex*, 4(6): 601–620.

Sereno, M. I., Pitzalis, S., and Martinez, A. (2001). Mapping of contralateral space in retinotopic coordinates by a parietal cortical area in humans. *Science*, 294: 1350–1354.

Shipp, S., Watson, J. D. G., Frackowiak, R. S. J., and Zeki, S. (1995). Retinotopic maps in human prestriate cortex: The demarcation of areas V2 and V3. *Neuroimage*, 2(2): 125–132.

Singh, K. D., Smith, A. T., and Greenlee, M. W. (2000). Spatiotemporal frequency and direction sensitivities of human visual areas measured using fMRI. *Neuroimage*,

12: 550–564.

Sled, J. G., Zijdenbos, A. P., and Evans, A. C. (1998). A non-parametric method for automatic correction of intensity non-uniformity in MRI data. *IEEE Trans. Med. Imag.*, 17: 87–97.

Smith, A. T., (1994). The detection of second-order motion. In Smith, A. T. and Snowdon, R. J., editors, *Visual detection of motion*. Academic Press, London, pp. 145–176.

Smith, A. T., Greenlee, M. W., Singh, K. D., Kraemer, F. M., and Hennig, J. (1998). The processing of first- and second-order motion in human visual cortex assessed by functional magnetic resonance imaging (fMRI). *J. Neurosci.*, 18(10): 3816–3830.

Smith, A. T., Hess, R. F., and Baker, Jr., C. L. (1994). Direction identification thresholds for second order motion in central and peripheral vision. *J. Opt. Soc. Am. A*, 11: 506–514.

Smith, A. T. and Ledgeway, T. (1997). Separate detection of moving luminance and contrast modulations: fact or artifact?. *Vision Res.*, 37(1): 45–62.

Smith, A. T., Singh, K. D., and Greenlee, M. W. (2000). Attentional suppression of activity in the human visual cortex. *Neuroreport*, 11: 271–277.

Smith, A. T., Singh, K. D., Williams, A. L., and Greenlee, M. W. (2001). Estimating receptive field size from fmri data in human striate and extrastriate visual cortex. *Cereb. Cortex*, 11: 1182–1190.

Smith, A. and Scott-Samuel, N. (2001). First-order and second-order signals combine to improve perceptual accuracy. *J. Opt. Soc. Am. A*, 18: 2267–2272.

Sobey, P. and Srinivasan, M. V. (1991). Measurement of optical flow by a generalized gradient scheme. *J. Opt. Soc. Am. A*, 8: 1488–1498.

Solomon, J. A. and Sperling, G. (1995). 1st- and 2nd-order motion and texture resolution in central and peripheral vision. *Vision Res.*, 35: 59–64.

Somers, D. C., Dale, A. M., Seiffert, A. E., and Tootell, R. B. H. (1999). Functional MRI reveals spatially specific attentional modulation in human primary visual cortex. *Proc. Natl. Acad. Sci. USA*, 96(4): 1663–8.

Steinmetz, H., Fürst, G., and Freund, H. J. (1989). Cerebral cortical localization: application

and validation of the proportional grid system in MR imaging. *J. Comput. Assist. Tomogr.*, 13(1): 10–9.

Steinmetz, H., Fürst, G., and Freund, H. J. (1990). Variation of perisylvian and calcarine anatomic landmarks within stereotaxic proportional coordinates. *Am. J. Neuroradiol.*, 11(6): 1123–30.

Steinmetz, H. and Seitz, R. J. (1991). Functional anatomy of language processing: neuroimaging and the problem of individual variability. *Neuropsychologia*, 29(12): 1149–61.

Stensaas, S. S., Eddington, D. K., and Dobelle, W. H. (1974). The topography and variability of the primairy visual cortex in man. *J. Neurosurg.*, 40: 747–755.

Sunaert, S., Van Hecke, P., Marchal, G., and Orban, G. A. (1999). Motion-responsive regions of the human brain. *Exp. Brain Res.*, 127(4): 355–370.

Talairach, J. and Tournoux, P. *Co-planar stereotaxic atlas of the human brain*. Thieme, New York, (1988).

Tolias, A. S., Smirnakis, S. M., Augath, M. A., Trinath, T., and Logothetis, N. K. (2001). Motion processing in the macaque: Revisited with functional magnetic resonance imaging. *J. Neurosci.*, 21(21): 8594–8601.

Tootell, R. B. H., Dale, A. M., Sereno, M. I., and Malach, R. (1996). New images from human visual cortex. *Trends Neurosci.*, 19(11): 481–9.

Tootell, R. B. H. and Hadjikhani, N. (1998). Has a new color area been discovered? *Nat. Neurosci.*, 1(5): 335–336.

Tootell, R. B. H. and Hadjikhani, N. (2001). Where is 'dorsal V4' in human visual cortex? Retinotopic, topographic and functional evidence. *Cereb. Cortex*, 11(4): 298–311.

Tootell, R. B. H., Hadjikhani, N., Hall, E. K., Marrett, S., Vanduffel, W., Vaughan, J. T., and Dale, A. M. (1998). The retinotopy of visual spatial attention. *Neuron*, 21(6): 1409–22.

Tootell, R. B. H., Hadjikhani, N. K., Vanduffel, W., Liu, A. K., Mendola, J. D., Sereno, M. I., and Dale, A. M. (1998). Functional analysis of primary visual cortex (V1) in humans. *Proc. Natl. Acad. Sci. USA*, 95(3): 811–7.

Tootell, R. B. H., Mendola, J. D., Hadjikhani, N. K., Ledden, P. J., Liu, A. K., Reppas, J. B., Sereno, M. I., and Dale, A. M. (1997). Functional analysis of V3A and related areas in human visual cortex. *J. Neurosci.*, 17(18): 7060–78.

Tootell, R. B. H., Mendola, J. D., Hadjikhani, N. K., Liu, A. K., and Dale, A. M. (1998). The representation of the ipsilateral visual field in human cerebral cortex. *Proc. Natl. Acad. Sci. USA*, 95(3): 818–24.

Tootell, R. B. H., Reppas, J. B., Dale, A. M., Look, R. B., Sereno, M. I., Malach, R., Brady, T. J., and Rosen, B. R. (1995). Visual motion aftereffect in human cortical area MT revealed by functional magnetic resonance imaging. *Nature*, 375(6527): 139–41.

Tootell, R. B. H., Reppas, J. B., Kwong, K. K., Malach, R., Born, R. T., Brady, T. J., Rosen, B. R., and Belliveau, J. W. (1995). Functional analysis of human MT and related visual cortical areas using magnetic resonance imaging. *J. Neurosci.*, 15(4): 3215–30.

Tootell, R. B. H., Hadjikhani, N. K., Mendola, J. D., Marrett, S., and Dale, A. M. (1998). From retinotopy to recognition: fMRI in human visual cortex. *Trends Cogn. Sci.*, 2 (5): 174–183.

Turner, R., Le Bihan, D., Moonen, C. T., Despres, D., and Frank, J. (1991). Echo-planar time course MRI of cat brain oxygenation. *Mag. Res. Med.*, 22: 159–166.

Tyler, C. W. (1987). Analysis of visual modulation sensitivity. II. Peripheral retina and the role of photoreceptor dimensions. *J. Opt. Soc. Am. A*, 2(3): 393–398.

Vaina, L. M. and Cowey, A. (1996). Impairment of the perception of second order motion but not first order motion in a patient with unilateral focal brain damage. *Proc. Natl. Acad. Sci. USA*, 263: 1225–1232.

Vaina, L. M., Cowey, A., and Kennedy, D. (1999). Perception of first- and second-order motion: separable neurological mechanisms? *Hum. Brain. Mapp.*, 7(1): 67–77.

Vaina, L. M., Makris, N., Kennedy, D., and Cowey, A. (1998). The selective impairment of the perception of first-order motion by unilateral cortical brain damage. *Vis. Neurosci.*, 15: 333–348.

Vaina, L. M., Solomon, J., Chowdhury, S., Sinha, P., and Belliveau, J. W. (2001). Functional

neuroanatomy of biological motion perception in humans. *Proc. Natl. Acad. Sci. USA*, 98(20): 11656–11661.

Vaina, L. M., Soloviev, S., Bienfang, D. C., and Cowey, A. (2000). A lesion of cortical area V2 selectively impairs the perception of the direction of first-order visual motion. *Neuroreport*, 11(5): 1039–1044.

Van de Grind, W. A., Koenderink, J. J., van Doorn, A. J., Milders, M. V., and Voerman, H. (1992). Inhomogeneity and anisotropies for motion detection in the monocular visual field of human observers. *Vision Res.*, 33: 1089–1107.

Van der Smagt, M. J., Verstraten, F. A. J., and Van de Grind, W. A. (1999). A new transparent motion aftereffect. *Nat. Neurosci.*, 2: 595–596.

Van Essen, D. C. and Drury, H. A. (1997). Structural and functional analyses of human cerebral cortex using a surface-based atlas. *J. Neurosci.*, 17(18): 7079–7102.

Van Essen, D. C., Drury, H. A., Joshi, S., and Miller, M. I. (1998). Functional and structural mapping of human cerebral cortex: Solutions are in the surfaces. *Proc. Natl. Acad. Sci. USA*, 95: 788–795.

Van Essen, D. C., Drury, H. A., Joshi, S., and Miller, M. I. (2000). Functional and structural mapping of human cerebral cortex: Solutions are in the surfaces. *Adv. Neurol.*, 84: 23–34.

Van Essen, D. C., Lewis, J. W., Drury, H. A., Hadjikhani, N., Tootell, R. B. H., Bakircioglu, M., and Miller, M. I. (2001). Mapping visual cortex in monkeys and humans using surface-based atlases. *Vision Res.*, 41(10-11): 1359–78.

Van Oostende, S., Sunaert, S., Van Hecke, P., Marchal, G., and Orban, G. A. (1997). The kinetic occipital (KO) region in man: an fMRI study. *Cereb. Cortex*, 7(7): 690–701.

Van Santen, J. P. H. and Sperling, G. (1985). Elaborated Reichardt detectors. *J. Opt. Soc. Am. A*, 2: 300–321.

Vanduffel, W., Fize, D., Mandeville, J. B., Nelissen, K., Van Hecke, P., Rosen, B. R., Tootell, R. B., and Orban, G. A. (2001). Visual motion processing investigated using contrast agent-enhanced fMRI in awake behaving monkeys. *Neuron*, 32: 565–577.

Voyvodic, J. T. (1999). Real-time fMRI paradigm control, physiology, and behavior com-

bined with near real-time statistical analysis. *Neuroimage*, 10: 91–106.

Wallach, H. and O'Connell, D. (1953). The kinetic depth effect. *J. Exp. Psychol.*, 45: 205–217.

Wandell, B. A. (1999). Computational neuroimaging of human visual cortex. *Ann. Rev. Neurosci.*, 22: 145–173.

Wang, Y. Z., Hess, R. F., and Baker, Jr., C. L. (1997). Second-order motion perception in peripheral vision: limits of early filtering. *J. Opt. Soc. Am. A*, 14: 3145–3153.

Warnking, J., Dojat, M., Guérin-Dugué, A., Delon-Martin, C., Olympieff, S., Richard, N., Chehikian, A., and Segebart, C. (2002). fMRI retinotopic mapping — step by step. *Neuroimage*, 17(4): 1665–1683.

Warren, W. H. and Kurtz, K. J. (1992). The role of central and peripheral vision in perceiving the direction of self-motion. *Percept. Psychophys.*, 51: 443–454.

Warren, Jr, W. H., Kay, B. A., Zosh, W. D., Duchon, A. P., and Sahuc, S. (2001). Optic flow is used to control human walking. *Nat. Neurosci.*, 4(2): 213–216.

Watanabe, T., Harner, A. M., Miyauchi, S., Sasaki, Y., Nielsen, M., Palomo, D., and Mukai, I. (1998). Task-dependent influences of attention on the activation of human primary visual cortex. *Proc. Natl. Acad. Sci. USA*, 95: 11489–11492.

Watson, J. D. G., Myers, R., Frackowiak, R. S. J., Hajnal, J. V., Woods, R. P., Mazziota, J. C., Shipp, S., and Zeki, S. (1993). Area V5 of the human brain: evidence from a combined study using positron emission tomography and magnetic resonance imaging. *Cereb. Cortex*, 3: 79–94.

Westheimer, G. (1982). The spatial grain of the perifoveal visual field. *Vision Res.*, 22: 157–162.

Williams, D. S., Detre, J. A., Leigh, J. S., and Koretsky, A. P. (1992). Magnetic resonance imaging of perfusion using spin inversion of arterial water. *Proc. Natl. Acad. Sci. USA*, 89(1): 212–216.

Wilson, H. R., Ferrera, V. P., and Yo, C. (1992). A psychophysically motivated model for two-dimensional motion perception. *Vis. Neurosci.*, 9(1): 79–97.

Wilson, J., Robinson, J., and Piggins, D. (1983). Wobble cones and wobble holes: the

stereokinetic effect revisited. *Perception*, 12: 187–193.

Wong, A. M. F. and Sharpe, J. A. (1999). Representation of the visual field in the human occipital cortex - a magnetic resonance imaging and perimetric correlation. *Arch. Ophthal.*, 117(2): 208–217.

Woods, R. P., Cherry, S. R., and Mazziotta, J. C. (1992). Rapid automated algorithm for aligning and reslicing PET images. *J. Comput. Assist. Tomogr.*, 16: 620–633.

Woods, R. P., Grafton, S. T., Holmes, C. J., Cherry, S. R., and Mazziotta, J. C. (1998). Automated image registration: I. general methods and intrasubject, intramodality validation. *J. Comput. Assist. Tomogr.*, 22: 139–152.

Worsley, K. J., Liao, C., Aston, J., Petre, V., Duncan, G. H., Morales, F., and Evans, A. C. (2002). A general statistical analysis for fMRI data. *Neuroimage*, 15(1): 1–15.

Worsley, K. J., Marrett, S., Neelin, P., Vandal, A. C., Friston, K. J., and Evans, A. C. (1996). A unified statistical approach for determining significant signals in images of cerebral activation. *Hum. Brain. Mapp.*, 4: 58–73.

Zanker, J. M. (1993). Theta motion: a paradoxical stimulus to explore higher order motion extraction. *Vision Res.*, 33(4): 553–569.

Zanker, J. M. (1997). Second-order motion perception in the peripheral visual field. *J. Opt. Soc. Am. A*, 14: 1385–1392.

Zanker, J. M. and Burns, N. R. (2001). Interaction of first- and second-order direction in motion-defined motion. *Vision Res.*, 18(9): 2321–2331.

Zeki, S., McKeefry, D. J., Bartels, A., and Frackowiak, R. S. J. (1998). Has a new color area been discovered? *Nat. Neurosci.*, 1(5): 335.

Zhou, Y.-X. and Baker, Jr., C. L. (1993). A processing stream in mammalian visual cortex neurons for non-fourier responses. *Science*, 261: 98–101.

Zhou, Y.-X. and Baker, Jr., C. L. (1994). Envelope-responsive neurons in areas 17 and 18 of cat. *J. Neurophysiol.*, 72: 2134–2150.

Zhou, Y.-X. and Baker, Jr., C. L. (1996). Spatial properties of envelope-responsive cells in area 17 and 18 neurons of the cat. *J. Neurophysiol.*, 75: 1038–1050.

Ziegler, L. R. and Hess, R. F. (1999). Stereoscopic depth but not shape perception from

second-order stimuli. *Vision Res.*, 39(8): 1491–1507.

Zihl, J., von Cramon, D., and Mai, N. (1983). Selective disturbance of movement vision after bilateral brain damage. *Brain*, 106: 313–340.

Zijdenbos, A. P., Forghani, R., and Evans, A. C. (1998). Automatic quantification of MS lesions in 3D MRI brain data sets: Validation of INSECT. In *Proceedings of the First International Conference on Medical Image Computing and Computer-Assisted Intervention (MICCAI)*, pp. 439–448, Cambridge MA, USA.

13 March 2003

Dr Serge O Dumoulin
McGill University
Vision Research Unit

Dear Dr Dumoulin

NEUROLMAGE, 2003, Dumoulin et al, "Automatic volumetric segmentation of human visual retinotopic cortex", (in press)

As per your letter dated 12 February 2003, we hereby grant you permission to reprint the aforementioned material at no charge **in your thesis** subject to the following conditions:

1. If any part of the material to be used (for example, figures) has appeared in our publication with credit or acknowledgement to another source, permission must also be sought from that source. If such permission is not obtained then that material may not be included in your publication/copies.

2. Suitable acknowledgment to the source must be made, either as a footnote or in a reference list at the end of your publication, as follows:

   "Reprinted from Publication title, Vol number, Author(s), Title of article, Pages No., Copyright (Year), with permission from Elsevier".

3. Reproduction of this material is confined to the purpose for which permission is hereby given.

4. This permission is granted for non-exclusive world **English** rights only. For other languages please reapply separately for each one required. Permission excludes use in an electronic form. Should you have a specific electronic project in mind please reapply for permission.

5. This includes permission for the National Library of Canada to supply single copies, on demand, of the complete thesis. Should your thesis be published commercially, please reapply for permission.

Yours sincerely

Helen Wilson
Rights Manager

Your future requests will be handled more quickly if you complete the online form at www.elsevier.com/homepage/guestbook/?form=permis

February 21, 2003

Serge Dumoulin
McGill Vision Research Unit
Dept. of Ophthalmology
McGill University

Dear Mr. Dumoulin:

The Optical Society of America considers the below requested use of its copyrighted material to be allowed under the OSA Author Agreement submitted by the requestor on acceptance for publication of his/her manuscript. It is requested that a complete citation of the original material be included in any publication. If you require any confirmation or permission other than what this letter grants, please feel free to contact me.

Article: S.O. Dumoulin, C.L. Baker Jr., R.F. Hess "Centrifugal bias for second-order but not first-order motion," J. Opt. Soc. Am. A 18: 2179-2189
(2001). (In author's PhD thesis.)

Sincerely,

Susannah Lehman
Authorized Agent
Optical Society of America